CLOUD CONDENSATION NUCLEI

A

THESIS

Presented to the Faculty

of the University of Alaska Fairbanks

in Partial Fulfillment of the Requirements

for the Degree of

DOCTOR OF PHILOSOPHY

By

Qiang Ji, B.S., M.S.

Fairbanks, Alaska

May 1996

CLOUD CONDENSATION NUCLEI

By

Qiang Ji

RECOMMENDED:

Knut Stamnes, Ph.D.

Sue Ann Bowling, Ph.D.

Richard Benner, Ph.D.

Juergen Kienle, Ph.D.

Brenton Watkins, Ph.D.

Glenn Shaw, Ph.D., Chairman, Advisory Committee

John Morack, Ph.D., Head, Physics Department

APPROVED:

Paul Reichardt, Ph.D., Dean, College of Natural Science

Joseph Kan, Ph.D., Dean, Graduate School

Dec 7, 1995

Date

ABSTRACT

In this study the supersaturation spectra of Cloud Condensation Nuclei (CCN) and the size distribution spectra of aerosols were investigated. These studies were conducted because it is believed that atmospheric aerosols, especially CCN, can affect the climate of the Earth.

First, the size distributions of aerosols and the number concentrations of CCN were measured at different times in different meteorological airmass systems. The results indicate that the CCN supersaturation spectrum can be calculated from the size distribution of aerosols in only a few cases, suggesting that the direct measurement of CCN is of importance.

Second, based on the measurements, a new general equation is proposed to describe the CCN supersaturation spectrum for some types of aerosols. The corresponding equation for CCN size distribution is derived. It is also shown theoretically that, with certain assumptions, the aerosol size distribution in the accumulation mode can be described by a bell-shaped distribution, in agreement with our measurements. The new equations are compared with actual data.

Finally, a new method is devised to facilitate the measurement of CCN. The new instrument, which we call the "CCN Remover", separates CCN from the rest of aerosols by activation and removal. Together with a particle sizer, a new CCN measurement system, the CCN Remover Spectrometer, can provide information on both the supersaturation spectrum and the size distribution of CCN. Preliminary laboratory tests show close agreement between measurement results and theoretical predictions. The Remover Spectrometer was successfully tested in the NASA SCAR-B (Smoke, Clouds, and Radiation - Brazil) biomass burning experiment.

TABLE OF CONTENTS

LIST OF FIGURES

LIST OF TABLES

ACKNOWLEDGMENTS

I would like to give special thanks to Professor Glenn E. Shaw for his encouragement, support, and guidance over the course of this research. Similar thanks to Professor Knut Stamnes for his constant support and assistance; to Professor Richard Benner for his suggestions and support on experimental work; to Professor Sue Ann Bowling for her helpful suggestions; and to Professor Juergen Kienle for encouraging me to study the coalescence of volcanic ash. Special thanks go to Dr. Yongxiang Hu for constructive conversations; to Dr. Si-Chee Tsay and Dr. Yoram J. Kaufman for supporting me in building a CCN Remover and helping to arrange my attendance at the NASA SCAR-B field measurement in Brazil. The prototype Remover was built in the machine shop of the Geophysical Institute under the expert guidance of Larry Kozycki. Thanks to all who helped get the instruments up and running. Thanks to Professor Hiroshi Tanaka for giving me the chance to come to Alaska and for his encouragement and support.

I thank my wife Qingling and my son Robin for the patience and love they have shown over the last several

years. Without their support it would have been impossible for me to earn this degree.

It has been gratifying to be part of the Geophysical Institute at University of Alaska Fairbanks. Thoughts of the awesome nature of Alaska and the unique research environment at the Geophysical Institute will always be pleasant ones for me.

This research has been conducted under the support of the contract to the University of Alaska from the US Department of Energy's Environmental Sciences Division, the ARM program (Department of Energy contract 091574-A-Q1), and the NASA Aerosol Interdisciplinary Project (grant 2818-AERO92-0049). The attendance at the SCAR-B experiment has been partly supported by the "Subcontract Agreement between Science Systems and Applications, INC. and Mr. Qiang Ji" (QJ061995).

CHAPTER 1

INTRODUCTION

1.1 Aerosol and climate

"I have said that if there was no dust there would be no fogs, clouds, nor mists; ...", John Aitken wrote in 1880. Today, it is generally believed that if the properties of dust change, clouds and radiative transfer in the atmosphere will be influenced, and the climate may change.

Systematic study of atmospheric aerosol began over a hundred years ago. "After the publication of his great paper, on 'Fogs and Clouds,' John Aitken was recognized as one of the original experimenters of his day" (Knott, 1923). Aitken made many measurements of "dust" by using his dust counter, which operated on the principle of the expansion cloud chamber. He discovered that there are between several hundreds to tens of thousands of particles in a cubic centimeter of air. He demonstrated that no cloudy condensation is produced in saturated dust-free air upon slight cooling (low supersaturation).

Observations of aerosols in cities, in the countryside, on mountains and over oceans show that the concentration of

aerosols varies greatly and the compositions of aerosols are complex (e.g., Junge, 1958; Landsberg, 1938). Usually the air is clean over oceans, and dirty in cities. In most practical cases in the atmosphere, condensation of a vapor takes place in the presence of small dust particles making unnecessary the extremely high supersaturations required for homogeneous condensation. These small dust particles are given the generic name of condensation nuclei (CN). They can range in size from near molecular sizes to greater than 1 μm. Among CN, the larger, soluble particles are of interest for the formation of clouds. These particles are called Cloud Condensation Nuclei (CCN).

Ever since the pioneering work in the late nineteenth century by John Aitken, we have known that some fraction of the available aerosol participates in the cloud condensation process. When air is slightly supersaturated, water vapor will condense on these particles to form cloud droplets. The growth of these early formed droplets pull water vapor out of the air and prevent the supersaturation from rising enough to activate the remaining particles. Thus the available water released in an air mass cooled below its dew point spreads out among activated CCN. These activated CCN determine the droplets' number concentration and hence a number of important parameters related to atmospheric

chemical properties and climate influences of clouds (surface area, optical depth, scattering phase function, etc.). Obviously, changes in CCN have the potential to introduce climatic or chemical perturbations.

Aerosol and clouds play a central role in the atmospheric water cycle, the so-called hydrological cycle, and the planet's outgoing radiation (e.g., Twomey, 1991). Under certain conditions, if there are more CCN, more cloud droplets form and the average size of cloud droplets decreases (Warner and Twomey, 1967; Pruppacher and Klett, 1978; Hudson, 1983; Twomey et al., 1984). In clouds, if the same amount of condensed water is divided among more but smaller droplets, then the optical depth of clouds in visible wavelengths will increase. Also due to the lack of large droplets, the coalescence process in clouds may be influenced and the probability of rainfall may decrease. Increases in aerosol concentrations over the oceans may increase the amount of low-level cloudiness, through a reduction of drizzle, in a process that regulates the liquid water content and the energetics of shallow marine clouds (Albrecht, 1989). Air pollution can increase the number of CCN (Hobbs et al., 1974; Braham, 1974). Fossil fuel and biomass burning can also affect climate (Kaufman, et al., 1991). In short, cloud condensation nuclei (CCN) can have a

significant indirect effect on climate through their influence on the formation and microstructure of clouds.

In a highly simplified model, a possible link between CCN and climate can be illustrated in Figure 1-1. The actual physical processes are much more complex.

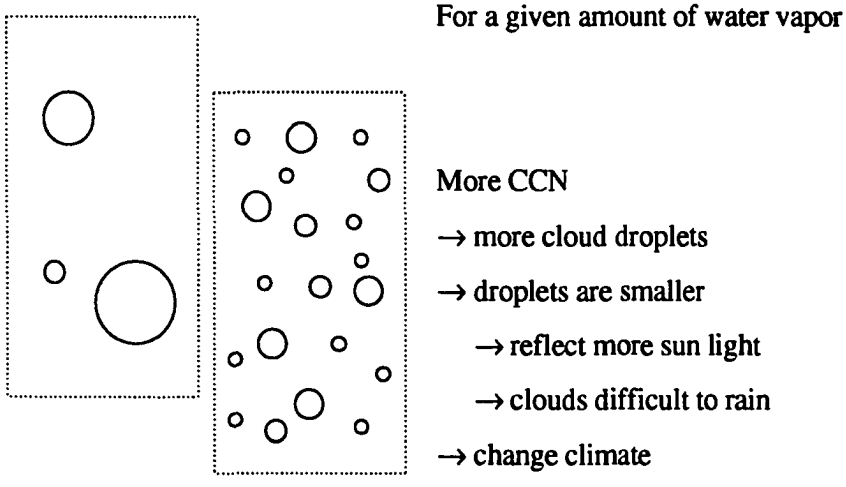

Figure 1-1 A possible link between CCN and climate.

Aerosols may affect radiation directly and indirectly though their effects on clouds. One piece of observational evidence is the "ship track" phenomenon (Radke, et al., 1989; Coakley, et al., 1987). It was observed from satellite images that under certain conditions clouds formed, apparently nucleated by the pollutants released from a ship, and left a visible track behind the ship. Another example is

Arctic Haze in polar regions (Shaw and Stamnes, 1980). Comprehensive models were built to study the influences of aerosols and clouds on the radiative transfer and energy budget in the atmosphere (e.g., Tsay, et al., 1989).

It is stated in the preface of a recent book entitled "Aerosol-Cloud-Climate Interactions" (Hobbs, 1993):

> Together with molecular scattering from gases, aerosol and clouds determine what fraction of the solar radiation incident at the top of the atmosphere reaches the earth's surface, and what fraction of the long wave radiation from the earth escapes to space. Consequently, aerosol and clouds play an important role in determining the earth's climate. Much remains to be learned about the properties of atmospheric aerosol and clouds and their effects on the radiative balance of the earth. The problem stems, in part at least, from the fact that unlike gases, aerosol and clouds are distributed very unevenly in the atmosphere. Also, many of the relevant properties of aerosol and clouds are not well defined. Finally, there are strong interactions between aerosol, clouds, and climate, many of which we are only just beginning to understand, let alone incorporate into climate models.

Although aerosols have been studied for many years, there is neither a theoretical nor an empirical basis to allow the necessary global modeling of the radiative effects that depend on the number of CCN (Penner, 1994). This situation is partly due to the lack of measurement of the cloud condensation nuclei, the CCN. Significant uncertainties about global climate change cannot be reduced without expansion of the knowledge base of CCN (Hudson, 1992).

The key to predicting cloud microphysical parameters, for example, droplet diameter, droplet number concentration, etc., is knowledge of the CCN supersaturation spectrum, $N(S)$, where N is the number concentration of CCN at supersaturation S.

1.2 CCN measurements

The CCN we measure are some aerosols in the sub-micron range as shown in Figure 1-2. Most of them are smaller than the wave lengths of visible light. Cloud droplets formed on CCN can grow up to larger than the 10 μm range.

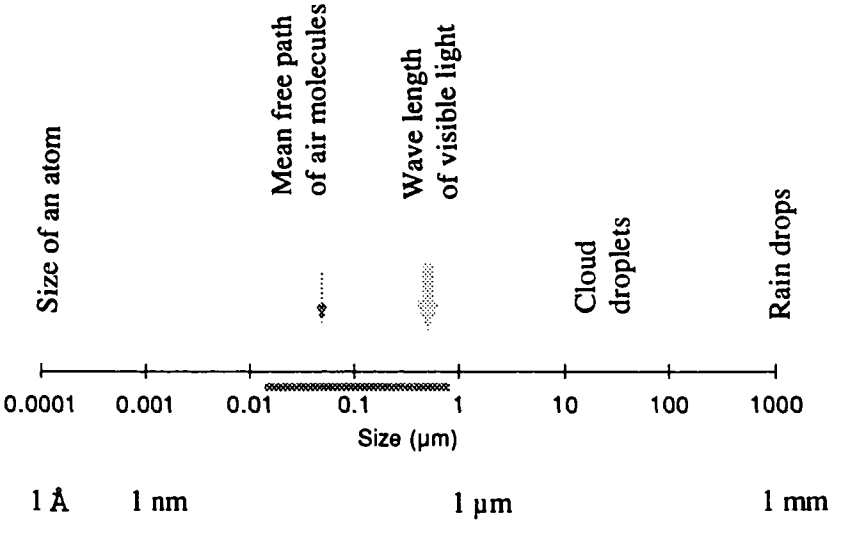

Figure 1-2 The CCN we measure are some aerosols in the sub-micron range.

To measure CCN number concentration, the aerosol must be put into a supersaturated environment. There are typically two laboratory methods to produce supersaturated air. Expansion chambers were widely used in the early days of aerosol measurements. When moist air expands rapidly, it becomes supersaturated. However, it is difficult to control the supersaturation accurately in an expansion chamber, especially at low supersaturations. The second method, which can be used for quantitative measurement of CCN, was introduced by Wieland (Radke and Jiusto, 1977). Wieland's technique is called the thermal-gradient diffusion cloud chamber. His cloud chamber was adapted from a chamber originally developed by Langsdorf in 1936. The thermal diffusion chamber is the basic design used for virtually all the CCN counters developed to date.

Experiments investigating the chemistry of CCN indicate that the chemical composition of the cloud condensation nuclei is mainly sulfur compounds. The major source of CCN over the oceans appears to be dimethylsulfide (DMS) produced by planktonic algae in sea water and oxidized in the atmosphere to form a sulfate aerosol (Charlson et al., 1987). It has been proposed that biogenic and anthropogenic sulfate aerosol could modify the Earth's radiation budget and cool the climate (Shaw, 1983a; Wigley, 1989). Most

particles in the atmosphere, including bacteria (Maki and Willoughby, 1978), can potentially be CCN.

1.3 The objectives of the project

It is believed that the CCN supersaturation spectrum is primarily -- though not entirely -- determined by the aerosol size distribution spectrum rather than by aerosol composition (Junge and McLaren, 1971; Fitzgerald, 1972). Size distribution is now relatively easy to measure with modern instrumentation. This is a great change from the situation that existed just a decade or so ago. The new particle sizing system (Model 3934) manufactured by TSI (Minneapolis, MN) allows one to measure size distribution virtually in real time, so aerosols can be measured in more detail than ever before. It is now possible to examine the assumption that the supersaturation spectrum of CCN can be obtained from the size distribution of aerosol. Because the CCN supersaturation spectrum is difficult to measure, it would be a distinct scientific advance if the CCN supersaturation spectrum could be reliably obtained simply from the aerosol size distributions.

The primary objective of this project is to look at the relationship between the CCN supersaturation spectrum and aerosol size distribution. The original plan consisted of

two steps. The first step was to make more measurements to establish a CCN or aerosol "climatology". An automated CCN counter (Model M1, DH Associate, Tucson, AZ) was used to measure the number concentrations of CCN. Sub-micron particles were measured. The second step was to analyze the data and build models that describe some characteristics of aerosol and CCN.

During the progress of this project, it was found that the thermal gradient CCN counter has a number of errors which are difficult to correct. This led to an effort to improve the CCN counter. The effort resulted in the invention of a new instrument, the CCN Remover. The "CCN Remover Spectrometer" is the new aerosol measurement system. It is a combination of a CCN Remover and a particle sizing system, and it can be used to measure both the supersaturation spectrum and the size distribution of CCN.

1.4 Organization of the thesis

A new equation for the CCN supersaturation spectrum is proposed in Chapter 2. It is shown that the bell-shaped size distribution can be derived from the new equation. A theoretical argument is presented that explains why the size distribution of accumulation mode aerosols can be bell-shaped as we often see in the atmosphere.

In Chapter 3, a simple model is used to simulate the performance of a thermal diffusion chamber and CCN counters based on the chamber. It helps to explain why this type of CCN counter has errors that cause biases in measured CCN number concentrations. The new CCN measurement method and the design of a CCN Remover are described.

Chapter 4 summarizes some of the measurements of aerosol size distribution spectra and cloud condensation nuclei concentration in the atmosphere. Four types of air-masses are described. They are winter and late summer episodes in Alaska, and marine boundary layer and free troposphere airmasses in Hawaii. A few cases are chosen from thousands of measured particle size distribution spectra to demonstrate cases where the CCN number can and cannot be obtained from the measured size distribution. Some results of CCN counter intercomparison and laboratory tests are presented.

Laboratory and field tests of the CCN Remover Spectrometer are discussed in Chapter 5. Chapter 6 gives the conclusions and suggests some important future work.

CHAPTER 2

CCN AND AEROSOL MODELING

2.1 CCN supersaturation spectrum

The activation of CCN in the cloud condensation process was summarized by Köhler (1923). He used two basic principles of physical chemistry. One is Raoults' law, which supposes the depression of equilibrium vapor pressure to be proportional to the mole fraction of solute. The other one is Kelvin's law, which specifies enhanced vapor pressure necessary to maintain surfaces of curved liquid in equilibrium. Thus, the saturation vapor pressure (e') over a solution droplet of radius r that contains a mass m of a dissolved salt of molecular weight M_s can be expressed as:

$$e' = e_s \left(\exp \frac{2\sigma'}{n' k T r}\right) \left[1 + \frac{i m M_w}{M_s\left(\frac{4}{3} \pi r^3 \rho' - m\right)} \right]^{-1}$$

where e_s is the saturation vapor pressure over the flat pure water surface; σ' and n' are the surface energy and number density of water molecules, respectively, in the solution; k is the Boltzmann constant; T is the temperature; M_w is the molecular weight of water; each molecule of the salt

dissociates in water into i ions and the density of the solution is ρ' (Wallace and Hobbs, 1977). By solving $de'/dr = 0$, we can find the maximum of e' and the size of the droplet, r_c, at which e' reaches maximum. r_c is the critical size. If the vapor pressure in the air is higher than the maximum e' for a droplet, or if the size of a droplet is larger than the critical size at a given vapor pressure, then water vapor will continue to condense on the droplet. By Köhler's theory, at a given supersaturation S, all CCN larger than the critical radius r_c will be activated. For soluble salts,

$$r_c = const/S^{2/3},$$

where *const* is a constant depending on the chemical composition of the CCN. Therefore, for CCN with known chemical composition, if we know the size distribution of CCN, we can calculate the supersaturation spectrum and vice versa.

2.1.1 An equation for CCN supersaturation spectrum

A widely used expression of the CCN supersaturation spectrum is an empirically fitted power law expression described by Twomey (1959).

2.1.1.1 The power law

The power law gives us the number concentration (N) of activated CCN at a given supersaturation (S)

$$N = C S^{K} \tag{2.1}$$

where C and K are empirical coefficients. The power law is widely used because it is relatively simple. With the power law assumption, the nonlinear activation equation can be solved approximately to predict the number concentration of cloud droplets (Twomey, 1959). Twomey recognized that the power law expression is only approximate and is not valid over a wide range of supersaturation.

2.1.1.2 Limitations of the power law

Several decades ago, researchers found that atmospheric aerosol size distribution can be approximated by the Junge distribution (see section 2.4 B). This distribution works fairly well for the large particles (around 1 μm) of the bell-shaped size distribution. Instruments available then could not see the entire size distribution in detail because the small particles are smaller than the wave length of light and are difficult to collect. Nevertheless, the "Junge Law" was extrapolated to very small particle sizes without knowledge of its validity. If the size distribution of CCN

obeys the Junge law, then the supersaturation spectrum of CCN seems to obey power law.

Due to the limitations of CCN instruments and the knowledge about aerosol, the power law was proposed to fit measurements for only a narrow range of supersaturation. For supersaturation of 0.2% to 1%, it was believed to be good enough for some purposes. However, "a uniform K does not hold for the laboratory generated aerosol, and it is not always an accurate approximation in ambient air" (Jiusto and Lala, 1981). The reason for this can be seen from the new equations below.

2.1.2 New equations

Let us take our measurements of the aerosol size distribution on Mauna Loa Observatory (MLO) as an example. When the air is not polluted, most particles in the accumulation mode at MLO are soluble sulfate compounds and can act as CCN (Sheridan, et. al., 1994; Bigg, 1977).

Our measured size distributions are bell-shaped as shown in Figure 2-1. Assume all aerosol are ammonium sulfate, then the CCN supersaturation spectrum can be computed from the measured size distribution by using Köhler theory. The calculated supersaturation spectrum is S-shaped as shown in Figure 2-2.

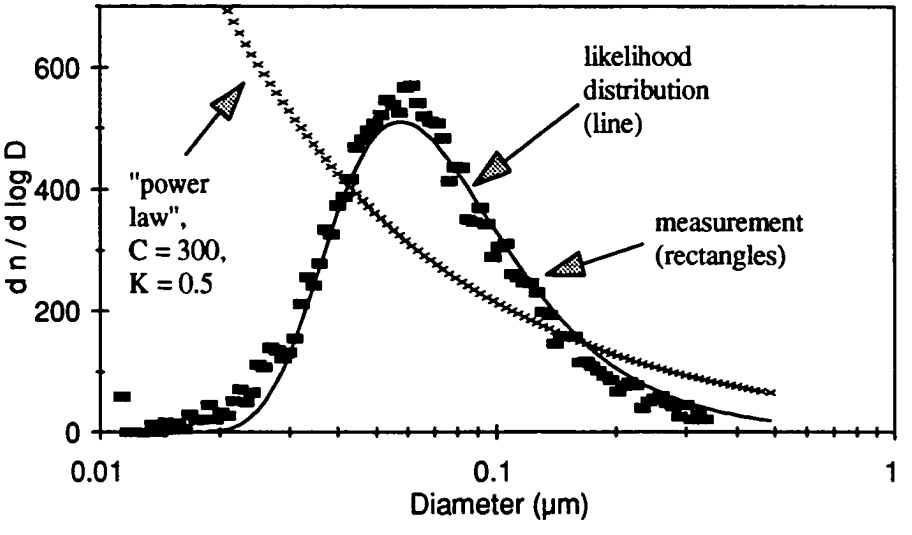

Figure 2-1 Aerosol size distributions (1): the rectangles (■) are measured; the solid curve (—) is calculated by using equation 2.15; the × curve is calculated by using the size distribution derived from the power law expression, equation 2.24, assuming C = 300 and K = 0.5.

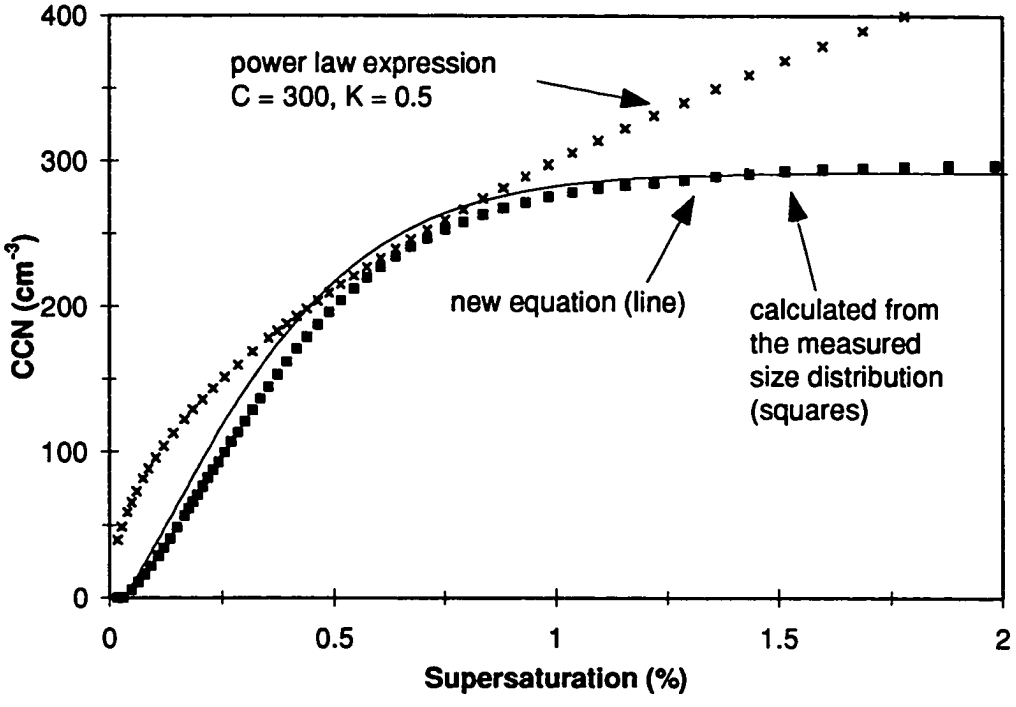

Figure 2-2 Supersaturation spectra (1): the squares (▪) are calculated form the measured bell-shaped size distribution; the solid curve (—) is calculated from the new equation, equation 2.2; the × curve is calculated by using the power law expression, equation 2.1, assuming C = 300, K = 0.5.

Usually, the power law is used to fit part of the S-shaped spectrum. To fit the entire spectrum, a new equation for CCN supersaturation spectrum is proposed. The size distribution derived from the new equation is bell-shaped size distribution. All parameters in the new equation have

clear physical meanings and are not merely empirical coefficients.

2.1.2.1 CCN supersaturation spectrum

The new equation being proposed for the CCN supersaturation spectrum is

$$N = A\,[1 - \exp(-B\,S^K)] \qquad (2.2)$$

The original idea is

(1) If the total CCN number under the bell-shaped curve is A, then as $S \rightarrow \infty$, $N \rightarrow A$.

(2) It was speculated that the power law was probably a reduced form of a more general equation, so the form BS^K was chosen. The new equation will reduce to the form of the power law formally when $S \rightarrow 0$; or, for fixed S, if B is very small, then from Taylor expansion, we can see that the equation reduces to

$$N = ABS^K$$

which is identical to Twomey's power law.

2.1.2.2 CCN size distribution

As mentioned before, by activation theory, the critical size of activated CCN depends on the supersaturation by

$$D = c/S^{2/3}$$

or $$S = (c/D)^{3/2} \qquad (2.3)$$

where c is a constant depending on the chemical composition of the CCN (e.g., Twomey, 1977). Traditionally, the unit of c is μm and S is expressed in %. Equation 2.3 states that at supersaturation S, all CCN larger than D will be activated.

The following shows how to derive the CCN size distribution from the CCN supersaturation spectrum:

First, substituting S from equation 2.3 into the new equation 2.2, we get

$$N = A \{ 1 - \exp[- B (c/D)^{3K/2}] \} \qquad (2.4)$$

where N should be the number concentration of activated CCN at supersaturation S, and correspondingly, at the critical size D. In other words, N is the number concentration of all the CCN larger than D.

Second, since the number of particles smaller than D is

$$n = A - N \qquad (2.5)$$

From equation 2.4 and 2.5, we have

$$n = A \exp[- B (c/D)^{3K/2}] \qquad (2.6)$$

Then from equitation 2.6, the derivative of n with respect to D yields the CCN size distribution

$$\frac{dn}{dD} = \frac{3K}{2} A B (\frac{C}{D})^{3K/2} \frac{1}{D} \exp[-B (\frac{C}{D})^{3K/2}] \qquad (2.7)$$

with $$\int_0^{\infty} \frac{dn}{dD}\, dD = A$$

where A is the total number concentration of CCN. B and K will be derived in the following sections.

2.2 Likelihood size distribution

Generally, the size distribution of aerosols varies so much that there is no simple parameterization to describe them. Lognormal distributions, power law expressions and exponential and gamma functions have been used with varying degrees of success (Fuchs, 1964).

Following its discovery by Whitby et al. (1971), the trimodal mass distribution has been widely observed (Whitby, 1978; Hering et al., 1981). One mass mode is usually found in the diameter range between 0.1 to 1 μm. It is the removal-resistant mode, sometimes called the "accumulation mode", that in certain circumstances may be the primary source of CCN (Jensen and Charlson, 1984). This aerosol contributes significantly to the chemical composition of rainwater, most importantly to the content of dissociated species such as sulfate, ammonium, and hydrogen ions (Junge, 1963; Charlson and Rodhe, 1982; Charlson et al., 1983; Lawson and Winchester, 1979; Duce, 1983).

Measurements show that the size distribution of aerosol in the accumulation mode tends to be bell-shaped as shown in Figure 2-1. A possible explanation comes from the removal mechanism of aerosols. The larger the particle, the faster it is removed by settling; the smaller the particle, the faster it is removed by diffusion to a larger particle or other surfaces. The result is the build up of an intermediate "accumulation" mode. Particles that are neither too large nor too small are therefore removal-resistant.

To describe the accumulation mode analytically, let us consider a highly simplified model.

2.2.1 Theory

Assumptions:

(1) The evolution of particle size is related to coagulation, which means when smaller particles collide with each other, they stick together and are therefore "removed", forming larger particles.

(2) The speeds of particles in the air are affected by perturbations in the atmosphere, such as micro-turbulence in the air or compressional waves associated with sound.

(3) The coagulation rate is related to the speed of particles in a special manner: if a particle moves fast relative to other particles, it has a better chance to

collide with other particles; and if a particle moves slowly relative to other particles, it has a better chance to be impacted by other particles.

(4) The coagulation rate is proportional to the number concentration of particles.

When air moves, the force it exerts on a small particle is given by Stokes drag

$$F = 3\pi \eta u D / C_c$$

where η is the coefficient of viscosity of air, u is the relative velocity between air and the particle, D is the diameter of the particle, C_c is the Cunningham slip correction factor. For particles with diameters smaller than 1 μm and larger than 0.1 μm:

$$C_c \approx 1 + 2.52\ \lambda/D$$

where λ is the mean free path of air molecules (e.g., Finlayson-Pitts, 1986).

Consider the acceleration of a particle due to the drag force (F), by Newton's second law of motion

$$F = \frac{d}{dt}(m\ v)$$

where m is the mass of the particle and v is the velocity of the particle, therefore,

$$3\pi\,\eta\,u\,D/C_c = m\,\frac{d}{dt}(v)$$

If the velocity of air is U, then

$$u = U - v \qquad (2.8)$$

and $$3\pi\,\eta(U - v)D/C_c = m\,\frac{d}{dt}(v)$$

or $$\omega_0\,(U - v) = \frac{d}{dt}(v)$$

with $$\omega_0 = 3\pi\,\eta\,D\,/(C_c\,m)$$

where, ω_0 can be regarded as a kind of eigenfrequency of particles, with diameter D and mass m, in the air with viscosity η.

Let $$m = \rho(\pi/6)D^3$$

where ρ is the density of the particle,

then $$\omega_0 = 18\eta\,/(\rho\,C_c\,D^2) \qquad (2.9)$$

Let $$\tau = 1\,/\,\omega_0$$

$$= \rho\,C_c\,D^2/(18\eta)$$

then τ is the relaxation time. It characterizes the time required for a particle to adjust or relax its velocity to a new condition of forces. For a given kind of particle, ρ, C_c and η can be regarded as constants, so τ is proportional to the square of the size of the particle (Figure A-1 in Appendix A.4). This means that, in responding to a

perturbation, a smaller particle will accelerate faster and reach a higher speed than a larger one. The result is that particles of different sizes tend to collide with each other, introducing an evolution in the size distribution of particles.

Let us consider a simple case, assume

$$U = U_0 \sin(\omega t) \tag{2.10}$$

and $v = 0$ at $t = 0$

solving for v gives the equation

$$v = \frac{U_0 \omega_0}{\omega_0^2 + \omega^2} [\, \omega \exp(-\omega_0 t) - \omega \cos(\omega t) + \omega_0 \sin(\omega t) \,]$$

(Appendix A.1, also see Figure A-2 in Appendix A.5).

According to assumptions (3) and (4), the change of the number concentration of particles is

$$\frac{d}{dt}(n) = - \alpha\, n\, v\, u \tag{2.11}$$

where α is a proportional factor or the "combination" factor of particles. It has the units $s\, m^{-2}$ (the reciprocal of the diffusion coefficient). It is expected to depend on some physical and chemical properties of particles, such as the surface properties of particles, the coagulation efficiency, etc. (*cf.* equations 2.25 and 2.13 below).

From equation 2.8 and equation 2.11 we can have

$$\frac{dn}{n} = -\alpha v (U_0 - v) dt$$

To solve the above equation, let us consider the microphysical process. According to the equation 2.10, the perturbation or the forcing velocity U changes periodically. In half of a period, the speed starts from 0 and increases to U_0, and comes back to 0. In the next half of the period, U changes direction and the speed changes the same way as in the first half of the period. Since the speed is the concern here, not the moving direction, we need to consider only half of a period. Figure A-2 shows an example of the change of v with time and with size during half of a period. As we can see, the speeds of large particles (small ω_0) change less than the speeds of small particles (large ω_0).

To find out how the change of v modifies n, let us consider the integral

$$\int_{n0}^{n1} \frac{dn}{n} = -\alpha \int_0^{\pi/\omega} v(U_0 - v)dt$$

where $n0$ is the initial value of n, $n1$ is the modified n after a half period π/ω, and ω is the angular frequency of the sound or the perturbation. The integral on the right hand of the equation is given in Appendix A.2. The expression is not simple. However, if ω is very large, the

integral approaches a simple form $\pi U_0^2 \omega_0 / \omega^2$ as shown in Appendix A.3. Therefore,

if $\omega >> \omega_0$

then $\ln(n1/n0) = - \pi \alpha U_0^2 \omega_0 / \omega^2$

or $n1 = n0 \exp(- \pi \alpha U_0^2 \omega_0 / \omega^2)$

Substitute ω_0 from equation 2.8 into the above equation, and we have

$$n1 = n0 \exp[-18 \pi \alpha \eta U_0^2 / (\rho C_c \omega^2 D^2)]$$

Notice that the new equation has a special form

$$n1 = n0 \exp(- \beta/D^2)$$

with $\beta = 18 \pi \alpha \eta U_0^2 / (\rho C_c \omega^2)$

During next half period, there will be

$$n2 = n1 \exp(- \beta/D^2)$$

$$= n0 \exp(-2 \beta/D^2)$$

After j half periods

$$nj = n0 \exp(-j \beta/D^2)$$

since the time now will be $t = j \pi/\omega$, we have

$$j = \omega t/\pi$$

then we get

$$n(t) = n0 \exp[- \beta \omega t / (\pi D^2)]$$

or $$n(t) = n0 \exp(- J\, t/D^2) \qquad (2.12)$$

with $$J = \beta\, \omega / \pi$$

$$= 18\, \alpha\, \eta\, U_0^2 / (\rho\, C_c\, \omega) \qquad (2.13)$$

The aging process of aerosol is characterized by the parameter J.

For particles in the accumulation mode, assume $n0 = n_0$ is a constant, then from equation 2.12, the derivative of n with respect to D is

$$\frac{dn}{dD} = 2\, n_0\, J\, t\, \frac{1}{D^3} \exp(- J\, t\, \frac{1}{D^2}) \qquad (2.14)$$

Let us call the new equation 2.14 the *likelihood size distribution of aerosol in the accumulation mode*. It is the size distribution that particles in the accumulation mode tend to reach under the influence of perturbations such as sound waves and turbulence in the atmosphere. Only a removal mechanism is considered to derive the new equation 2.14, so it is not called the maximum likelihood size distribution here.

At a given time t,

let $$H = J\, t$$

then equation 2.13 becomes

$$\frac{dn}{dD} = 2\, n_0\, H\, \frac{1}{D^3} \exp(- H\, \frac{1}{D^2}) \qquad (2.15)$$

2.2.2 Evaluation

To see whether the assumption that $\omega >> \omega_0$ is reasonable, let us calculate ω_0. Table 2-1 is a list of some properties of air and aerosols. The value of U_0 depends on the perturbation. U_0 = 0.01 m s^{-1} is used in equation 2.25. Table 2-2 shows the calculated relaxation time and ω_0 for different particle sizes. It is also shown in Figure A-1.

As an example, Let us consider the upper limit of audible sound; the frequency is ≈20,000 Hz, or $\omega \approx 1.3 \times 10^5$; it is close to ω_0 for 0.1 μm particles. Therefore, for particles larger than 0.1 μm, the assumption $\omega >> \omega_0$ holds well in the atmosphere. It is expected that the equation of likelihood distribution will agree well with measurements for particles with diameter near 0.1 μm.

Table 2-1 Some parameters used in calculations (1 atm, 20°C)

Property	**Symbol**	**Value**	**Units**
Speed of perturbation	U_0	0.01	(m s^{-1})
Viscosity	η	1.81×10^{-7}	(N s m^{-2})
Mean free path	λ	6.6×10^{-8}	(m)
Density of particle	ρ	1000	(kg m^{-3})

Table 2-2 Relaxation time of particles

Particle Diameter (μm)	C_c	τ (s)	$\omega_0 = 1/\tau$ (s^{-1})
0.02	≈ 10	3×10^{-7}	3.3×10^{6}
0.1	2.66	8.16×10^{-6}	1.2×10^{5}
1	1.17	3.59×10^{-4}	2.8×10^{3}

2.3 Relations between equations

A. The relation between the CCN size distribution and the likelihood size distribution

If $K = 4/3$, then the CCN size distribution described by equation 2.7 becomes

$$\frac{dn}{dD} = 2A\,B\,c^2\,\frac{1}{D^3}\,\exp(-B\,c^2\,\frac{1}{D^2})$$

which has the same form as the likelihood size distribution described by equation 2.15, with

$$n_0 = A$$

$$H = B\,c^2$$

By equation 2.2, the corresponding supersaturation spectrum is $N = A\,[\,1 - \exp(-B\,S^{4/3})\,]$

with $B = H / c^2$

$= J\,t / c^2$

i.e. $B = 18\,\alpha\,\eta\,U_0^2\,t\,/(c^2\,\rho\,C_c\,\omega)$ (2.16)

where an unknown parameter is the combination factor α, which is introduced in equation 2.11. We shall later estimate the value of α from measurements as shown in equation 2.25.

B. Other relations

Since $(dn)/(d \log D)$ ($\log = \log_{10}$) is more often used than dn/dD, we can change equation 2.7 to

$$\frac{dn}{d \log D} = \ln(10) \frac{3K}{2} AB\left(\frac{C}{D}\right)^{3K/2} \exp\left(-B\left(\frac{C}{D}\right)^{3K/2}\right) \qquad (2.17)$$

To find out the relation between B and the shape of the size distribution, let us consider

$$\frac{d}{dD}\left(\frac{dn}{d \log D}\right) = 0$$

which gives

$$B = \left(\frac{D_m}{C}\right)^{3K/2}$$

or

$$D_m = c\, B^{2/(3K)} \qquad (2.18)$$

where D_m is the diameter at which $dn/d\log D$ reaches the maximum or the position of the top point of the bell-shaped size distribution curve on a commonly used $dn/d\log D$ vs. D plot.

Substituting c or B from equation 2.18 back into equation 2.17, we have

$$\frac{dn}{d\log D} = const\ D^{-3K/2} \exp[-(\frac{D_m}{D})^{3K/2}] \qquad (2.19)$$

Notice that equation 2.19 is similar to the equation obtained from an "aerosol particle cloud erosion model" described by Shaw (1985c)

$$\frac{dn}{d\log r} = const\ r^{-\nu} \exp[-\frac{\nu}{2}(\frac{r_m}{r})^2] \qquad (2.20)$$

where r is the radius of aerosol, and ν is the Junge power law exponent in the initial condition of the model. The assumption is that small particles will diffuse to large particles (cloud droplets) and are thus removed.

In Junge law, $\nu \approx 3$ is expected. However, for $\nu = 2$ and $K = 4/3$, the equation 2.20 is the same as a likelihood size distribution. Of course, because the assumption behind equation 2.20 is related to diffusion, the parameter r_m has a different formula from equation 2.18

$$r_m = \sqrt{\frac{4R_c N_c kT\lambda t_c}{3\nu\eta}} \qquad (2.21)$$

where t_c is the time the aerosol-charged air mass has spent coexisting with cloud water droplets of mean radius R_c and in concentration N_c, k is the Boltzmann's constant, and T is the Kelvin temperature of the air (Shaw, 1985c, 1986).

As a comparison, for $K = 4/3$, from equation 2.18 and 2.16, we have

$$
\begin{aligned}
D_m &= c\sqrt{B} \\
&= c\sqrt{\frac{18\alpha\eta U_0^2 t}{c^2 \rho C_c \omega}} \\
&= \frac{3U_0}{c}\sqrt{\frac{2\alpha\eta t}{\rho C_c \omega}}
\end{aligned}
\qquad (2.22)
$$

Equation 2.21 shows that $r_m \propto \sqrt{t_c}$ and equation 2.22 shows that $D_m \propto \sqrt{t}$. Although derived from different physical processes, both equations show that the peak of the aerosol size distribution is proportional to the square root of time. The peak shifts to a larger particle size with time. The shifting rate depends on different physical parameters.

Because smaller particles are lost faster than larger particles in coagulation, if the coagulation rate is increased, then the peak of the size distribution will shift to a larger size faster. Equation 2.22 shows that as the perturbation speed (U_0) increases, the coagulation rate increases, and the peak of the size distribution (D_m) shifts to larger sizes faster. Similarly, if the combination factor (α) increases, then colliding particles have a higher probability of adhering, the coagulation will be more rapid, thus D_m will shift faster. If the viscosity (η) increases, then small particles follow the perturbation better and

reach higher speed, thus coagulation will be faster and D_m will shift faster. Also, if the time (t) is longer, more particles will coagulate and D_m will be larger. On the other hand, higher density (ρ) particles have larger inertia, and will not follow the perturbation well, so the coagulation will be slower and D_m will shift more slowly. Also, if the frequency of perturbation (ω) is higher, then each period is shorter and the displacements of particles are smaller, therefore particles have less chance to collide with one another, and D_m will shift more slowly. We can also see that D_m depends on the chemical composition of particles via the parameter c.

If we assume that the speed U_0 is related to the sound wave, and substitute $U_0 = s_0 C_s = s_0\sqrt{RT c_p / c_v}$, where s_0 is a coefficient related to the amplitude of pressure wave and the atmospheric pressure (e.g. Wood, 1955) and C_s is the speed of sound, into equation 2.22, then

$$D_m = \frac{3}{c} s_0 \sqrt{\frac{2\alpha \eta c_p R T t}{\rho c_v C_c \omega}} \qquad (2.22)$$

where R is the gas constant, T is the temperature of air, c_p and c_v are specific heat values at constant pressure and at constant volume respectively. Both equations 2.21 and 2.23

show that if the air temperature is higher, then the peak of the aerosol size distribution will shift faster. This can be tested by laboratory experiments.

2.4 Comparison with measurements

The example shown here is a measurement from the Mauna Loa Observatory during "clean" conditions (free troposphere). All aerosol are soluble and are potential CCN, so the supersaturation spectrum can readily be calculated.

A. Likelihood size distribution and field measurement

In Figure 2-1, the total number concentration is ≈300 cm^{-3}. Let us fit the likelihood size distribution to these data. Let A = 300, K = 4/3, and assume the particles are ammonium sulfate, so $c \approx 0.03$. Then choose B = 3.5 to fit the measurement. Figure 2-1 shows that the likelihood size distribution agrees closely with the measured size distribution. As predicted by the theory, for small particles, the new equation gives a small error. By the way, since the Scanning Mobility Particle Sizer is not accurate in the small particle range, a large uncertainty is expected.

Figure 2-2 shows that the new equation 2.2 for the CCN supersaturation spectrum agrees reasonably well with the measurement. Notice that when the size distribution is known, the supersaturation spectrum is fixed accordingly.

B. Size distribution associated with power law expression

Similarly to the derivation in section 2.1.2.2, we can find out what the size distribution should be if the power law expression, equation 2.1, is used to describe the supersaturation spectrum. The result is

$$\frac{dn}{d\log D} = \ln(10)\, C\, \frac{3K}{2} \left(\frac{C}{D}\right)^{3K/2} \qquad (2.24)$$

It looks like a Junger law.

C. Power law and measurement

In the power law expression, C is the number concentration at S = 1%. The critical size of ammonium sulfate CCN at 1% supersaturation is ≈0.03 μm, thus, almost all particles under the bell-shaped size distribution will be activated. Let us assume C = 300; K can be chosen arbitrarily depending on the supersaturation at which we want the power law expression to agree with the measurement. Let us assume K = 0.5, the size distribution calculated by using equation 2.24 is shown in Figure 2-1. In this case,

the size distribution derived from the power law expression overestimates the CCN number for both large and small particles; it underestimates for intermediate-sized particles.

The supersaturation spectrum can be calculated by integrating the particle number starting from large particles. Therefore, the power law expression will overestimate the CCN number at both low and high supersaturations. In the middle, while the underestimation cancels the overestimation at certain supersaturation, the power law expression will agree with the measurement there; in the case shown in Figure 2-1 and 2-2, it agrees with measurement at $S \approx 0.6\%$.

A change in C and K will change the slope and the position of the size distribution described by equation 2.24. This will let the power law expression agree with the experiment at different supersaturations. Figure 2-3 and 2-4 show an example when the power law expression agrees with the new equation for low supersaturations, and the corresponding size distributions agree with each other for large particles.

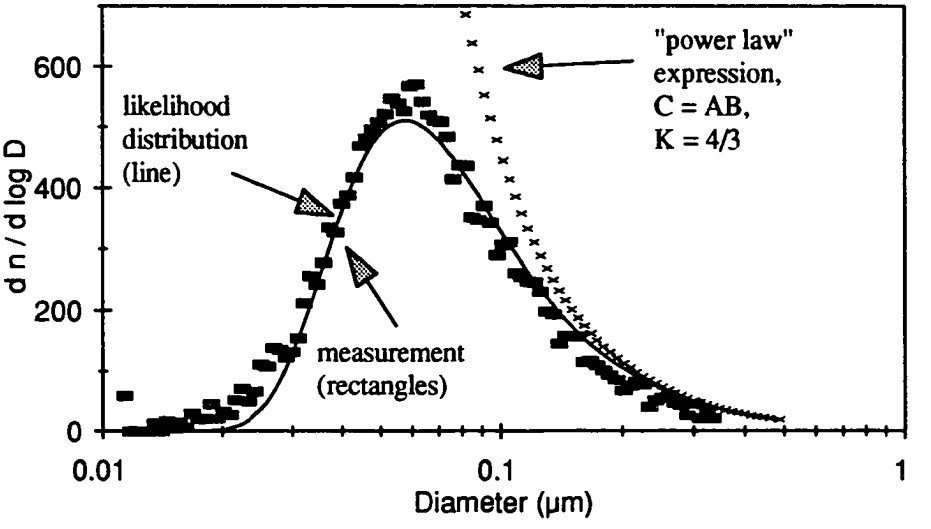

Figure 2-3 Aerosol size distributions (2): the rectangles (▪) are measured; the solid curve (—) is calculated by using equation 2.15; the × curve is calculated by using the size distribution derived from the power law expression, equation 2.24, assuming $C = AB$ and $K = 4/3$. In this case, the size distribution derived from the power law expression approaches the likelihood distribution for large particles.

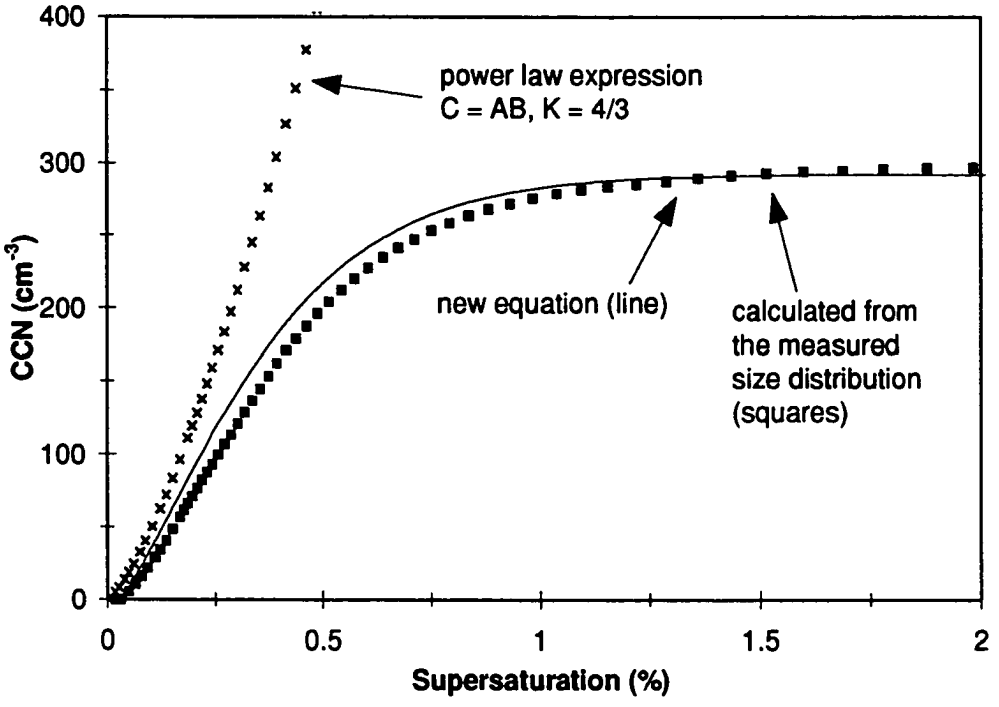

Figure 2-4 Supersaturation spectra (2): the squares (▪) are calculated form the measured bell-shaped size distribution; the solid curve (—) is calculated from the new equation, equation 2.2; the × curve is calculated by using the power law expression, equation 2.1, assuming $C = AB$, $K = 4/3$. In this case the power law expression agree with the new equation at low supersautration.

D. Likelihood size distribution and laboratory test

Notice that our likelihood distribution is time-dependent. We can test this aspect in the laboratory. Figure 2-5 is a measured result. The total particle number concentration was initially about 98,000 cm^{-3}. The aerosol was put in a large aluminized mylar bag. One hour later, the total number concentration dropped to about 50,000 cm^{-3}. The air bag can hold ≈1 m^3 of air. The gravitational settling speed of a 1 μm particle is only about 3.5×10^{-3} cm s^{-1}, so it can be ignored. Let us also ignore the wall effects, and assume the evolution of the aerosol size distribution is mainly due to coagulation caused by perturbations in the air. Let us compare the measured size distributions with the calculated likelihood distributions. Figure 2-6 shows the results calculated by using equation 2.6 with A = 98,000 cm^{-3}. $J = 0.8 \times (10^{-9})^2$ m^2 s^{-1} was chosen to fit the measurement. The calculations closely agree with the measurements.

In Figure 2-6, although the total particle number decreases to about 50% after 1 h, the total mass does not change much because it depends primarily on large particles. In Figure 2-5, there seems to be more large particles after 1 h. This is probably due to the uncertainty of measurement

in this particular case, which shows a higher total mass after 1 h.

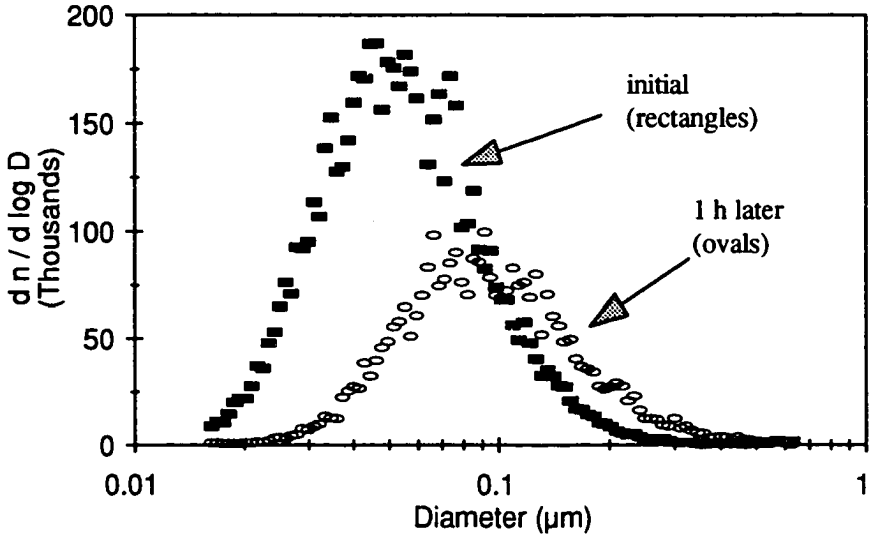

Figure 2-5 Measured size distribution of aerosol in an air bag. The initial distribution is shown as rectangles. One hour later, the size distribution changed, it is shown in ovals. The total particles number concentration dropped from 98,000 cm^{-3} to 50,000 cm^{-3}. The size shifted a little to the larger particle side.

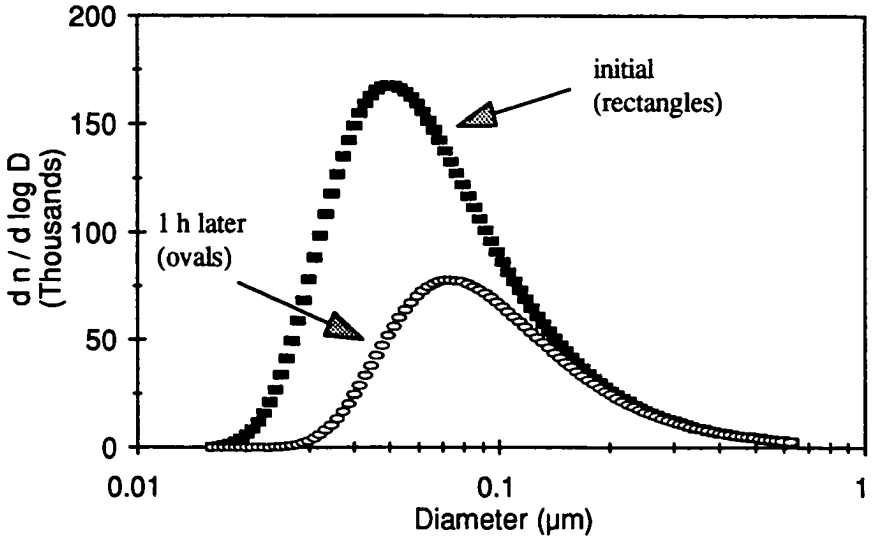

Figure 2-6 Calculated aerosol size distribution spectra by using the likelihood size distribution (compare with Figure 2-5). The initial distribution is show as rectangles. The parameters in the likelihood size distribution equation was chosen to fit the measured size distribution. The calculated size distribution for one hour later is shown as ovals. The equation considered only the removal of particles. The coagulation growth of particles was not included, so there is no increase of particle numbers at larger sizes.

The discrepancy between Figure 2-5 and Figure 2-6 may be explained by

(1) the assumptions for the likelihood distribution are highly simplified; only one possible removal mechanism of aerosol is considered, therefore, Figure 2-6 does not show an actual increase in the numbers of large particles;

(2) the initial aerosol in Figure 2-5 was not aged, so the size distribution shows more smaller particles and less larger particles than the calculated one in Figure 2-6.

A more detailed model should consider the formation of new particles, the coagulation and the condensation growth, the influence of cloud droplets, precipitation scavenging etc. (e.g., Hoppel, et. al., 1988).

E. Estimation of the "combination factor", α

From equation 2.13 and Table 2-1, we can calculate the combination factor α introduced in equation 2.11.

Let $J = 0.8 \times (10^{-9})^2 \ (m^2 \ s^{-1})$

$\omega = 10^5 \ (s^{-1})$

$C_c = 1$

then

$$\alpha = \rho \, C_c \, J \, \omega \, / \, (18 \, \eta \, U_0^2) \qquad (2.25)$$

$$= 10^3 \times 1 \times 0.8 \times (10^{-9})^2 \times 10^5 \, / \, (18 \times 1.81 \times 10^{-7} \times 0.01^2)$$

$$= 0.24 \ (s \ m^{-2})$$

2.5 Discussion

A. New equations and the power law

One important aspect of the new equation for the CCN supersaturation spectrum is that the new coefficients A, B and K have clear meanings. They can be measured and can be derived from basic physics. When the chemical composition and the size distribution of CCN are known, the supersaturation spectrum can be calculated.

The power law expression can be a reduced form of the new equation if B is very small. From equation 2.18 and equation 2.19, formally,

if $B \rightarrow 0$

then $D_m \rightarrow 0$

and $$\frac{dn}{d \log D} \rightarrow const\ D^{-3K/2}$$

which is the same as equation 2.24.

In other words, when the peak of the bell-shaped size distribution shifts to small size, or B, which is described in equation 2.16, is very small, then for $D >> D_m$, the new equation can be approximated by the power law expression with $C = AB$.

Generally, if the CCN size distribution is bell-shaped, similar to what we usually obtained in the laboratory, the

power law expression should not be used to fit the supersaturation spectrum of CCN. Because although the power law expression seems to agree with measurements at certain supersaturations as shown in Figure 2-2, Figure 2-1 shows that the agreement does not come from correct physics.

The parameter K in the new equation for CCN supersaturation spectrum seems to be a constant according to the likelihood size distribution. In the power law, K is usually called the slope of the power law; the physical meaning of K is not clear. The efforts of trying to fit K in the power law has never been succeeded. Without knowledge of the CCN size distribution, attempting to use the power law may be misleading.

B. Junge distribution

"The most striking feature of the size distribution is their almost straight-line segment extending over two orders of magnitude from 0.1 μm to 10 μm. It can be approximated by

$$\frac{dN}{d\log r} = \frac{const}{r^{\gamma}}$$

where γ is equal to about 3" (Junge, 1958). Many measurements show that γ is not a fixed number; sometimes it is larger than 4 (Lechner, et al, 1989, Hoppel, et al, 1983), sometimes it is around 2 (Parungo, et al, 1987). It

seems that γ tends to be 2 in ocean air (e.g., Gras, 1995). Some other measurements indicate that γ can be between 3/4 and 3/2 (Jiusto, 1967). One reason for this uncertainty is that the instruments did not have a high enough resolution, and researchers tried to fit the measurement results into a "law".

In the likelihood size distribution, γ seems to be 2 for large particles. Of course, according to the assumptions, the likelihood size distribution is valid only for particles in the accumulation mode. For particles larger than 1 μm, other physical processes may need to be considered.

It is mentioned by Twomey (1975):

"Particle distributions in the atmosphere are, however, far from smooth even when averaged, for they are known to exhibit behavior of the form $f(r) \equiv A\, r^{-\alpha}$ with $\alpha \sim 4$ over a portion of the range, but fall toward zero below some size which is a priori unknown. If, for example, one plots the distribution

$$f(x) = Ar^{-3}\exp(-10^{-12} r^{-2}), \qquad (x = \ln r),$$

the result is a distribution which is probably close to that of many real atmospheric particle distributions." The unit

of r is cm. The distribution mentioned by Twomey looks like the likelihood distribution.

C. Discussion of the lognormal distribution

The size distribution of particles is usually described as a lognormal distribution or a superposition of several lognormal distributions, especially in aerosol and cloud models (e.g., Ghan, et al., 1993; Dellago and Horvath, 1992). Lognormal distributions are widely used in modeling because they have statistical characteristics that are well understood; there are analytical expressions for mean, variance, and other high order moments. (Aitchison and Brown, 1957). Numerous processes have been devised that may underlie the generation of the lognormal distribution. One of them is the *law of proportionate effect*, so called by Gibrat (Crow and Shimizu, 1988).

According to Gibrat, suppose V_0 is the initial volume of a particle. If the change of the volume in the j^{th} step can be expressed as

$$V_j - V_{j-1} = \varepsilon_j V_{j-1}$$

where $\{\varepsilon_j\}$ is a set of mutually independent and identically distributed random variables and is also statistically

independent of $\{V_j\}$, then the process $\{V_j\}$ is said to obey the law of proportionate effect. Thus

$$V_j = V_{j-1}(1 + \varepsilon_j)$$

$$V_n = V_0 \prod_{j=1,n}(1 + \varepsilon_j)$$

Assuming that the absolute value of ε_j is small compared with 1, we can approximate from the Taylor expansion of $\ln(1 + \varepsilon_j)$ that

$$\ln V_n = \ln V_0 + \sum_{j=1,n} \varepsilon_j$$

By the additive central limit theorem $\ln V_n$ is asymptotically normally distributed and hence V_n is asymptotically lognormally distributed in a two-parameter form. In other words, if the volume of a particle changes randomly and proportionally to its volume, then the distribution of the volume (thus the size distribution) may become lognormal.

Unfortunately, there is no clear physical explanation why the size distribution should be lognormal. The lognormal distribution, although widely used elsewhere, is not suitable for most aerosol particle size distributions (Hinds, 1982). It is interesting to see that the likelihood size distribution derived above is not lognormal.

CHAPTER 3

A NEW CCN MEASUREMENT METHOD

3.1 Thermal diffusion chamber

To know whether a kind aerosol is cloud condensation nuclei, the aerosol must be put into a supersaturated environment. The most common method to obtain the low supersaturations found in clouds is the thermal diffusion chamber as shown in Figure 3-1. It is used in most CCN counters of static and flow designs (e.g., Twomey, 1959; Storozhilova, 1960; Laktionov, 1965; Saxena and Carstens, 1971; Judson and Squires, 1973; Sinnarwalla and Alofs, 1973; Fukuta and Saxena, 1974; Hoppel and Wojciechowski, 1976; Radke, Domonkos and Hobbs, 1981).

3.1.1 Advantages of thermal diffusion chamber

One advantage of a static plane parallel plate thermal diffusion chamber is that it produces a stable supersaturation. The theory is simple. As shown in Figure 3-2, the saturation vapor pressure can be calculated by the Clausius-Clapeyron equation. At the ceiling and bottom surfaces, the actual vapor pressure is supposed to be the

same as that predicted by the Clausius-Clapeyron equation. In between the two surfaces, the actual vapor pressure inside the chamber is expected to change linearly due to diffusion. Thus the air in the middle of the chamber will be slightly supersaturated with water vapor.

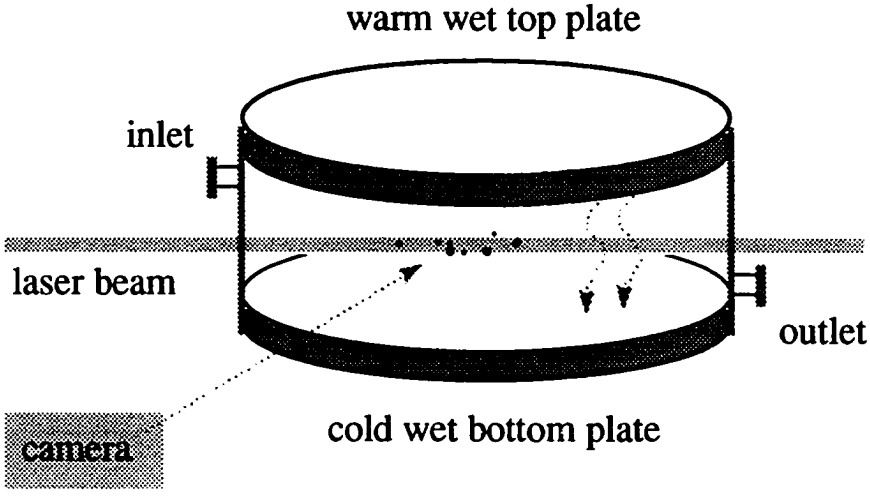

Figure 3-1 A sketch of a thermal diffusion chamber. Both the ceiling and the bottom surfaces inside the chamber are wet. Heat and water vapor are transported from the top plate to the bottom plate. The activated CCN will form droplets which fall due to the gravity. These droplets can be seen when illuminated by a laser beam.

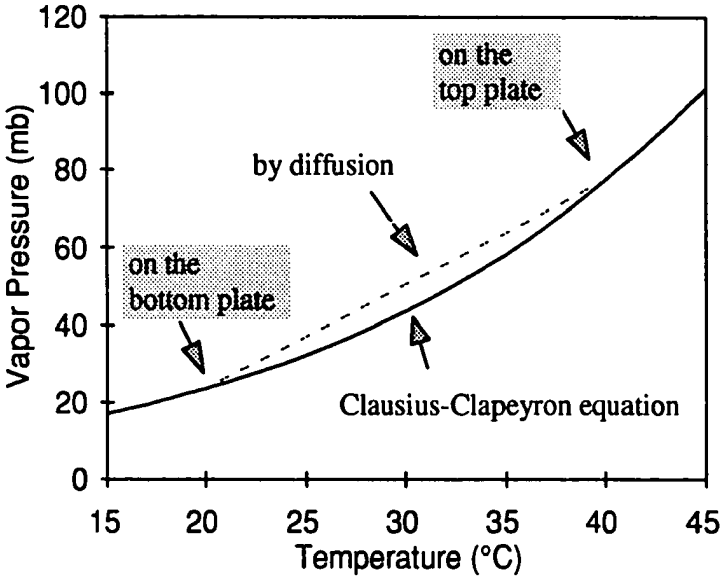

Figure 3-2 Vapor pressure in a thermal diffusion chamber. The actual vapor pressure is expected to change linearly between the top plate and the bottom plate due to diffusion.

A thermal diffusion chamber can be used as a static chamber in which the sample air does not move while measurements are taken, or as a flow chamber where the sample air flows continuously. In most of the applications the chamber is used horizontally, with the bottom plate cooler than the top plate providing a stable temperature profile.

As a comparison, another kind of chamber is the expansion chamber, which can be used to produce high supersaturation over a short time. It is seldom used in CCN counters now because the supersaturation is difficult to control, especially for the long time required for droplet growth at low supersaturations. (Miller and Bodhaine, 1982).

3.1.2 Limitations of thermal diffusion chamber

The supersaturation inside a thermal diffusion chamber is not uniform; it is zero at the plates and maximum near the chamber's central plane as shown in Figure 3-3. Due to wall effects and the possible uneven distribution of temperatures in the top and bottom plates, the supersaturation is usually not uniform horizontally either. Supersaturation reaches the maximum in the center. In a laminar flow type thermal diffusion chamber, clean sheath air can be used to carry the sample air through the chamber. With sheath air, the sample air is confined within the central plane of the chamber where the supersaturation is close to a constant.

A problem with the thermal diffusion chamber is the thermal gradient. The typical thermal gradient can be as high as $3^{\circ}C\ cm^{-1}$. In the real atmosphere, the typical thermal gradient is the dry lapse rate, which is about $1^{\circ}C$ per 100 m

or 10^{-4} °C cm^{-1}. With four orders of magnitude difference in thermal gradient, some physical process, such as thermophoresis, will be altered. Therefore, although the air in a thermal diffusion chamber is supersaturated, the micro-physical process may differ from those in the real atmosphere.

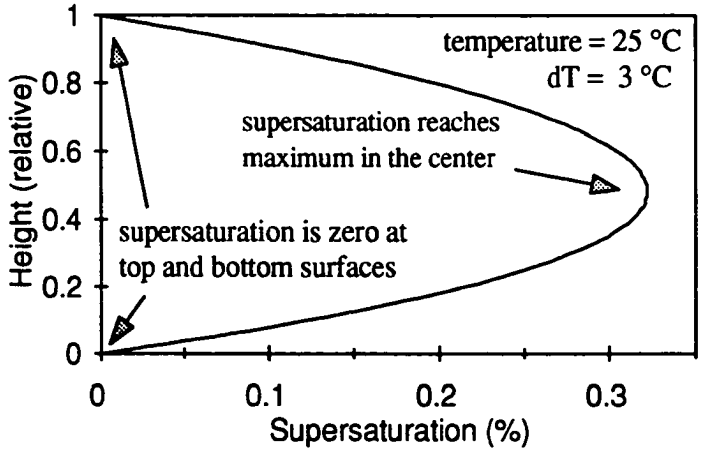

Figure 3-3 Supersaturation in a thermal diffusion chamber. If the temperature at the top plate is 25°C and the temperature difference between the top and bottom plates is 3°C, then the maximum supersaturation in the chamber is about 0.3%.

Note: the supersaturation is not symmetry above and below the mid-plane.

Another problem is that if the temperature of the sample air is lower than the temperature at the top plate of the chamber, the transient supersaturation in the chamber may cause some errors (Fitzgerald, 1970; Saxena, et al., 1970). Also, water depletion due to the removal of water vapor by droplets would lower the supersaturation in a thermal diffusion chamber.

There are other questions. For example, if a laser beam is used to illuminate the chamber, is there an influence of a high intensity laser beam on the microphysical process in the chamber? In spite of the problems discussed above, the thermal diffusion chamber remains the best tool available for achieving a relatively stable supersaturated environment.

3.2 Numerical simulation of a thermal diffusion chamber

The air in a thermal diffusion chamber is supersaturated. Unfortunately, there is no good method to measure the supersaturation in the chamber directly, so the supersaturation is calculated.

3.2.1 Thermal diffusion chamber model

Let us assume that the temperature and the density of water vapor change linearly inside the thermal diffusion

chamber from the top to the bottom due to diffusion. If we assume that the height of the chamber is H; the temperature and the water vapor density at the bottom of the chamber are $T(0)$ and $\rho(0)$, respectively, then the temperature at the height z in the chamber is

$$T(z) = T(0) + \frac{T(H) - T(0)}{H} z \tag{3.1}$$

and the density of water vapor at z is

$$\rho(z) = \rho(0) + \frac{\rho(H) - \rho(0)}{H} z \tag{3.2}$$

The saturation vapor pressure e_s obeys the Clausius-Clapeyron equation

$$e_s(z) = e_0 \exp\left[\frac{L}{R_v}\left(\frac{1}{273} - \frac{1}{T(z)}\right)\right] \tag{3.3}$$

where the unit of T is K, e_0 = 6.11 mb at 0°C (273K), $L = 2.5 \times 10^6$ J kg^{-1} is the latent heat of evaporation at 0°C, and R_v = 461 J deg^{-1} kg^{-1} is the gas constant for water vapor. From the gas law, the saturation water vapor density is

$$\rho_s = \frac{e_s}{R_v T} \tag{3.4}$$

At the top and bottom of the chamber,

$$\begin{aligned} \rho(H) &= \rho_s(H) \\ \rho(0) &= \rho_s(0) \end{aligned} \tag{3.5}$$

From equations (3.1) to (3.5), the supersaturation can be calculated as

$$S(z) = \frac{\rho(z) - \rho_s(z)}{\rho_s(z)} \tag{3.6}$$

The values of the saturation vapor density can be obtained from standard tables such as Smithsonian Meteorological Tables, Table 108, pp. 382-383 (1949).

The principle of a thermal diffusion chamber can be found in many references (e.g., Götz, 1991). It is illustrated in Figure 3-2.

According to the activation theory in a supersaturated environment all CCN larger than the critical size will be activated to form water droplets. The critical size, r_c, is related to the supersaturation by

$$r_c = \frac{const}{S^{2/3}} \tag{3.7}$$

where *const* is a constant depending on the chemical composition of the CCN (Towmey, 1977).

The air in a thermal diffusion chamber is supersaturated everywhere, so the droplet will keep growing. Because the CCN are very small, when droplets are formed, they soon become dilute solutions. For a droplet with radius r, the growth of a droplet can be estimated by

$$r\frac{dr}{dt} = G\,S \tag{3.8}$$

where G may be considered a constant for a given environment at a fixed temperature (Wallace and Hobbs, 1977).

All particles in the atmosphere fall due to gravity. If there is no turbulence in the air, the falling speed for small particles can be calculated by the Stokes' relation

$$v = \frac{2\,r^2\,\rho_d\,g}{9\,\eta} \tag{3.9}$$

where ρ_d is the density of the droplet, g = 9.81 m s^{-2} is the acceleration due to gravity at the surface of earth, and η is the viscosity of the air.

By using equations 3.6 to 3.9, the growth and the trajectory of the droplet can be estimated in a thermal diffusion chamber. The Quick Basic program is listed in Appendix C.1.

Figure 3-4 shows some calculation results. The sample air is supposed to be injected into the chamber at different initial heights. The CCN size is 0.072 μm; the maximum supersaturation is about 0.3%. In the center part of the chamber, where the supersaturation is high, CCN will activate and form droplets. Most of the droplets will fall to the bottom of the chamber within 20 s. CCN in the upper half of the chamber may also fall into the high

supersaturation zone and be activated if given a long enough time. This result agrees with observations.

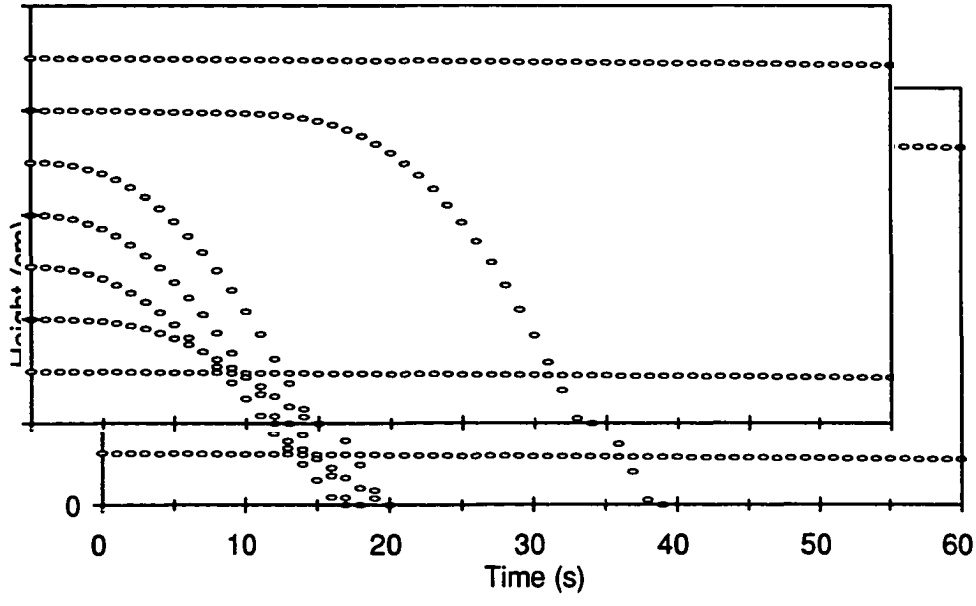

Figure 3-4 Trajectory of activated CCN in a thermal diffusion chamber. S = 0.3%, CCN diameter = 0.072 μm. All particles will fall due to gravity. Bigger droplets fall faster.

Figure 3-5 shows the change in droplet size as a function of time. It indicates that a droplet can grow to a few microns when it reaches the bottom of the chamber.

For some thermal diffusion chambers, observations show that there may be a "Plateau" (Hudson, 1972, 1976). This means that the number concentration of droplets in the laser

beam will stay relatively constant for a while, this allows stable counting of the droplets. Our static CCN counter does not show a good plateau. The following simulation demonstrates what happens in the chamber.

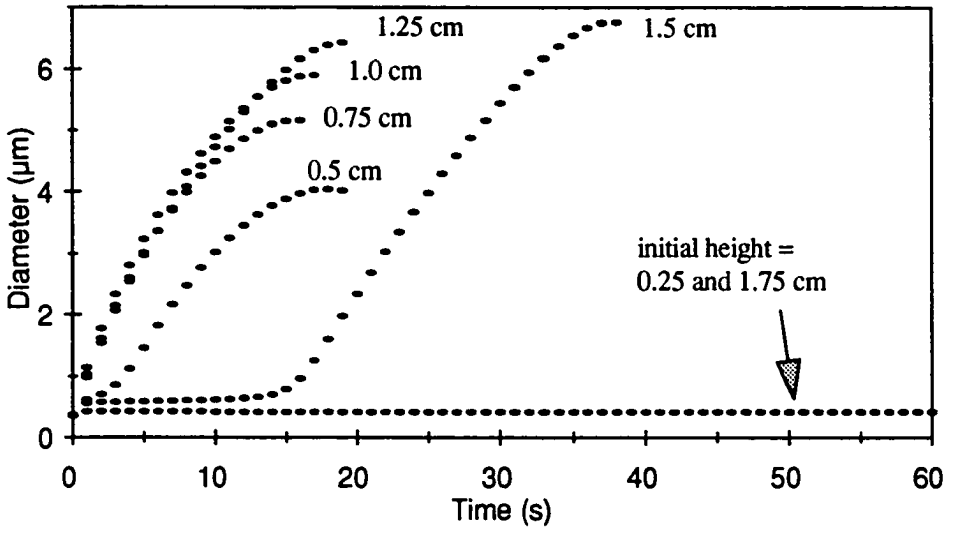

Figure 3-5 Evolution of droplet diameters in a thermal diffusion chamber. The trajectories are shown in Figure 3-4. Initial heights of particles (droplets) are labeled.

A. counting efficiency for CCN of different size at a fixed supersaturation

By using the CCN chamber model, we can calculate the time when a droplet falls into the laser beam, as well as how large it is. Thus, we can estimate how many droplets may

be counted. Figure 3-6 is a simulation result for a static CCN counter, assuming the CCN are monodisperse and S = 0.3%. For the calculation, the upper half of the chamber is divided into 500 layers, the laser beam is 1 mm wide, the threshold for the camera is 0.5 μm, exposure = 1 s, and

$$counting\ efficiency = \frac{droplet\ number\ seen\ in\ the\ beam\ (cm^{-3})}{CCN\ number\ (cm^{-3})}$$

If a CCN counter works perfectly, the counting efficiency should be 1.

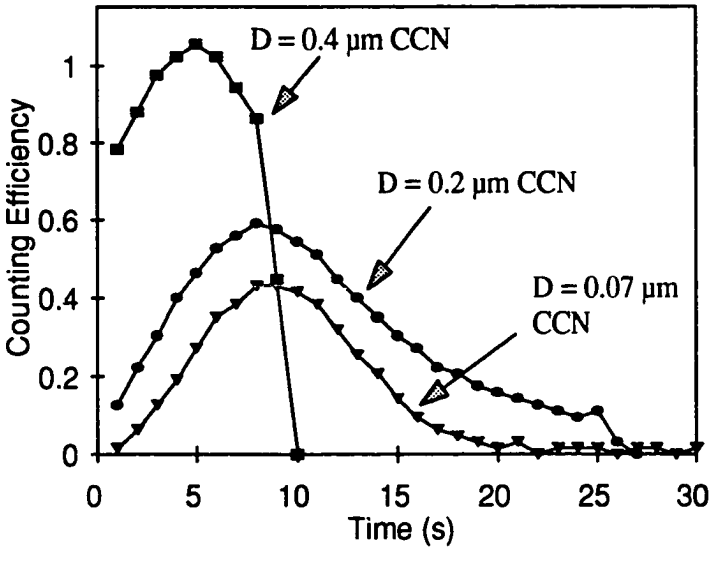

Figure 3-6 Simulated counting efficiency of a CCN counter; at supersaturation 0.3%, for different CCN diameter D. The smaller the CCN, the lower the maximum counting efficiency and the later it happens.

The result shows that, after the chamber is flushed with the sample air, the number concentration of droplets in the laser beam will reach a maximum within a few seconds. The maximum does not last long, so there will be a small "hill" instead of a "plateau." This illustrates that the smaller the CCN size, the lower the counting efficiency of the instrument, suggesting that the CCN counter will be influenced by the size distribution of CCN. The implication is that even if two air samples have exactly the same number of CCN larger than a critical diameter, a CCN counter will give different counts if the size distributions vary.

B. counting efficiency for CCN of a fixed size at different supersaturations

In Figure 3-7, the counting efficiency is calculated for fixed particle sizes but for different supersaturations. The result shows that the higher the supersaturation, the higher the counting efficiency. This agrees with the results from laboratory tests discussed in chapter 2. The simulation may not be very accurate however because the water depletion and other effects were not considered. In short, there seems to be no simple way to accurately relate the number concentration of droplets to the number concentration of CCN.

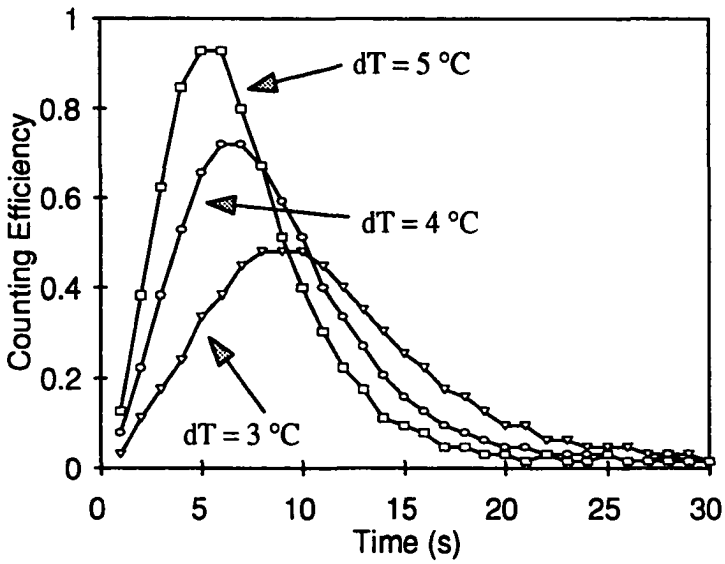

Figure 3-7 Simulated counting efficiency of a CCN counter; the diameter of CCN is 0.1 μm, for different dT, which is the temperature difference between the top and the bottom plates of the thermal diffusion chamber. The supersaturation is about 0.3% when dT = 3°C, and about 1% when dT = 5°C.

3.2.2 Additional problems with static CCN counters

The fallout of droplets in a static chamber imposes difficulties in detection and counting, because particles constantly fall into and out of the laser beam. In a flow type chamber, the fallout of droplets limits the time they remain in the chamber. Thus, small droplets may not have

time to grow large enough to be seen and large droplets may be lost before they can be counted. In a vertical chamber, particles fall but do not fall out. However, the falling speeds are not the same for different particle sizes, so there are still difficulties.

Since all activated CCN compete for water vapor, water depletion can be a problem, especially at high number concentration and in a static chamber, where the droplets outside the laser beam also consume water vapor.

A numerical simulation (Alofs and Carstens, 1975) indicates order of magnitude of uncertainty in the count at 0.1% supersaturation, and a factor of 2 uncertainty at 1.0% supersaturation. Another simulation also indicates a substantial underestimate of the actual CCN concentration (Hoppel and Wojeciechowski, 1976). Radke and Jiusto (1977) assert that "However, because the mutual agreement between the static chambers, horizontal and vertical continuous flow chambers, and isothermal haze chambers has generally been remarkably good these predictions of very poor absolute accuracy must be discounted." Nevertheless, there has been no very reliable absolute calibration of the CCN counters.

Our calibration by using the Scanning Mobility Particle Sizer (SMPS) shows that our CCN counter underestimates the

CCN concentration compared to prediction by activation theory.

3.3 A New CCN measurement method

To improve the CCN instrument, one may use a larger chamber, a wider laser beam, a more sensitive camera, and improve the image processing software. All of these are related to taking pictures of droplets which, unfortunately, does not guarantee getting the CCN number concentration correct.

After watching the formation and growth of droplets in a thermal diffusion chamber, it was natural to wonder why not simply let the droplets fall out and measure the particles left behind. It is obvious that the experiment could not have been possible before the development of new instrumentation, such as the fast scanning mobility particle sizer.

3.3.1 CCN Remover

A new method is suggested in which the thermal diffusion chamber simply becomes a "CCN Remover." As shown in Figure 3-8, the sample air is introduced into the Remover between the clean sheath air. Activated CCN (droplets) will fall out of the sample air flow. The side wall of the

prototype of the CCN Remover is made of clear glass, so we can see the droplets falling by shining a laser beam into the chamber. By introducing smoke to the sample air, it was possible to visually confirm that the air flow was laminar and remained in the center of the chamber as shown in Figure 3-8.

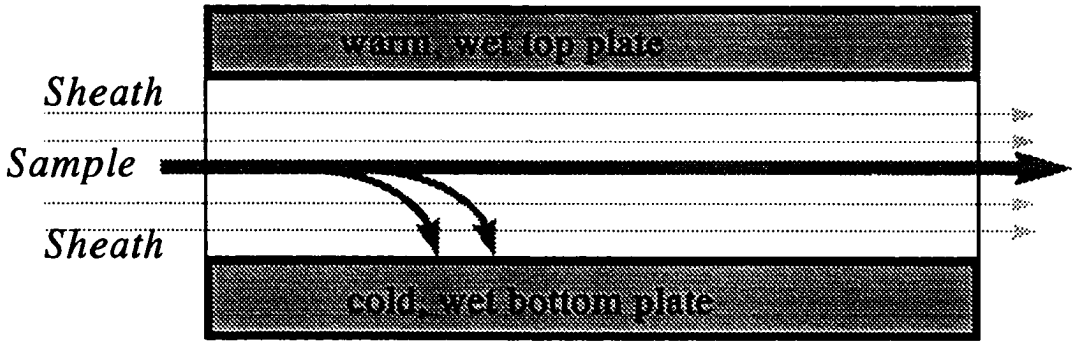

Figure 3-8 A side view of the CCN Remover. The sample air is injected in the center between clean sheath air. Activated CCN fall while particles not activated pass though the chamber.

Because there is no need to take photos of droplets in the CCN Remover, it removes not only activated droplets but also some difficult assumptions and problems that affected the CCN counting method. For example, the problems related to the illumination light, the camera system and the

corresponding data processing algorithm, etc. The sample air can remain in the chamber longer to let droplets grow and fall.

The CCN Remover can be regarded as an add-on to a particle sizing system, which measures the particle size distribution. The difference in size distributions before and after CCN are removed is expected to be the size distribution of CCN. The supersaturation spectrum of CCN can be obtained by scanning the supersaturation inside the CCN Remover.

3.3.2 Advantages of the new method

Figure 3-9 shows a set-up of a CCN Remover with a TSI Scanning Mobility Particle Sizer (SMPS). Depending on the air flow rate in the chamber, the sample air can stay in the chamber for several minutes. This is much longer than the typical 30 s in the old CCN counter. This will give the CCN more time to activate and grow. Also, since the sheath air is particle-free, water depletion is less of a problem. It is expected that this new method can measure CCN more accurately than our old CCN counter.

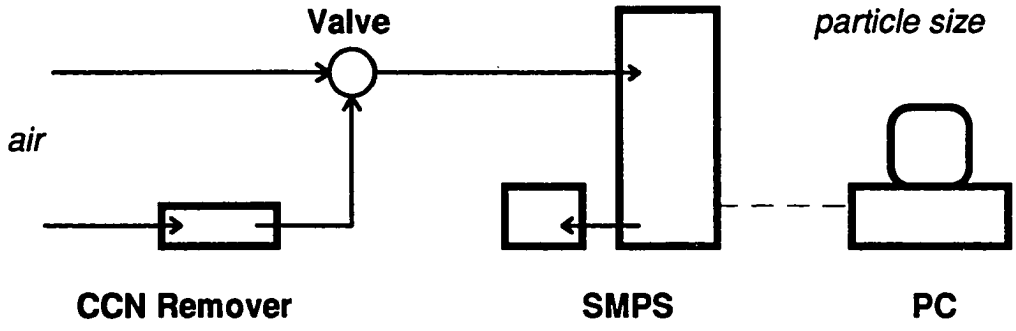

Figure 3-9 A setup of the new aerosol and CCN measurement system. The scanning mobility particle sizer can measure particle sizes and the number concentration before and after the CCN Remover.

A distinct advantage of the new system is that the size distribution of aerosols is measured. As we can see, the size distribution offers much more information about the aerosol than the total number concentration.

3.3.3 Evaluation

Temperature and water vapor reach equilibrium by diffusion in the chamber within a few seconds. In an ordinary CCN counter, droplets can be seen within 30 s (e.g., Bigg, 1986). Since the sample air remains in a CCN Remover for more than 60 s, equilibrium is achieved.

To estimate the diffusion loss of particles to the walls of a chamber, let us estimate how long it takes a particle to travel from the center of the chamber to the top or bottom surfaces of the chamber by diffusion. The mean square displacement of particles by diffusion is (Reist, 1984)

$$s^2 = 2\,D\,t$$

Assume s = 1 cm. For a spherical particle with a diameter of 0.01 μm, the diffusion coefficient D at normal temperature and pressure is 5.24×10^{-4} $cm^2 s^{-1}$ (e.g., Hinds, 1982). Therefore

$$t = \frac{s^2}{2\,D}$$

$$= 954 \text{ s}$$

$$= 16 \text{ min}$$

This estimation illustrates that the diffusion loss of particles to the wall of the chamber is not a problem inside the chamber. The problem will be at the inlet and outlet of the chamber, where the tube diameter is smaller.

Let us estimate whether a small particle can be lost by diffusion to large droplets. Assume the number concentration of droplets is 1000 cm^{-3}, then the distance between droplets is about $s' = 1/(1000)^{1/3}$ cm, or 0.1 cm. Similar to the estimation above, for a 0.01 μm particle to travel 0.1 cm,

it takes about 10 s. In 10 seconds, due to gravity, a 1 μm droplet will fall about 0.035 cm. This means that small particles have a chance to be captured by large particles. Since the new method measures the size distribution of aerosols, the diffusion loss of particles is measured directly.

When a temperature gradient is established in a gas, the aerosol particles in that gas experience a force in the direction of decreasing temperature. The motion of the aerosol particles that results from this force is called thermophoresis. All particles in a thermal diffusion chamber with the cold plate at the bottom will be pushed down by thermophoresis. The microphysical process is complex. Thermophoresis may play a role in the colliding of small particles with larger droplets (e.g., Hinds, 1982, Talbot, et al., 1980).

In a thermal diffusion chamber, a droplet must fall about a centimeter within a minute to be removed, which means that the droplet must increase in size to a few microns. This indicates that the CCN Remover is not expected to work well for very low supersaturation, in which case particles may not grow fast enough to be removed. Also, the particles close to the critical size need more time to activate and grow, so they may not be removed efficiently.

The result is a blurring of what otherwise would be a sharp decrease of particle number for particles larger than the critical size as predicted by the theory after using the CCN Remover.

Previous research shows that the effect of the vertical walls on the supersaturation inside a thermal diffusion chamber is reduced when a linear temperature gradient is maintained on these walls instead of an isothermal condition (Tomlinson and Fukuta, 1979). Compared to our old CCN counter, the thermal diffusion chamber of the CCN Remover has a much larger aspect ratio, and the sample air is far from walls. Thus, the wall effect is limited.

3.4 Discussion

Activation theory predicts that all CCN larger than critical size will be removed, and no particles smaller than critical size will be removed. However, there are two complications: (1) Some fraction of particles smaller than the critical size may be removed by diffusion or micro-turbulence. (2) Some of the larger particles may not fall sufficiently far to be removed, as discussed above. The two complications have opposite effects: one of them lets the Remover remove more aerosol than theoretically predicted; the other one lets the Remover remove less aerosol than

theoretically predicted. Since the size distribution of aerosol is measured, the effects can be seen directly.

The CCN Remover is relatively simple and inexpensive to build, as it relies on a commercially available particle sizing system. It eliminates many of the problems found with static counters. The new CCN measurement method is still in a state of development. Nevertheless, the new CCN measurement system is not simply a new CCN counter, nor is it just a new CCN spectrometer; it also provides important information about the size spectra of the cloud condensation nuclei. This in turn provides insights into the solubility of the particles. It provides a number of new possible research directions in studying the relationship between clouds and climate.

CHAPTER 4

MEASUREMENTS

"Never tear a page off the lab notes." - Glenn Shaw, April 1994.

4.1 Why more measurements?

"Dr. S. Twomey and other pioneers have been studying and measuring CCN for decades; what else is left for you to do?" This is a scary question posed by on of my fellow students. However, computer-controlled new instruments can produce vast amounts of data very rapidly nowadays. These data can help us to see the behavior of aerosol much better than ever before.

The aerosol instruments available for this project are listed in Table 4-1. A Scanning Mobility Particle Sizer, a CCN Counter (the old one in our laboratory, static thermal diffusion chamber type) and a Condensation Nucleus Counter were used in the preliminary measurements. Our Condensation Nucleus (CN) Counter uses butanol as working fluid and can count all particles larger than 0.02 μm. Those particles

counted by the CN counter are called CN. CCN is a subset of CN.

Table 4-1 List of instruments

Instrument	**Manufacture and Model**	**Purpose**
condensation particle counter [1]	TSI* 3020 TSI 3010	number concentration of condensation nuclei
differential mobility particle analyzer (DMA)	TSI 3071	separate aerosols as a function of size
scanning mobility particle sizer [2]	TSI 3934	size distribution of aerosol
CCN counter	DH** M1	CCN number concentration
CCN Remover (an add-on to a particle sizer)	Geophysical Institute UAF	number concentration and size distribution of aerosol and CCN

[1] abbreviated to CPC, uses butanol as working fluid

[2] abbreviated to SMPS, composed of a CPC and a DMA

* TSI Incorporated, 500 Cardigan Road, P. O. Box 64394, St. Paul, MN 55164

** DH Associates, 6633 E. Koralee, Tucson, AZ 85710

Table 4-2 List of preliminary measurements

Episode	**Location and Date**	**Instrument**	**Description**
Alaska winter	Ester Dome, AK Feb. to May 1993, Nov. 1993 to Mar. 1994	CCN, SMPS	there are three typical cases: 1. local pollution 2. Chinook 3. Arctic haze
Alaska summer	Ester Dome, AK Sept. and Oct. 1994	CCN, SMPS	later summer aerosols
marine boundary layer air	Kapoho, Hawaii April 1994	CCN, SMPS	double-peak size distributions
free troposphere	Mauna Loa, Hawaii April 1994, May 1995	CCN, SMPS	bell-shaped size distributions
laboratory		CCN, SMPS, CCN-Remover	supersaturation spectrum, size distributions

The preliminary measurements were taken mainly in Alaska and Hawaii. Some laboratory measurements were conducted to calibrate and test the instruments. Limited information about the chemical composition of aerosol was obtained by heating-tube tests, which had been calibrated in the laboratory with known salts. Sulfates and organic materials evaporate at 300°C; sea salts evaporate at much higher temperatures. Some meteorological data were acquired from Japanese weather maps (Japan Meteorological Agency, Tokyo, Japan) to help interpret the measurements. Some data are briefly summarized in Table 4-2. Selected examples are discussed in the following sections. All data are shown in corresponding local time.

4.2 Alaska

Figure 4-1 is a map of Alaska. Fairbanks lies in the Tanana flats in the center of the State between two major mountain ranges. The Alaska Range is located approximately 150 km to the south of our laboratory in Fairbanks; the Brooks Range is to the north. Most Alaskan data were taken on Ester Dome (64°53'N, 148°03'W, 715 m above sea level). Ester Dome is a hill located at the southern edge of the Yukon-Tanana Uplands north of the flood plains of the Tanana River flood plain. Ester Dome is approximately 10 km west of

Fairbanks, and about 550 meters above the flood plain of the Tanana river system. The Ester Dome Observatory was described by Shaw (1983b).

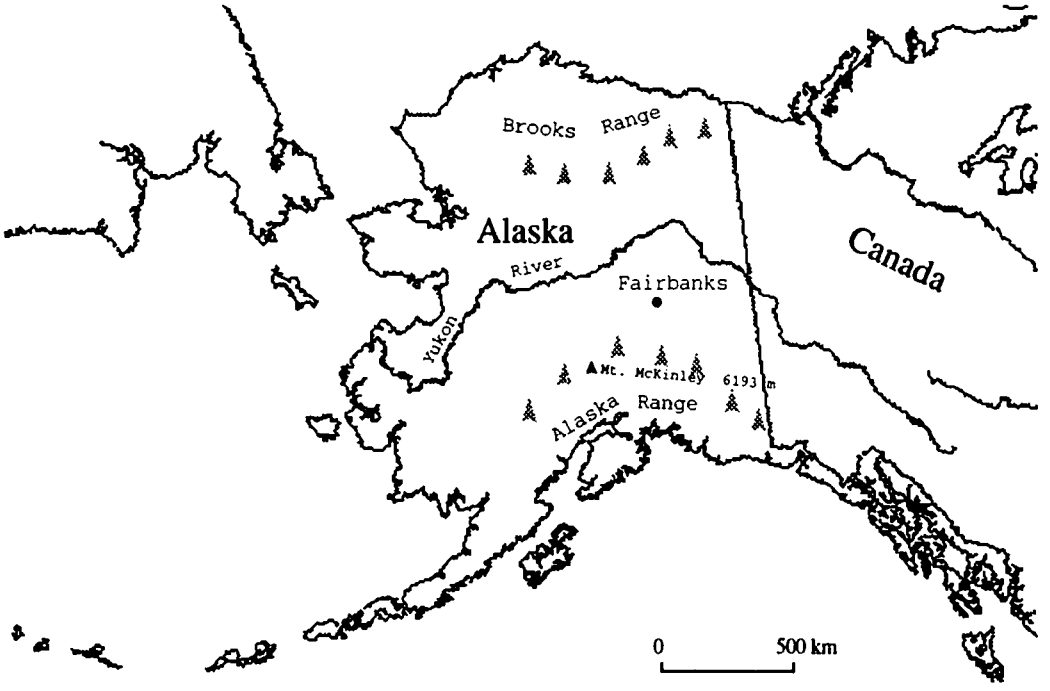

Figure 4-1 Map of Alaska showing location of Fairbanks in the center of the State and between the Brooks Range and the Alaska Range.

4.2.1 Ester Dome, winter

The local winter air pollution in Fairbanks is due to the persistence of intense ground-based inversions through the hours of maximum release of pollutants near the surface (Bowling, 1986). When we took measurements from the roof of the Geophysical Institute, we saw large amounts of particles and CCN during rush hours. Since Ester Dome is several hundreds meters above the city, we saw less pollution there.

The arctic airmass, which sometimes contains Arctic Haze, has been studied extensively by Shaw (1983b; 1985a; 1988; 1989). The measurements from our new aerosol instruments agree well with the previous results. A few typical cases are used here demonstrate how CCN number concentrations can be calculated from measured size distributions of aerosols.

The first case is for aerosols found during Chinook conditions. As shown in Figure 4-2, airflow from the south passing over the Cost and Alaska Ranges brings warm and relatively dry air to Interior Alaska. During a Chinook, when the air passes over the Alaska Range, precipitation washes out many large aerosols from the air.

The measurement made on December 9, 1993 is an example. The prevailing wind came from the south. The particle number concentrations were quite low as shown in Figure 4-3. After

15:00, the total particle number concentration in the 0.01 to 0.6 μm range was only about 200 cm^{-3}. This was a typical Chinook event. A size distribution spectrum at 20:00 is shown in Figure 4-4. It shows that large particles were essentially missing. The number concentration of particles larger than 0.03 μm was about 50 cm^{-3}. The supersaturation in the CCN counter was 1%, so it should have activated all particles larger than about 0.03 μm. Figure 4-3 shows that the CCN measurement seems to agreed with the theoretical estimation.

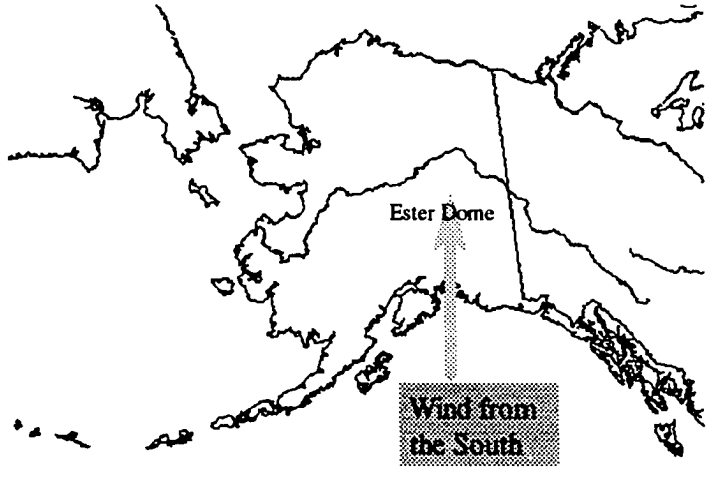

Figure 4-2 Wind is from the south during a Chinook event.

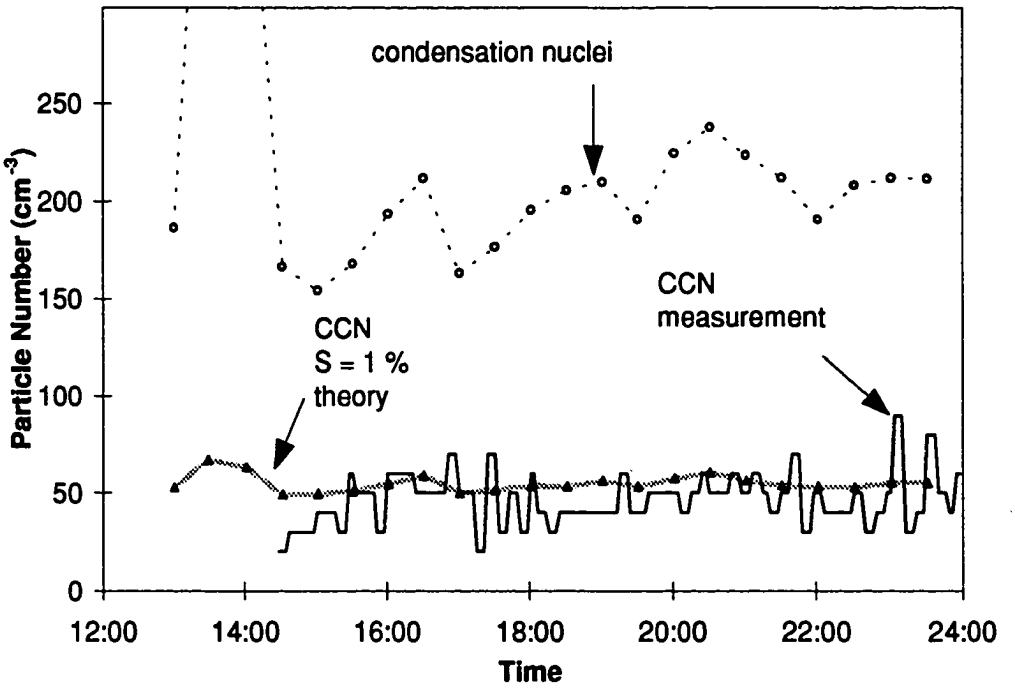

Figure 4-3 Particle number concentrations on December 9, 1993 during Chinook flow. The condensation nuclei are particles in the 0.01 to 0.6 μm range measured by the SMPS. The theoretical CCN are particles larger than 0.03 μm. The critical supersaturation for 0.03 μm $(NH_4)_2SO_2$ particle is 1%. The CCN measurement is measured by a CCN counter; the supersaturation was set to 1%.

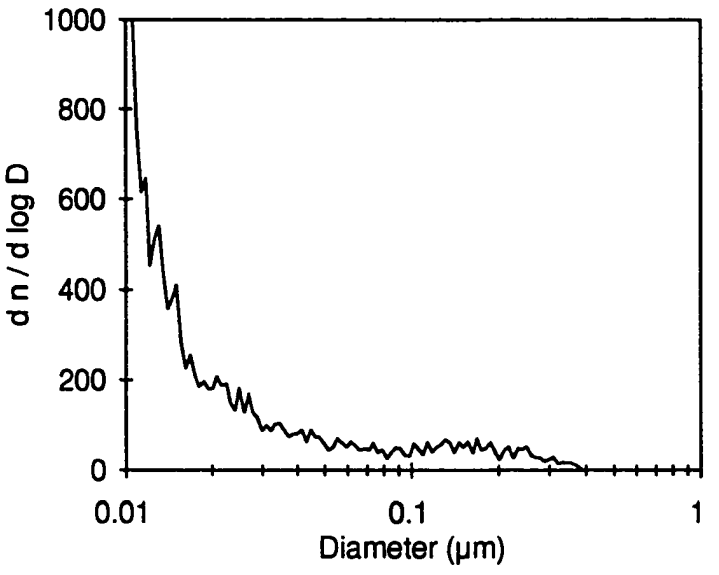

Figure 4-4 An aerosol size distribution measured during a Chinook event at 20:00 on December 9, 1993, Ester Dome Observatory, Fairbanks, Alaska. Large particles were washed out during air flow over the Alaska Range.

From the data collected during the Chinook event we can see that for this particular case:

(1) If the number concentration of particles is very low and the supersaturation is very high, then the CCN counter will count CCN particles correctly.

(2) It appears that during Chinook conditions we can estimate the CCN number quite accurately from the measured size distribution spectrum of the aerosols. This implies

that the particles consist mainly of soluble salts and the Köhler theory applies.

The second case is for polluted air. Figure 4-5 shows the particle number concentrations at Ester Dome on February 14, 1994. The total CN number was variable, but the CCN number at S = 1% was relatively constant at ≈100 cm^{-3}. A Size distribution for this episode is shown in Figure 4-6 which is for a period when CCN measurements agree with theoretical estimations. We can see a large particle mode and there are not many small particles. This is the typical Arctic Haze size distribution; the peak of the large particle mode is at 0.2 μm (Shaw, 1985b; 1984; 1983b; Staebler, et al., 1994). Figure 4-7 is a period when CCN measurements do not agree with theoretical estimates. The disagreement seems to be caused by the presence of a large number of small particles, which may be due to local pollution. Apparently some substantial fraction of these particles are either insoluble or have hydrophobic surface films that prevents their activation. Another reason is that the counting efficiency of the CCN counter is low for particles smaller than 0.1 μm.

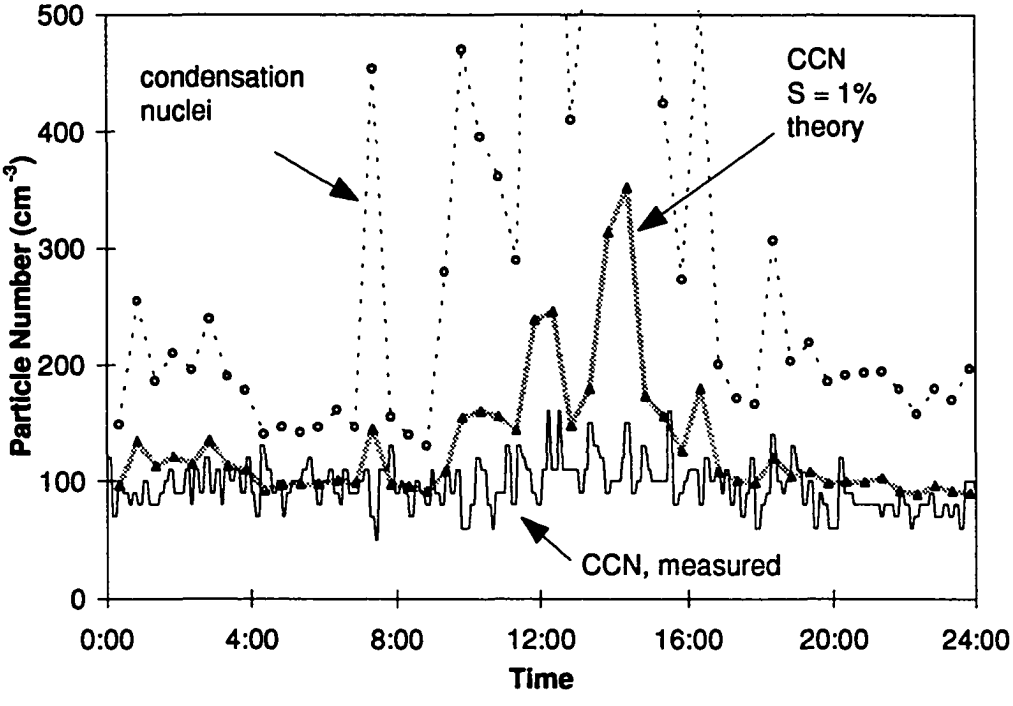

Figure 4-5 Particle number concentrations on Ester Dome on February 14, 1994. The condensation nuclei represents particles in the 0.01 to 0.6 μm range measured by the SMPS. The theoretical CCN at S = 1% are particles larger than 0.03 μm. The critical supersaturation for 0.03 μm $(NH_4)_2SO_2$ particle is 1%. The CCN measurement is measured by a CCN counter; the supersaturation was set to 1%.

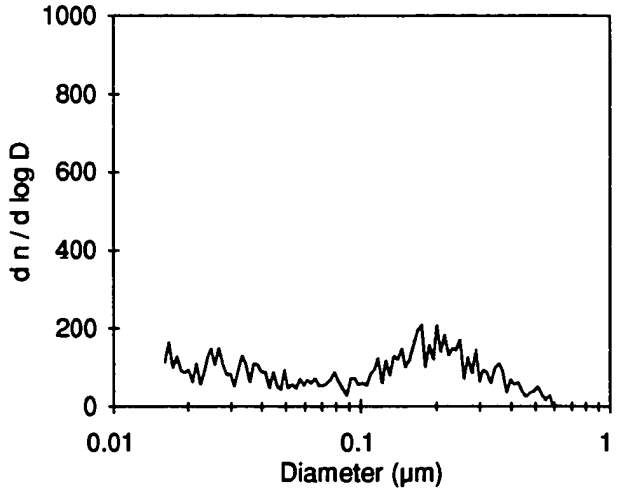

Figure 4-6 A size distribution measured on Ester Dome at 04:20 on February 14, 1994. Arctic haze.

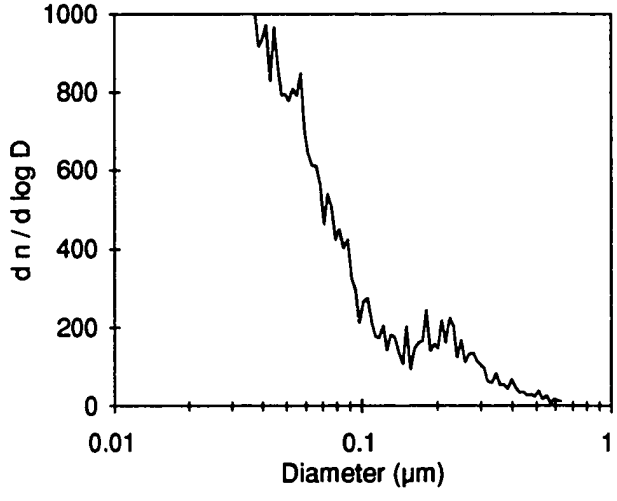

Figure 4-7 A size distribution measured on Ester Dome at 12:20 on February 14, 1994. The large particle mode at 0.2 µm was due to the Arctic haze. The particles smaller than 0.1 µm were probably local pollution.

4.2.2 Ester Dome, late summer

The air in Alaska during summer and autumn is often assumed to be clean because at this time of the year Arctic Haze contamination is at its minimum. Nevertheless, particle number concentration can be quite high. The following examples were taken in September, which was near the end of the summer season.

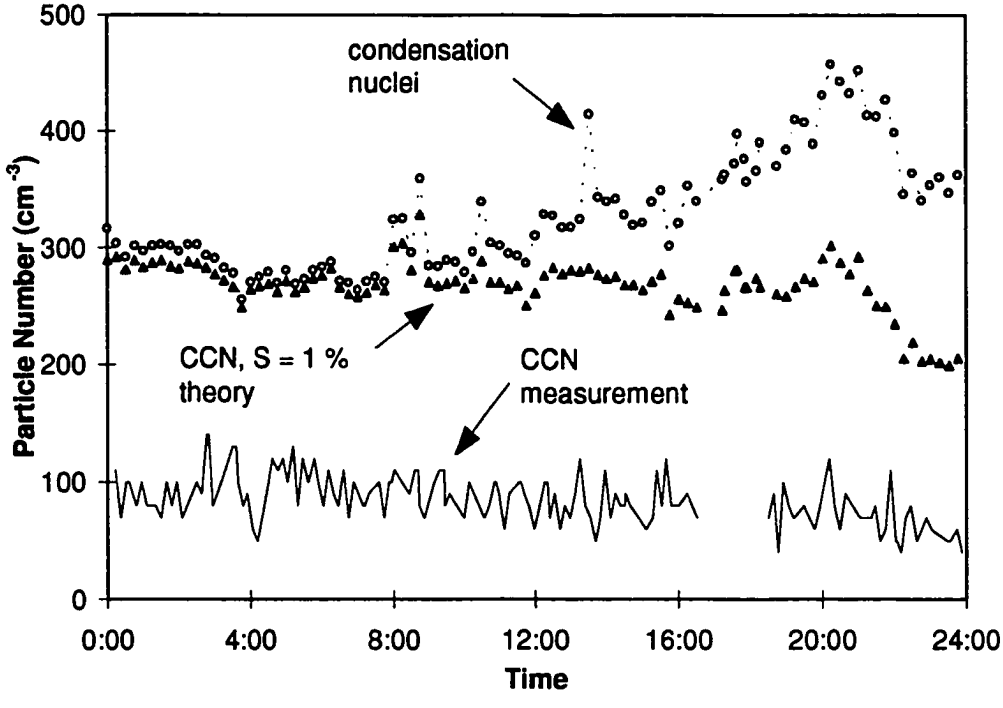

Figure 4-8 Aerosol number concentrations measured on Ester Dome, September 15, 1994. The condensation nuclei number concentration was about 300 cm^{-3} (circles).

Figure 4-8 shows the measurement on Ester Dome on September 15, 1994. In the early morning, the air was clean. The number concentration of condensation particles in the 0.015 to 0.7 μm range was about 300 cm^{-3}. A size distribution is shown in Figure 4-9. If we assume that all particles are soluble salts, then almost all of them should be activated at S = 1%, but the CCN counter counted only about 1/3 of the total particle number.

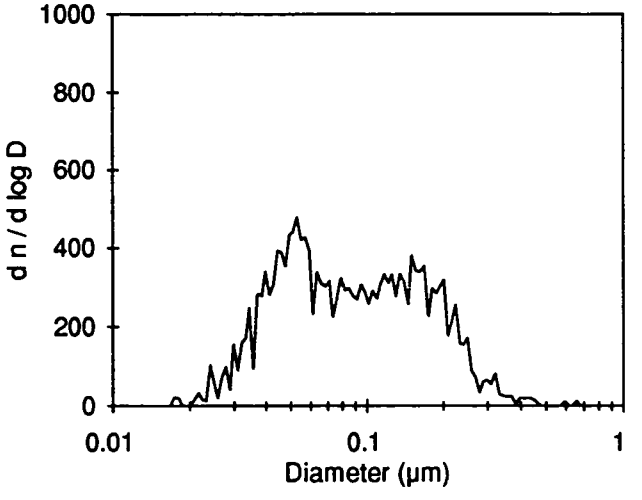

Figure 4-9 An aerosol size distribution measured on Ester Dome at about 0:30, September 15, 1994.

Compared to the size distribution in the morning, there were more small particles in the afternoon. A heating test showed that if the sample air was heated to 300°C, the total CN number dropped from 400 cm^{-3} to 100 cm^{-3}. Therefore, about 3/4 of the aerosols were volatile. The size distributions before and after the air was heated is shown in Figure 4-10. Most of large particles were volatile at 300°C. It is not clear whether they were all CCN or not.

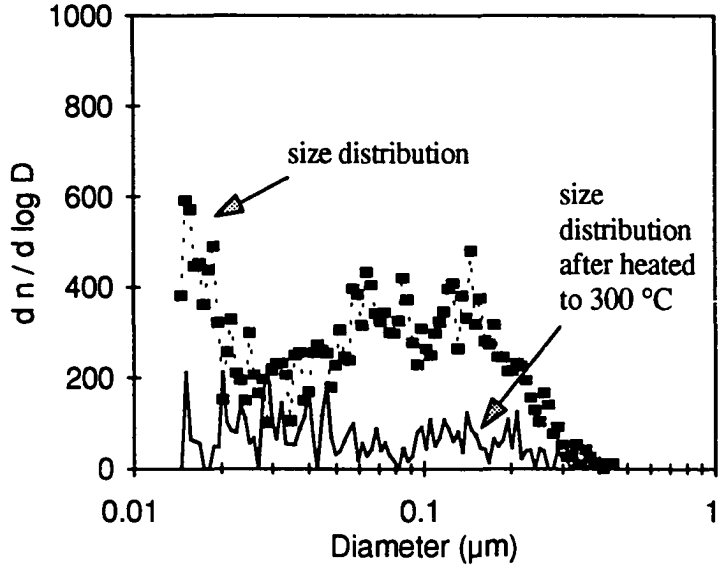

Figure 4-10 Aerosol size distributions measured on Ester Dome at 17:40, September 15, 1994. When the sample air was heated to 300°C, about 3/4 of the particles were disappeared (line).

Particles in the 0.3 to 5 μm range were also measured by a portable aerosol sizer, which is an optical instrument manufactured by Met One (Corvalis, Oregon). Figure 4-11 shows that most particles of all sizes were volatile at 300°C. If assume they were sulfate compounds then they could all be CCN.

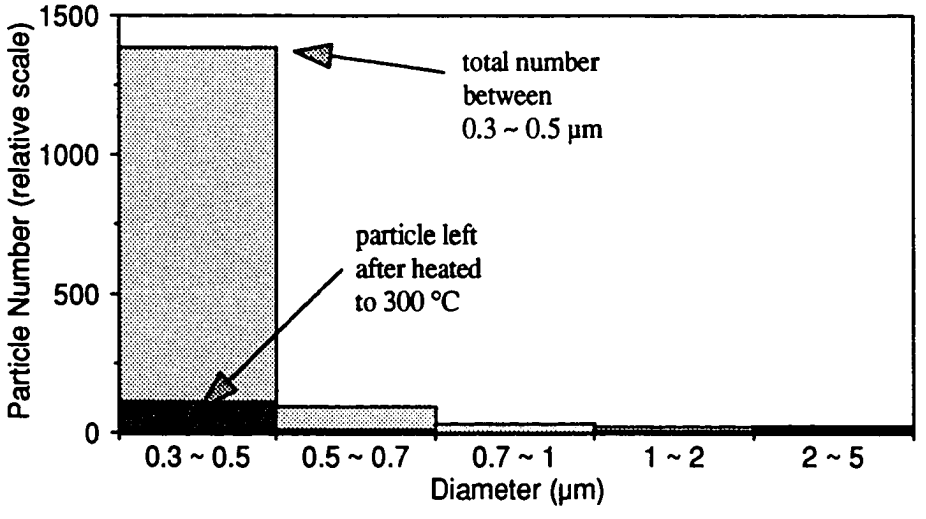

Figure 4-11 Number concentration of particles between 0.3 μm and 5 μm; measured by a portable particle sizer (Met One) on Ester Dome, around 17:35, September 15, 1994. When the sample air was heated to 300°C, most of the aerosols disappeared.

Figure 4-12 shows another example. The data were taken on September 22, 1994. It was cloudy in the morning; the wind came from the west. Figure 4-13 shows the aerosol size distribution. It was double peaked and appeared to be similar to that found in a marine air mass. The measured CCN number concentration was around 100 cm^{-3} at S = 1%. The total CN number was about 700 cm^{-3}, and the calculated CCN number was around 400 cm^{-3}.

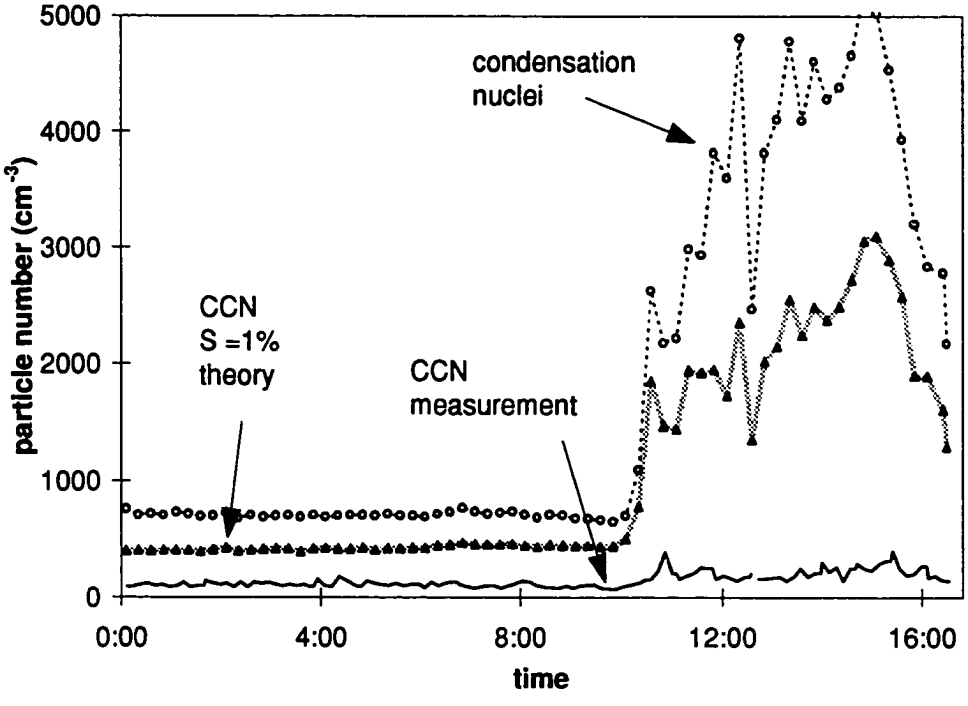

Figure 4-12 Aerosol number concentrations measured on Ester Dome, September 22, 1994. The heating test showed that most of the particles in the late afternoon were volatile.

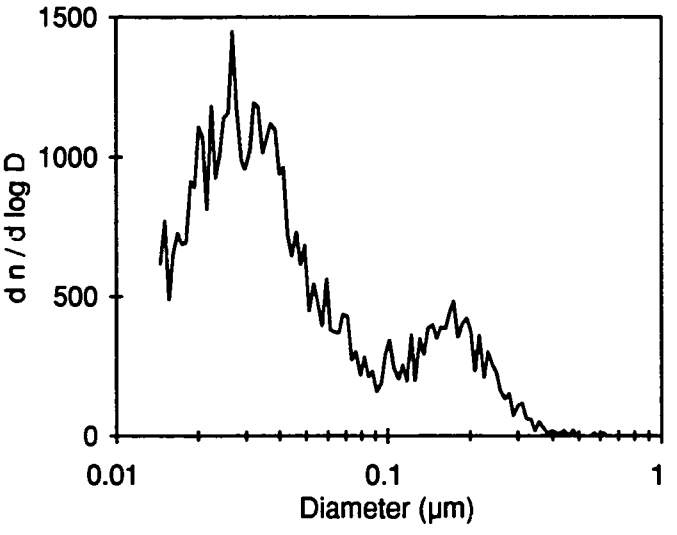

Figure 4-13 An aerosol size distribution measured on Ester Dome at 0:05, September 22, 1994. The wind came from the west. The size distribution looks like what we found in marine airmass.

Figure 4-14 show data acquired at 15:05. The number concentration of aerosol became very high; there was a forest fire nearby at the time of measurement. At about 17:00, the wind blew the smoke away and the air became clean for a while. The heating test result, Figure 4-15, shows that most of the aerosols were volatile, evaporating at 300°C. This suggests that if they were sulfate compounds, then they should be CCN and most of them should be activated because the critical size is about 0.03 μm for ammonium

sulfate. However, the CCN counter counted only a small fraction of them as shown in Figure 4-12, could underestimate their concentration.

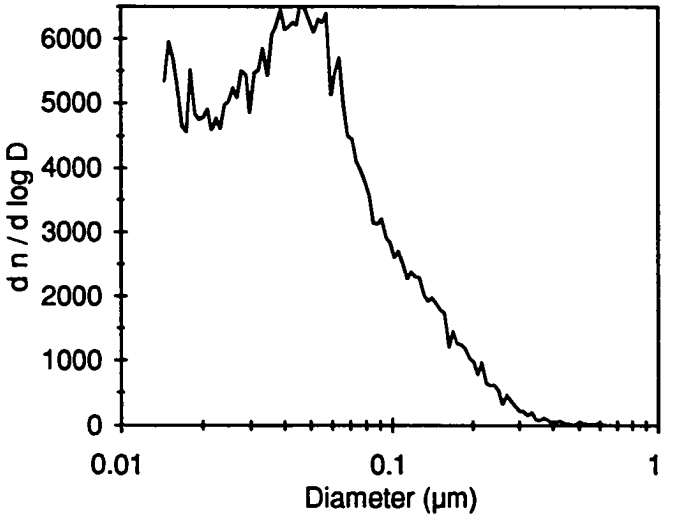

Figure 4-14 Aerosol size distribution measured on Ester Dome at 15:05, September 22, 1994. There was a forest fire nearby.

The autumn data seem to indicate that whenever there were a large number of particles smaller than 0.1 μm in diameter in the air, the CCN number concentration measured by our CCN counter would be much lower than the theoretical prediction. A similar behavior was noted during the winter data. Therefore, it was concluded that either the particles were "poisoned"; covered by insoluble films such as organic

material, or the CCN counter could not activate small particles efficiently. Further evidence for the latter was found in laboratory tests and in the CCN chamber model as was described in Chapter 3, section 3.2.1.

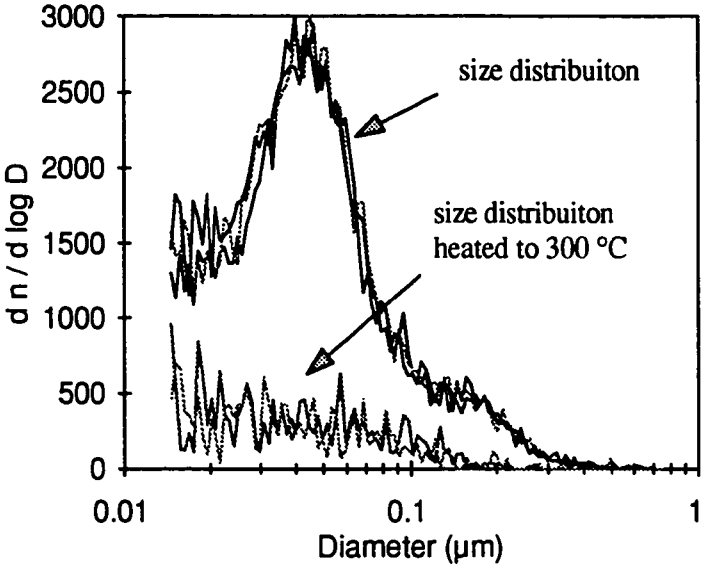

Figure 4-15 Aerosol size distributions measured on Ester Dome at 17:00, September 22, 1994. Several results are superposed. The heating test showed that when the sample air was heated to 300°C, most of aerosol disappeared, indicating that they might be sulfate compounds.

4.3 Hawaii

Hawaii is an excellent place to study "background" aerosols because of its clean location in the middle of the Pacific Ocean. Data were collected both on the easternmost point of the Island of Hawaii at Kapoho at sea level, and at Mauna Loa Observatory (MLO) at an altitude 3,400 m above sea level. Our sampling location was set up at the eastern tip of the island so clean air carried in by the Trade winds could be sampled. The MLO lies above the marine boundary layer for most of the day, and thus it is easy to measure the free-troposphere airmass. The same type of instruments as ours from Dr. Anthony Clark's research group at University of Hawaii were running along with ours at Kapoho.

4.3.1 Marine boundary layer

In the marine boundary layer, the aerosols have been cycled though numerous condensation-evaporation cycles without precipitation. This results in double-peaked aerosol size distributions (Hoppel et al., 1994; 1990; 1986). Figure 4-16 shows the typical double-peaked size distribution of aerosol found in the marine boundary layer during uncontaminated periods. On average, the air is clean compared to that found on the continent near Fairbanks. The heated tube test shows that about 30% of the aerosols are

refractory, probably sea salt. Figure 4-17 shows the measurement result on April 21, 1994, when the supersaturation was set to 0.3%. At this time the CCN counter underestimates the number of CCN. Because CCN data had a reasonable correlation with CN data, as shown in Figure 4-17 between 0:00 and 8:00, we can assume that the CCN counter functioned properly. Thus, there are three possible explanations to the underestimation:

(1) the actual supersaturation in the CCN counter was lower than the expected value;

(2) aerosols were "poisoned";

(3) the CCN counter could not activate small particles efficiently as suggested by the Alaskan data, the laboratory tests and the chamber model.

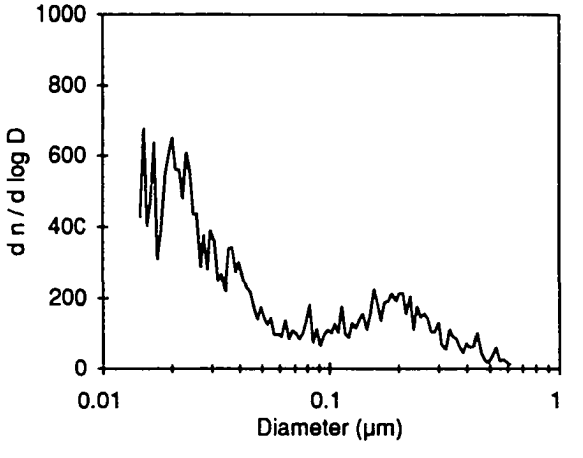

Figure 4-16 Bi-mode size distribution measured at Kapoho in Hawaii, at 0:00, April 21, 1994.

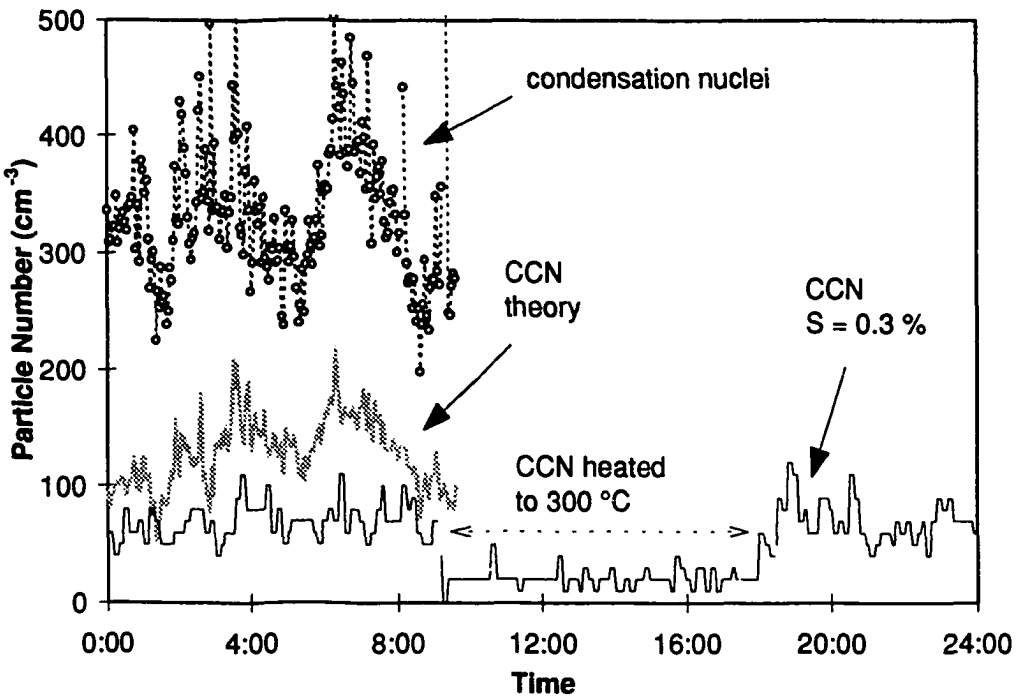

Figure 4-17 Particle number concentrations at Kapoho in Hawaii, April 21, 1994. The measured CCN number concentration was about 70 cm^{-3} at S = 0.3%. When heated up to 300°C, the CCN number concentration dropped to about 20 cm^{-3} (9:00 ~ 18:00). This suggests that about 30% of CCN were sea salt particles. The measured CCN number concentration was lower than the theoretical estimation though it had some correlation with the number concentration of condensation nuclei (circles).

4.3.2 Free troposphere

At the Mauna Loa observatory, at times when it was above the marine boundary layer, the size distributions of aerosol were bell-shaped as shown in Figure 4-18. All aerosols were volatile at 300°C. Figure 4-19 shows the particle number concentrations. On May 1, 1994, the CCN counter was programmed to scan the supersaturation. In Figure 4-19, when the supersaturation in the CCN counter was set to 1.3%, for example, around 4:00 and 20:00, the measurements agree with the theoretical estimation for S = 0.3%. As stated in previous cases, this could be an indication that the actual supersaturation in the CCN counter was lower than we expected.

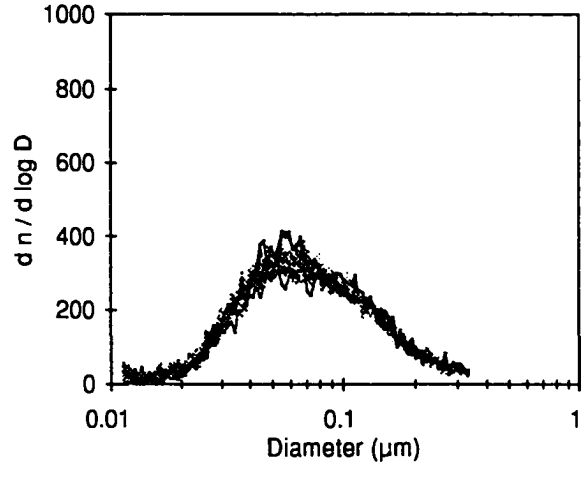

Figure 4-18 Bell-shaped aerosol size distributions measured on MLO between 18:50 and 20:20 on April 29, 1994. Ten distributions are superposed in the figure.

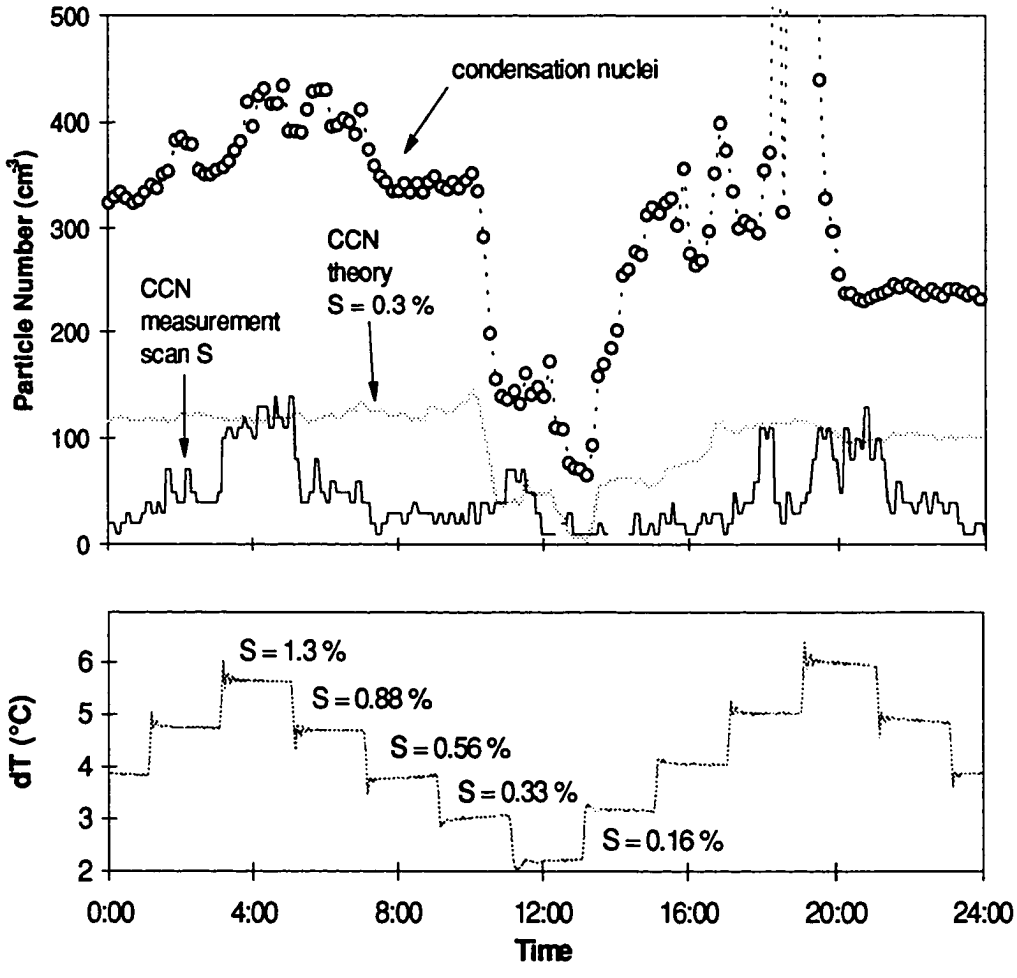

Figure 4-19 Aerosol number concentrations at Mauna Loa observatory, May 1, 1994. The condensation nuclei are aerosols in 0.01 to 0.34 μm range. The CCN counter was set to scan the supersaturation. The supersaturation was 1.3% around 4:00 and 20:00 when the measured CCN number seemed agree with the theoretical estimation for S =0.3%.

4.4 Instrument's intercomparison

Intercomparison is a useful method to see whether an instrument is functioning correctly. When the measurement results from two instruments designed on different physical principles agree with each other, one is confident in saying that both instruments are operating properly or subject to the same systematic error. Comparing two instruments of the same kind may give us some idea on the accuracy of the instrument and may assist in uncovering hidden errors or misadjustments.

4.4.1 Simultaneous measurement with CCN counter and other aerosol instruments

An example to show that our old CCN counter works properly comes from the April 1995 Mauna Loa data. Figure 4-20 shows the measurements from our CCN counter, a CN counter and a nephelometer. The supersaturation in the CCN counter was set to 2% (the real supersaturation is probably lower, see CCN counter calibration). It is not difficult to see that the three data time series have positive correlation. Figure 4-21 shows a period when the supersaturation was set to 0.5%; the CCN number was relatively constant, similar to previous measurement results at low supersaturation. It is concluded that the DH Model-1 CCN counter is measuring a

parameter that shows some degree of correlation with aerosol parameters.

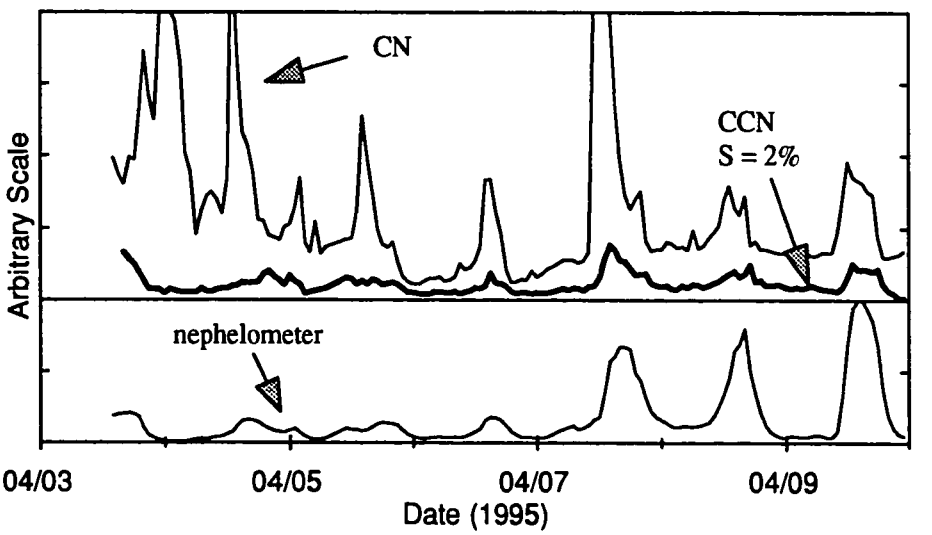

Figure 4-20 Correlation among condensation nuclei, cloud condensation nuclei, and nephelometer measurements. Mauna Loa Observatory, April 3 to 9, 1995. The data are shown on an arbitrary scale. The supersaturation in the CCN counter was 2%. Although the CCN counter did not activate all the CN as predicted by activation theory, the CCN data did have some correlation with CN and nephelometer data.

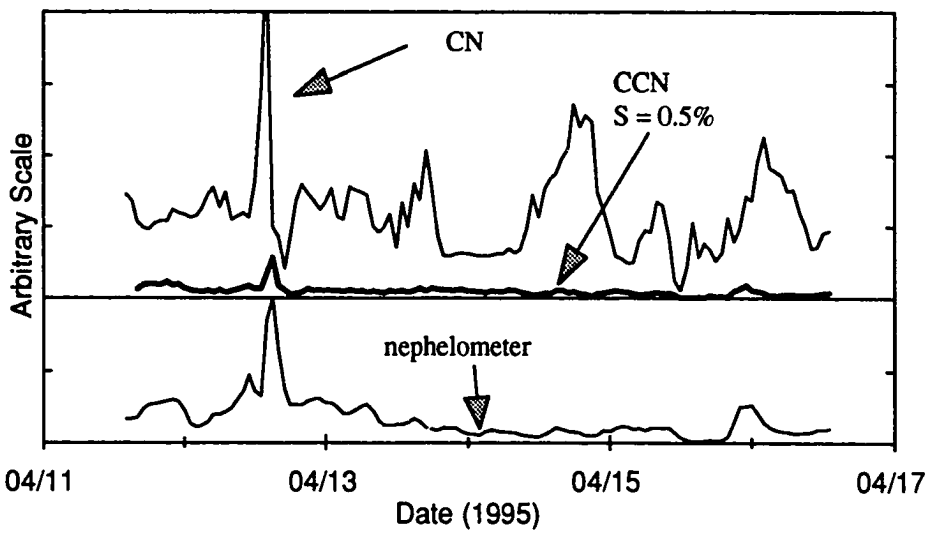

Figure 4-21 Correlation among condensation nuclei, cloud condensation nuclei, and nephelometer measurements. Mauna Loa Observatory, April 11 to 17, 1995. The data are shown on an arbitrary scale. The supersaturation in the CCN counter was 0.5%.

In Figure 4-20 and 4-21, the correlation between CCN and nephelometer data seems to be better than the correlation between CCN and CN data. This implies that the CCN counter does not measure small particles very well. It is understood why the nephelometer is insensitive to small particles a few hundredths of a micron in size, because they scatter light so inefficiently. The correlation between CCN

and CN data is lower because, as we know from previous measurements, when the CN number is very high, there are usually a large number of small particles.

4.4.2 A discussion of the classic thermal diffusion gradient chamber CCN counter

The University of Alaska Fairbanks' (UAF) CCN counter was manufactured by DH Associates in Tucson, Arizona. It was compared with a similar unit owned by the University of Hawaii (UH). Both counters were modified. A temperature controller was added to the UH counter, and the bottom plate of the chamber was rebuilt (a piece of copper was added) to even out the temperature distribution across the plate. Since the ambient temperature in Hawaii does not change much, it was assumed that the temperature on the top plate remains constant. The UAF CCN counter was modified for computer controlled supersaturation (Appendix B.3). This was necessary because of changes of the room temperature at the Ester Dome Observatory; the heater in the room turns on and off periodically. When the heater is off, the room temperature can drop more than 10°C. Fluctuating temperatures of this magnitude can introduce substantial errors in the supersaturation of the CCN counter (Appendix B.4).

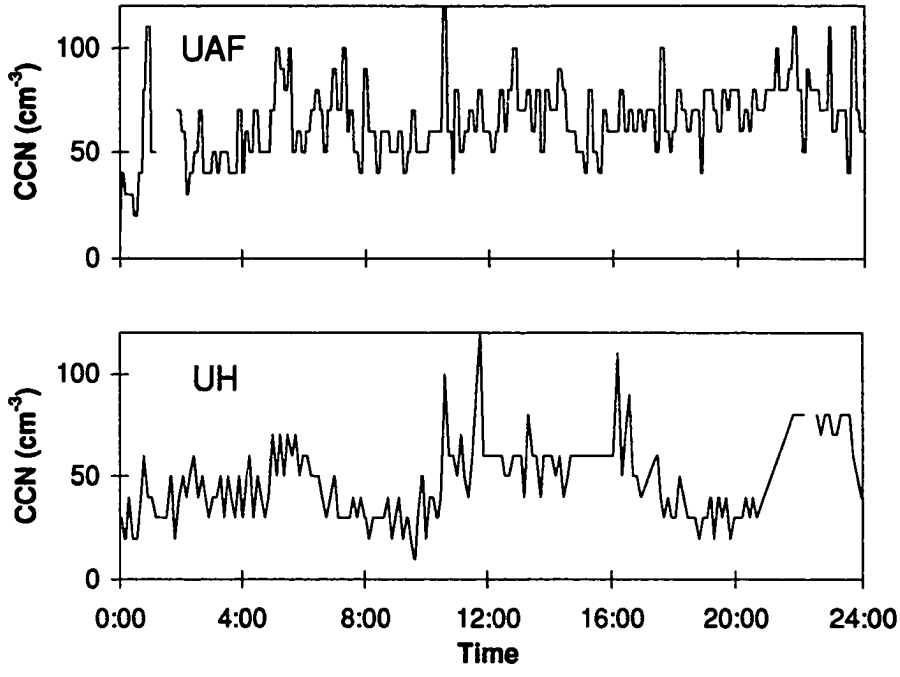

Figure 4-22 Intercomparison of UAF and UH CCN counters at Kapoho in Hawaii on April 20, 1994. The temperature difference between the top and the bottom plates of the thermal diffusion chambers was set to 3°C. The CCN number is obtained from the counting for 0.1 cm^{-3} sample air and multiplied by 10.

Figure 4-22 shows the result of an intercomparison between the UAF and UH CCN counters on April 20, 1994; where the temperature difference between the top and the bottom plates on the thermal diffusion chambers is controlled at

3°C. The CCN counters can sample 0.1 cc of air every 7 min. The sampling volume is small causing the uncertainty to be large.

Figure 4-23 is another intercomparison, from April 21, 1994. The UAF CCN counter controlled the supersaturation to 0.3%. UH CCN counter kept the temperature difference between the top and the bottom plates of the thermal diffusion chamber to 3°C. The theoretical CCN number is all particles between 0.07 μm and 0.5 μm, computed from the measured size distribution. It shows the advantage of controlling the supersaturation, because UAF data had a better correlation with the theoretical estimation. However, both counters underestimate the CCN number.

Figure 4-22 and 4-23 show only a short period of data, so the uncertainty seems large. If we look at a long period, as shown in Figure 4-24 and 4-25, then the two counters agree quite well, for example, around April 14 and April 18. Notice that the two counters were not running at the same supersaturation for all the time. The conclusion is that different counters can agree with each other quite well although they may not agree with the theoretical prediction.

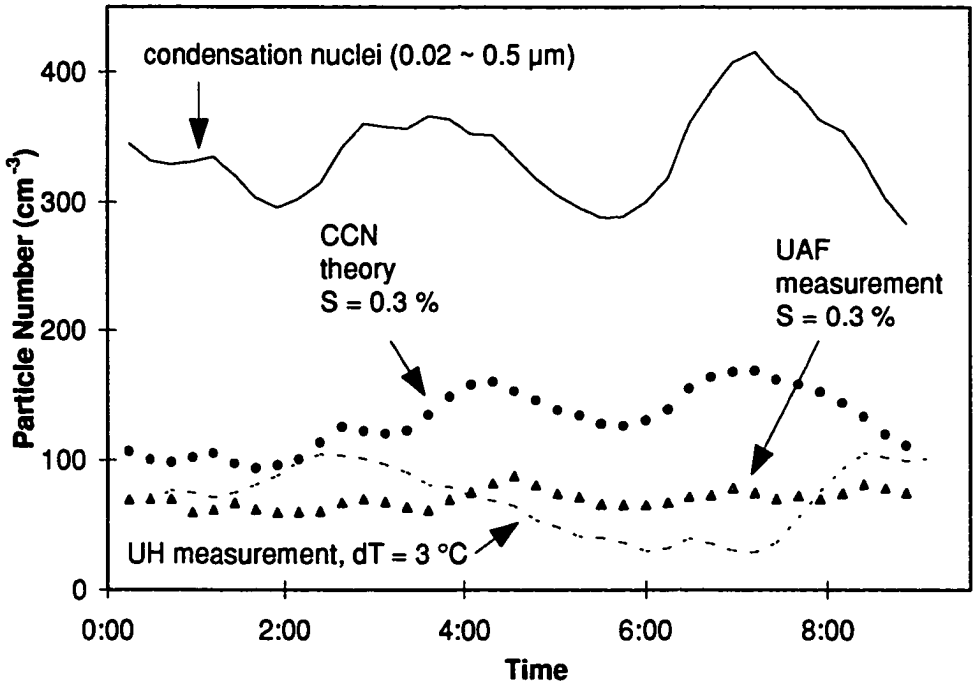

Figure 4-23 Intercomparison of UAF and UH CCN counters at Kapoho in Hawaii on April 21, 1994. The condensation nuclei number concentration (solid line) was obtained with a SMPS. Theoretical CCN number concentration was calculated from the size distribution (dots). The UAF CCN counter was set to S = 0.3% (triangles). The UH CCN counter controlled dT to 3°C (dotted line).

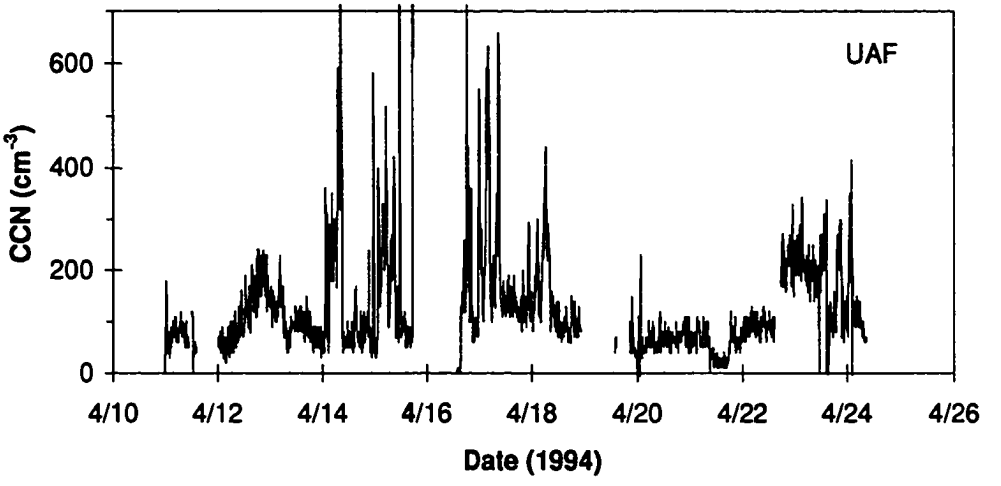

Figure 4-24 UAF CCN data measured in Hawaii, April 1994.

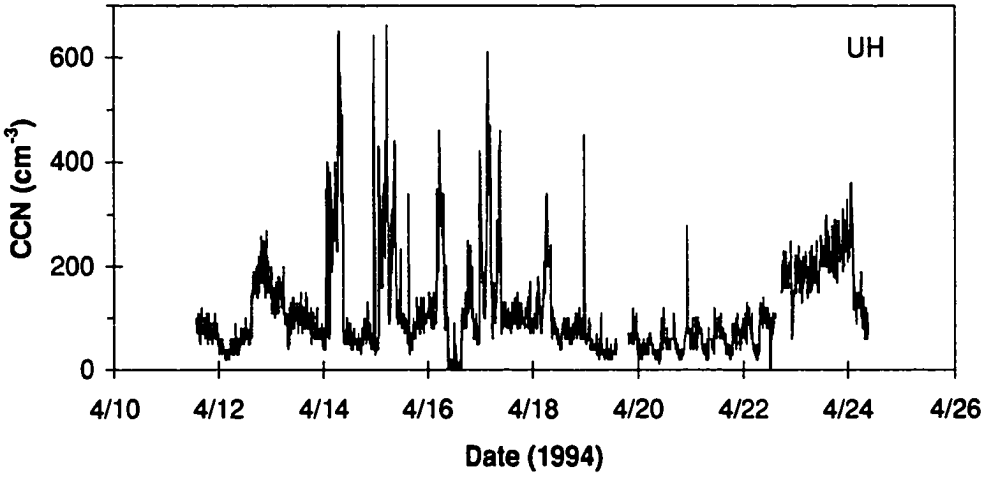

Figure 4-25 UH CCN data measured in Hawaii, April 1994.

4.5 CCN counter calibration

Recent advances in particle sizing and detecting equipment have led to methods that can be used to provide absolute calibrations of thermal diffusion gradient CCN counters. The idea is simple: as mentioned before, if we know the chemical composition and the size distribution of aerosol, we can calculate the supersaturation spectrum by using Köhler theory. If a CCN counter is operated correctly, then measurement results should agree with those predicted by theory.

By Köhler theory, for a 0.1 μm diameter ammonium sulfate aerosol, the critical supersaturation, S_c, is

$$S_c = (\frac{C}{D})^{3/2}$$

$$= (0.03/0.1)^{1.5}$$

$$\approx 0.16\ (\%)$$

This calculation illustrates that if the supersaturation is higher than 0.16%, then all particles larger than 0.1 μm will be activated.

To test our CCN counter, a monodisperse ammonium sulfate aerosol was generated in the laboratory as shown in Figure 4-26, and was measured by the CCN counter at different supersaturations.

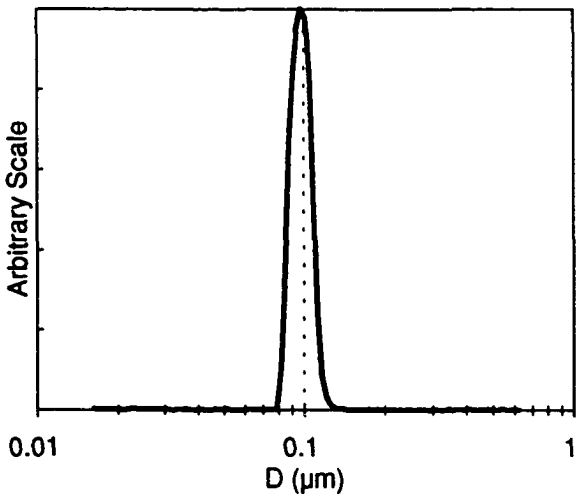

Figure 4-26 Size distribution of a monodisperse ammonium sulfate aerosol used in CCN counter calibration. It is shown in arbitrary scale.

Some results are listed in Table 4-3, where the total CCN number was about 150 cm^{-3}. The supersaturation was always higher than the critical value (0.16%), so the measured CCN number was expected to be 150 cm^{-3} for all cases. However, it was found that the measured CCN agreed with theory only when the supersaturation was set to a very high value, for example, to 2% supersaturation. This result agrees with predictions from the thermal diffusion chamber model in Chapter 3.

Table 4-3 A CCN counter calibration result. If the supersaturation is high (several percentages), and the number concentration of CCN is low, the CCN counter can count all the monodisperse CCN.

Supersaturation (%)	**Generated CCN (cm^{-3})**	**Measured CCN (cm^{-3})**	**Measured/Generated**
0.33	154	0	0
0.5	154	38	0.25
1.0	133	92	0.69
1.5	162	144	0.89
2.0	152	152	1

The result in Table 4-3 and some other results are shown in Figure 4-27, where

$$counting\ efficiency = \frac{measured\ CCN\ number\ concentration}{generated\ CCN\ number\ concentration}$$

The counting efficiency is expected to be one in all cases.

The conclusions are:

(1) If the CCN number concentration is high, the counting efficiency is low. This is probably due to the water depletion, the overlap of images, etc..

(2) If the supersaturation is low, the counting efficiency is low. This is a prediction we reached from the chamber model (see Figure 3-7).

(3) It is suggested in the field measurement results that, the smaller the CCN, the lower the counting efficiency. This is also a prediction from the chamber model (see Figure 3-6).

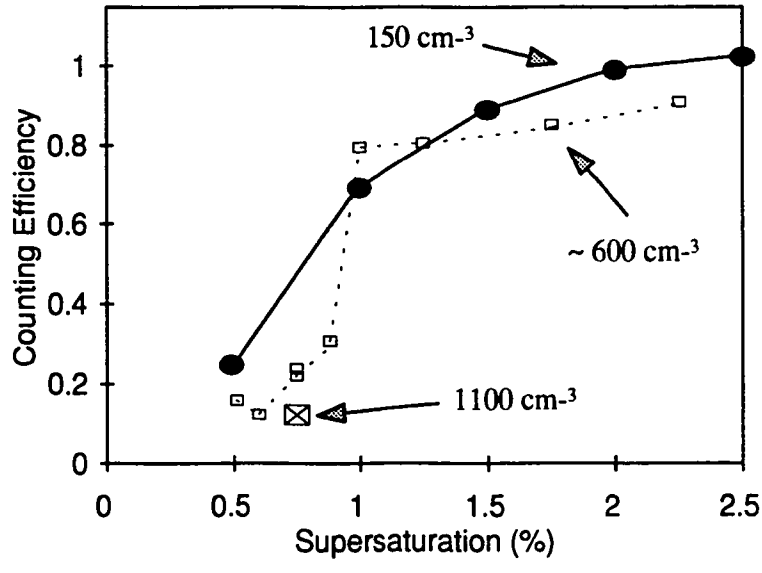

Figure 4-27 Some CCN counter calibration results. It is shown that (1) the instrument's counting efficiency falls with decreasing supersaturation; (2) the counting efficiency declines with increasing particle number concentration.

4.6 Discussion

The static thermal diffusion chamber possesses low counting efficiency. It appears that the actual supersaturation is lower than that calculated from the temperature difference between the top and the bottom plates of the thermal diffusion chamber. However, the problem can not be solved by simply introducing a correction factor to the calculated supersaturation or to the counted droplet number.

Another problem with the CCN counter we used is that the temperature is not evenly distributed in the top and bottom plates as shown in Figure 4-28. Thus, the supersaturation calculated for the chamber may not be accurate.

The effective light-scattering volume in the DH Model-1 CCN counter's thermal diffusion chamber is only about 6 mm^3 (Appendix B.2). In clean conditions it takes more than one hour to sample one cubic centimeter of air and give a CCN number at a single supersaturation. In contrast, the CCN Remover Spectrometer provides 40 data points (supersaturations) on a supersaturation spectrum, along with the 40 size distributions, in an hour's time.

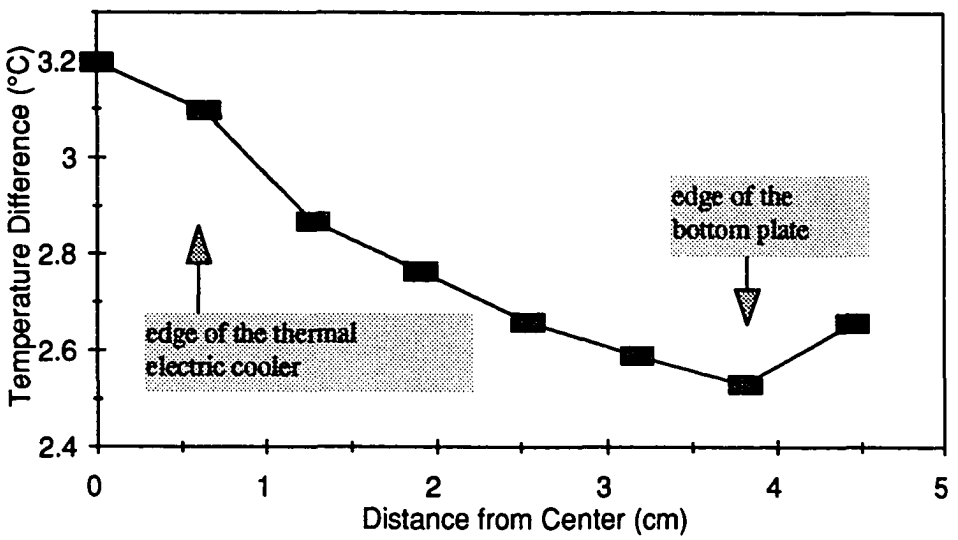

Figure 4-28 Temperature difference between the top and bottom plates of a thermal diffusion chamber. The thermocouple on the top plate was fixed while the thermocouple on the bottom plate was put at different distances from the center of the bottom plate.

CHAPTER 5

TESTS OF THE CCN REMOVER

"Save all the data you get; it may save your life someday." - Richard Benner, 1994.

5.1 Laboratory test

Before the prototype of the CCN Remover was built, two small test chambers were tested to check how CCN are removed.

5.1.1 Small test chambers

The two test chambers were made of clear plastic. The inside volume was about 25 × 20 × 1.5 cm each (0.75 L). The upper parts of the chambers were filled with "oasis" (found in flower shops, a green foam of material that holds water) to keep the ceiling wet. To get a wet bottom surface and to control the temperature, cold water was circulated in the bottom half of the chambers. A freezer was used to chill the water and thermocouples were used to measure temperatures.

The first chamber was divided with vertical walls, so the sample air would go though a labyrinth of channels as shown in Figure 5-1. A sample air flow rate of 0.3 L min^{-1} provided a residence time in the test chamber of about 2 min.

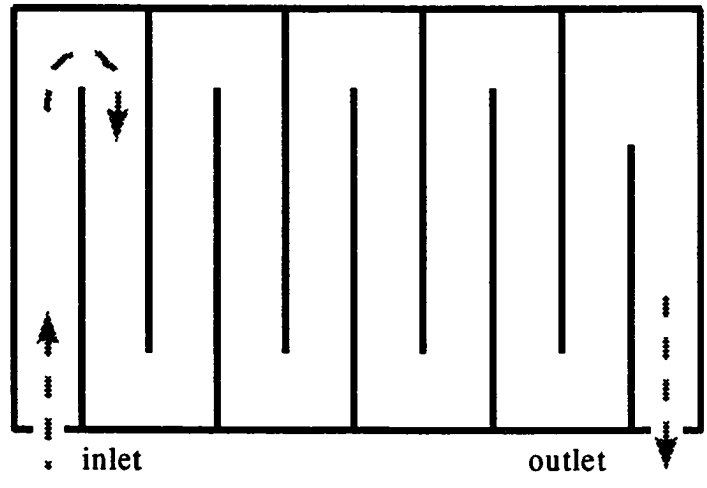

Figure 5-1 Top view of a test chamber. The sample air goes though a labyrinth channel.

The supersaturation was highest in the middle (the central horizontal plane) of the chamber; there, relatively small CCN could be activated and removed. Towards the top and bottom of the chamber, supersaturation decreases and only larger CCN could be removed. To allow most aerosols to experience the maximum supersaturation, we ran the air

through the labyrinth as shown in Figure 5-1. At each turn in the channel, turbulence mixes the sample air. Therefore, the air near the top or bottom of the chamber is mixed to the central horizontal plane and experiences the maximum supersaturation.

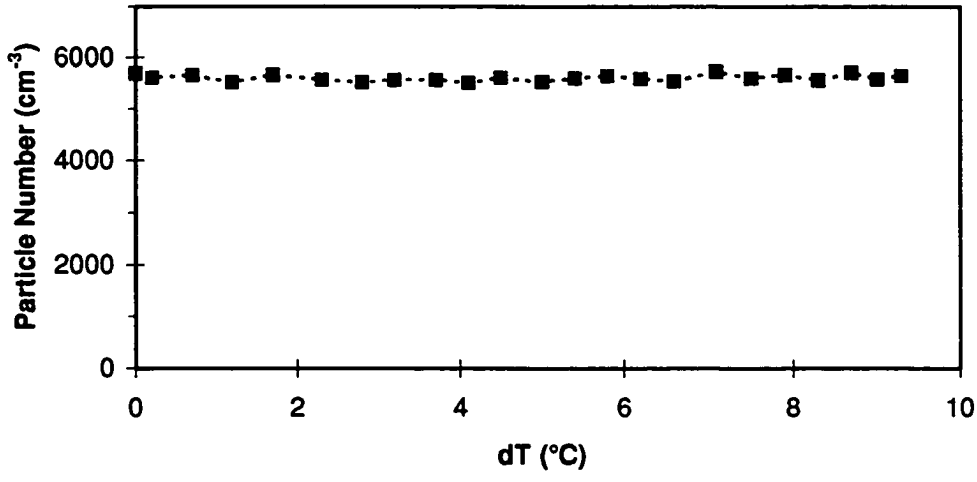

Figure 5-2 Particle number concentration after the chamber with a dry top plate.

Figure 5-2 demonstrates that if the top plate of the chamber is dry, the temperature difference between the top and bottom plates will not cause significant particle loss in the chamber. In other words, if the ceiling of the chamber is dry, there is no water vapor available in the chamber, so no CCN can be activated. The results show that diffusion loss of particles to the wall of the chamber is

small. Also, if the top plate of the chamber is not dry, but the temperature difference between the top and the bottom plates is zero, then particles will grow to haze droplets in the chamber by hygroscopic growth. However, they will not grow large enough to fall out.

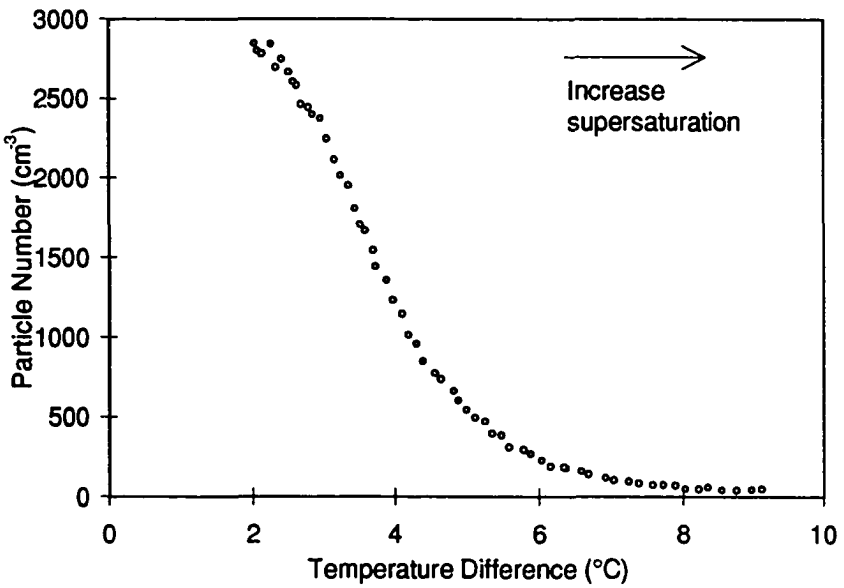

Figure 5-3 Particle numbers after the CCN Remover. The temperature difference is the temperature on the ceiling in the chamber minus the temperature on the bottom surface in the chamber. The higher the temperature difference, the higher the supersaturation. The corresponding size distributions are shown in Figure 5-4.

Figure 5-3 demonstrates that if the temperature difference between the bottom and top of the chamber is large, no CCN are left after the chamber. In this example, 80 size distributions was measured over two hours; 3 of them are shown in Figure 5-4.

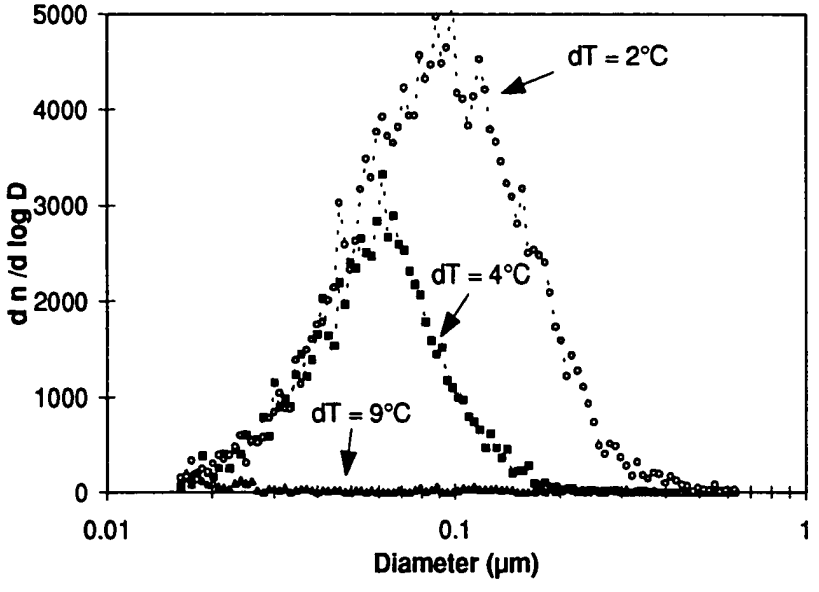

Figure 5-4 Size distributions after the CCN Remover. "dT" is the temperature difference between the top and bottom surfaces of the chamber. The higher the temperature different, "dT", the higher the supersaturation.

Although primitive, the test chamber demonstrated the following:

(1) If the top surface (ceiling) of the chamber is dry, then the temperature difference between the top and bottom surfaces will not cause significant loss of CCN.

(2) If the supersaturation is zero, there is no significant lost of CCN in the CCN Remover.

(3) The higher the supersaturation, the more CCN are lost in the chamber.

(4) Large particles can be removed at low supersaturation. When supersaturation increases, smaller particles will be removed.

The first test chamber did not show the theoretically predicted "cut off" of particles larger than the critical size. This is because not all the particles could stay in the highest supersaturation portion of the chamber, so some particles larger than the critical size could not be activated. For this reason the next version of the Remover used sheath air to confine the sample air into a thin layer at the center of the chamber. In this way the supersaturation experienced by all the particles is more nearly uniform.

The second version of the Remover was the same size as the first one, but was not divided by vertical walls. The

sample air was injected between sheath air flows (see Figure 3-8). When the chamber was illuminated by a laser beam, the trajectories of droplets could be clearly seen. Preliminary tests showed that because the chamber was small, the flow rate of sample air had to be very low to keep a proper sample-sheath flow ratio. Low air flow rate introduces larger errors. Therefore a bigger chamber is needed.

5.1.2 The final CCN Remover

The final version of the CCN Remover we built has a larger chamber. The dimensions of the chamber are 50 x 35 x 2 cm (3.5 L). The sheath air flow is about 2.7 L min^{-1}. The sample air is confined in the middle of the chamber as was shown in Figure 3-8, the flow rate is 0.3 L min^{-1}, and the air residence time in the chamber is 70 s. The bottom plate of the chamber is aluminum. Coolant circulates in the bottom plate to regulate the temperature difference between the top and bottom plates. The final design should not be considered optimal.

Figure 5-5 shows some measured size distributions obtained in the laboratory with ammonium sulfate aerosols. The number concentration of aerosol is about 2500 cm^{-3}, but the signal looks noisy. Smoothed curves are shown in Figure 5-6. They illustrate how the CCN Remover works. Activation

theory predicts a sharp cut in the size distribution after the CCN larger than the critical size are removed.

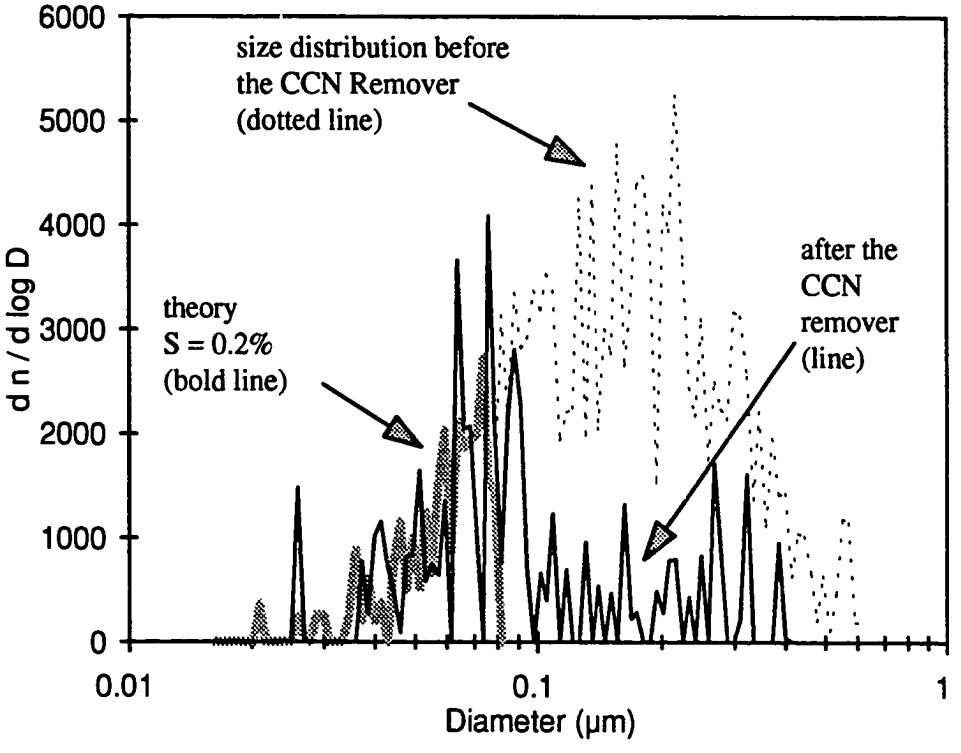

Figure 5-5 Aerosol size distributions measured before and after the CCN Remover. After the CCN Remover, some larger particles are removed (thin solid line). Activation theory predicts that all particles larger than the critical size will be removed and no particles smaller than the critical size will be removed (bold line). The original size distribution is shown with a dotted line.

The number of CCN at a particular supersaturation can be calculated by subtraction of the size distribution before and after the CN Remover. The supersaturation spectrum can be measured by scanning the temperature difference between the plates in the CCN Remover. A measured supersaturation spectrum is shown in Figure 5-7.

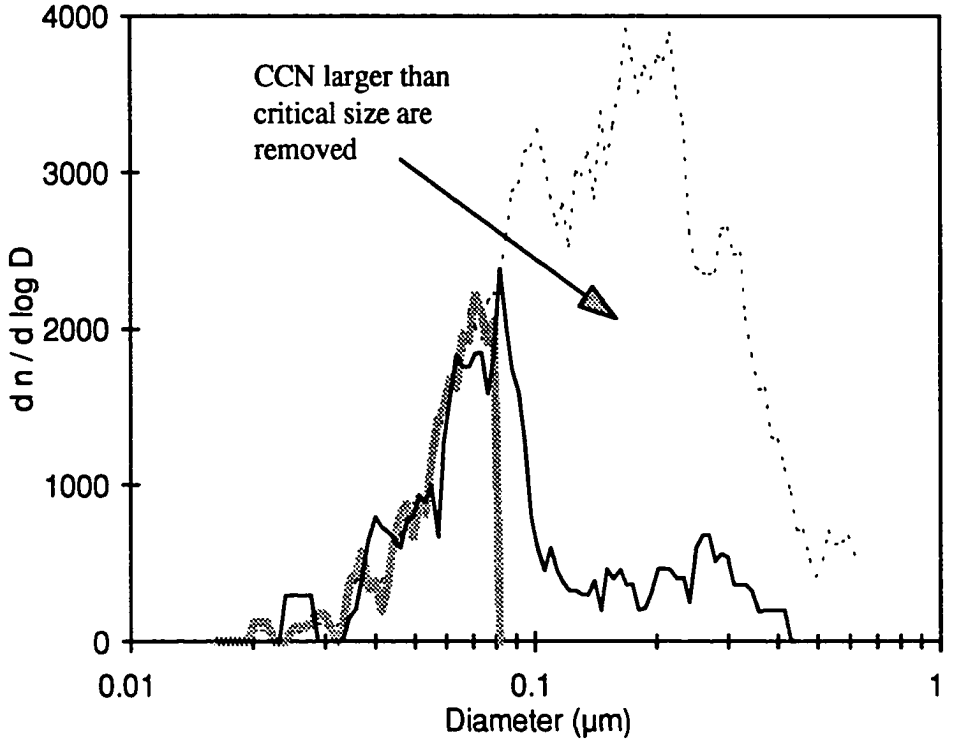

Figure 5-6 The same data as shown in Figure 5-5, but smoothed. It shows that most particles larger than critical size are removed. The particles left may due to the experimental error.

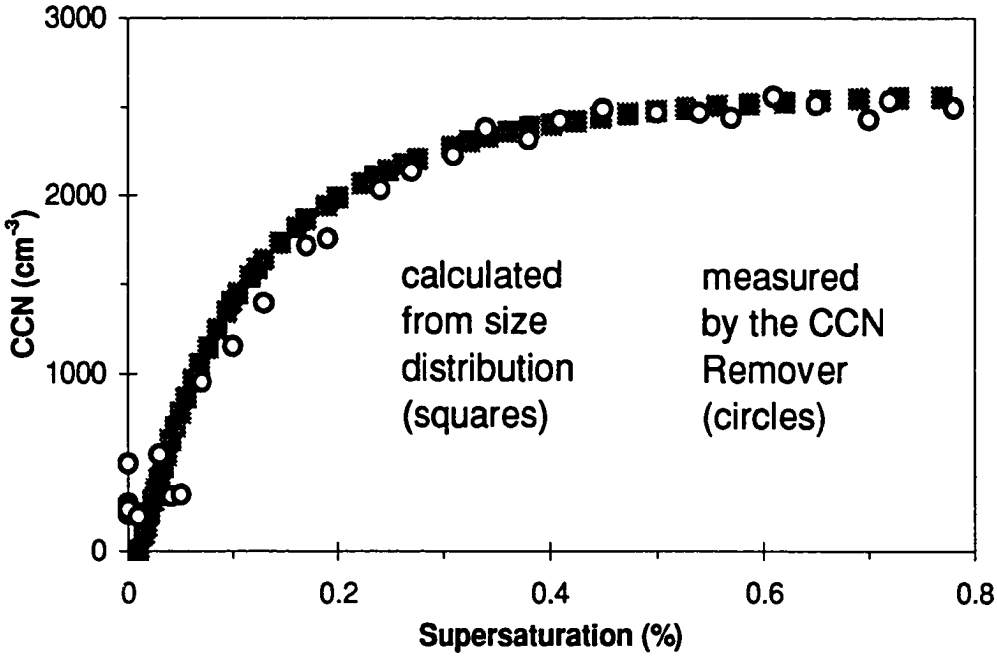

Figure 5-7 Measured and calculated supersaturation spectra in laboratory with ammonium sulfate aerosols. The removed CCN numbers are obtained from 27 scanned size distributions over one hour.

5.2 Field measurement in Brazil

The prototype CCN Remover-Spectrometer was tested in the 1995 NASA SCAR-B (Smoke, Clouds, and Radiation - Brazil) experiment. A Scanning Mobility Particle Sizer, a CCN Remover and a CCN counter were used to measure biomass burning aerosols near the ground in Cuiaba (16°S latitude, 56°W longitude), Brazil.

5.2.1 Background

In late August, the air in Cuiaba, Brazil is dry and charged with smoke. Fires were usually started by farmers in the area around 14:00 every day because the relative humidity reaches the lowest point around 14:00, and material is most combustible. The concentration of smoke would reach a maximum in the early morning due to the overnight build-up of an inversion layer. By mid-morning the smoke started to decrease due to atmospheric convection. During smoke-free "clean" periods, the particle number concentration would be a few thousands per cubic centimeter. If there were fresh fires nearby, the number concentration would be several tens of thousands per cubic centimeter. The SMPS showed smooth lognormal shaped particle size distributions. The concentrations were so high that the DH Model-1 CCN counter could not make valid measurements because it was saturated.

A large number of other instruments were in operation at the Brazil site, including an aethalometer that measured black carbon, a cascade impactor that sampled aerosols on filters for size-segregated chemical analysis, an O_3 detector, a CO_2 detector, and spectral sunphotometers. Weather balloons were launched daily and aerosol properties were measured by several aircraft nearby.

5.2.2 Preliminary results

Our measurements were taken between August 17 and September 3, 1995. Let us take the measurement on August 22 as an example. Figure 5-8 shows the CN and CCN number concentrations. The air was relatively clean between 8:00 and 16:00. For the CCN counter, the supersaturation was set to 0.3% at 8:00, and the measured CCN number was 170 cm^{-3}. Later, when the supersaturation was changed to 0.5%, the CCN number increased to 260 cm^{-3}. In the afternoon, the CCN number was 445 cm^{-3} at 0.7% supersaturation. In the late afternoon, the CCN number was about 1,000 cm^{-3} at 1% supersaturation. During the rest of the day, the supersaturation was kept at 1%, and the CCN counter showed that the CCN number varied between 1,000 cm^{-3} and 3,000 cm^{-3}.

The Scanning Mobility Particle Sizer was set to scan aerosol continuously before 8:00 and after 16:00. The number concentrations of the condensation nuclei (CN) in the 0.02 μm to 0.6 μm range were very high as shown in Figure 5-8 (circles). A large amount on aerosols was black carbon. The black carbon data measured by the aethalometer (University of Sao Paulo, Brazil) is shown in Figure 5-9. The CCN and CN data have positive correlation. However, the CCN counter could activate only a small fraction of the aerosols.

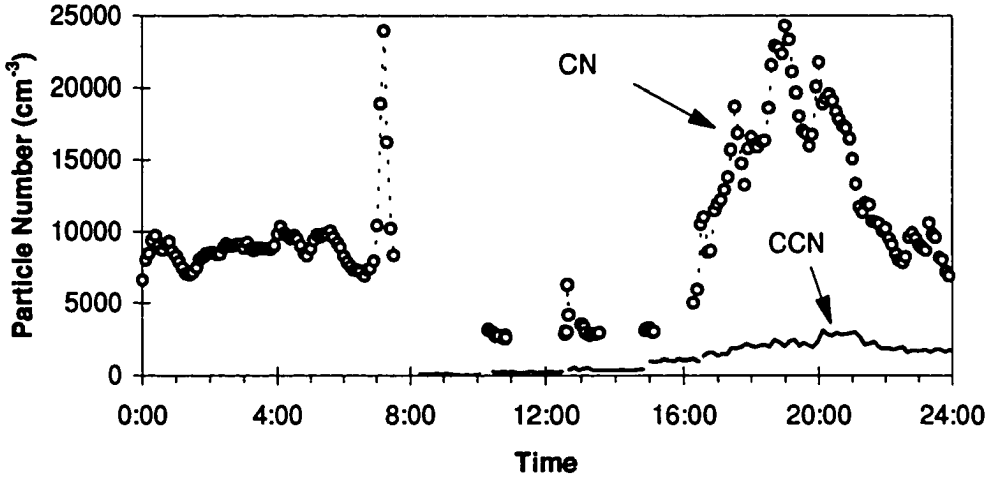

Figure 5-8 CCN number concentration measured by the CCN counter and CN number concentration measured by the SMPS. August 22, 1995, in Cuiaba, Brazil.

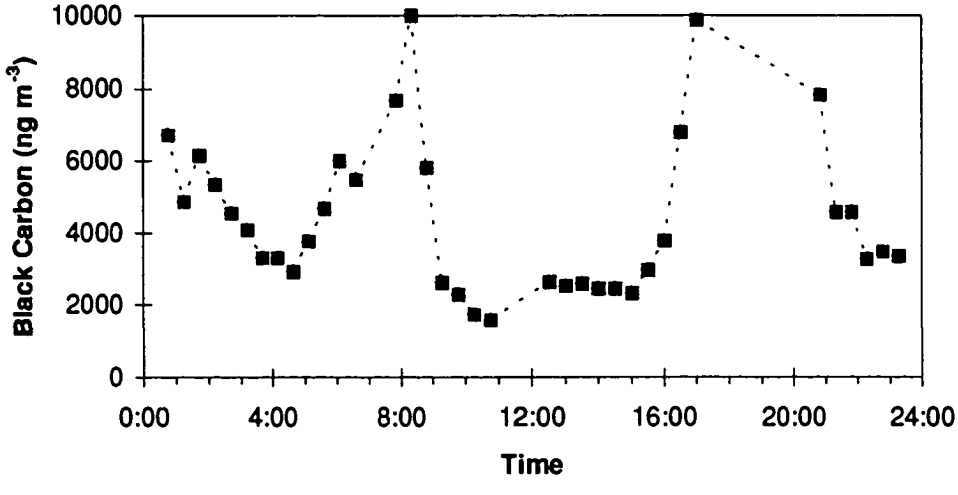

Figure 5-9 Black carbon measured on August 22, 1995, Cuiaba, Brazil.

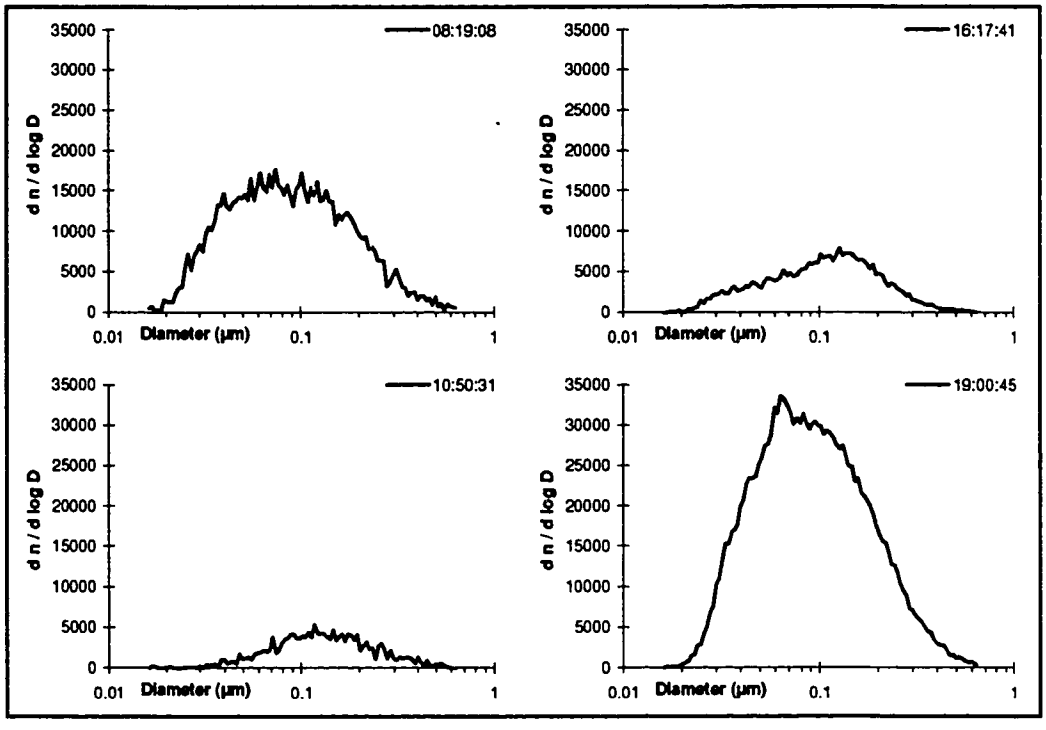

Figure 5-10 Some size distributions measured on August 22, 1995, in Cuiaba, Brazil. Most size distributions were lognormal-shaped.

Figure 5-10 shows some size distributions of aerosol. Most size distributions were lognormal-shaped. For aerosol measured at 8:19 (top left case in Figure 5-10), as a rough estimation, if we assume all particles are CCN, then the theoretical estimation of the CCN number is ≈8,500 cm^{-3}. This is much higher than 170 cm^{-3} measured by the CCN counter. As discussed in Chapter 4, the disagreement between

the CCN counter measurement and the theoretical estimation is probably due to two reasons: (1) The CCN counter underestimates CCN number, especially when CN numbers are large. (2) Not all particles are CCN; some may be hydrophobic or insoluble.

The measurements obtained by using our new CCN measurement system, the CCN Remover Spectrometer, show higher CCN numbers than the measurements obtained using the CCN counter. Figure 5-11 shows the particle number concentrations before and after the CCN Remover measured around 8:30. Sample air was drawn into an air bag, the number concentration in the air bag dropped from ≈13,200 cm^{-3} to ≈9,800 cm^{-3} in about 40 min. The CCN Remover scanned the supersaturation from 0% to 0.6%. At 0.3% supersaturation, ≈6,000 cm^{-3} particles were removed. Some particles would be removed by diffusion loss as discussed in Chapter 4, thus not all 6,000 cm^{-3} particles might be CCN. However, comparing to the ≈170 cm^{-3} measured by the CCN counter, the difference is an order of magnitude significant. This demonstrates that the CCN Remover has a much higher counting efficiency than the CCN counter. Figure 5-12 shows a size distribution before and after the CCN Remover at 0.3% supersaturation. It indicates that most

particles larger than 0.2 μm were removed; many small particles were also loss probably due to diffusion.

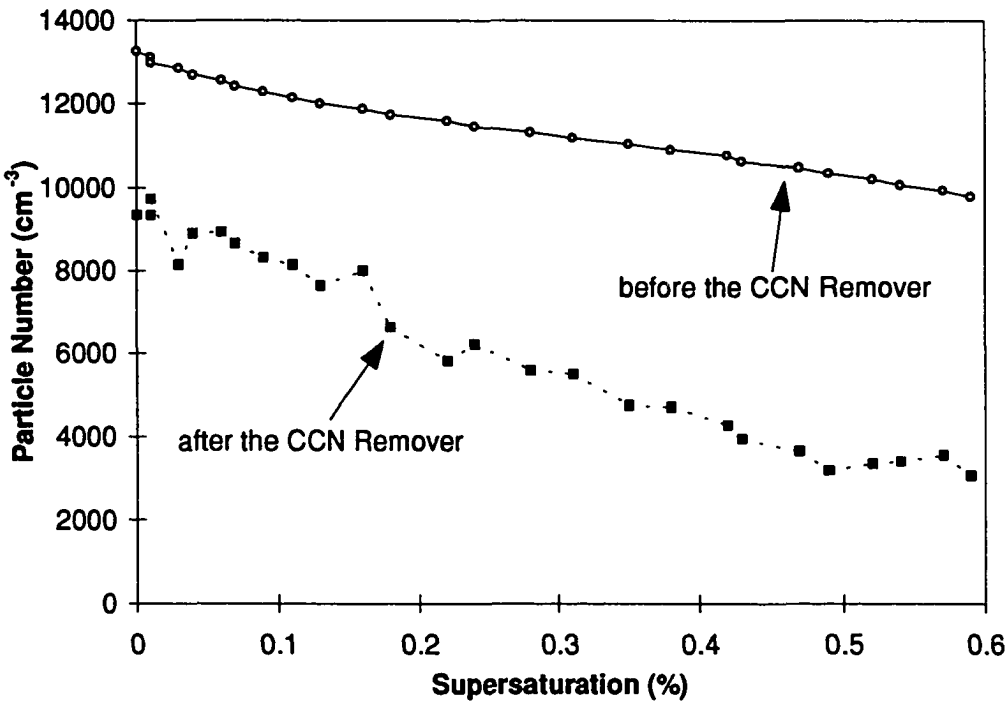

Figure 5-11 Particle number concentrations before and after the CCN Remover measured around 8:00 on August 22, 1995, in Cuiaba, Brazil. The sample air was stored in an air bag (≈1 m^3). The number concentration of particles in the air bag dropped form ≈13,200 cm^{-3} to ≈9,800 cm^{-3} in about 40 min. Meanwhile, the Scanning Mobility Particle Sizer scanned particle size distributions 26 times, and the supersaturation in the CCN Remover scanned from 0% to 0.6%.

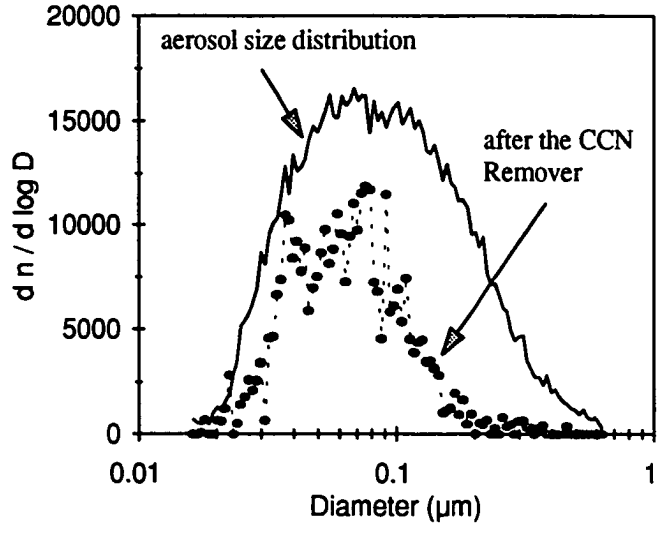

Figure 5-12 Size distribution of aerosol before and after the CCN Remover at 9:00, August 22, 1995, in Cuiaba, Brazil. The supersaturation in the CCN Remover was about 0.3%.

Figure 5-13 show another example. It is a measured CCN supersaturation spectrum by using the CCN Remover Spectrometer at ≈11:30, on August 21, 1995, in Cuiaba, Brazil. The supersaturation in the CCN Remover was scanned from 0% to ≈0.9% in about 20 min, and the scanning mobility particle sizer gave 12 size distributions during the same period. The result is compared with a theoretical estimation assuming all particles are ammonium sulfate. The aerosol size distribution is shown in Figure 5-14.

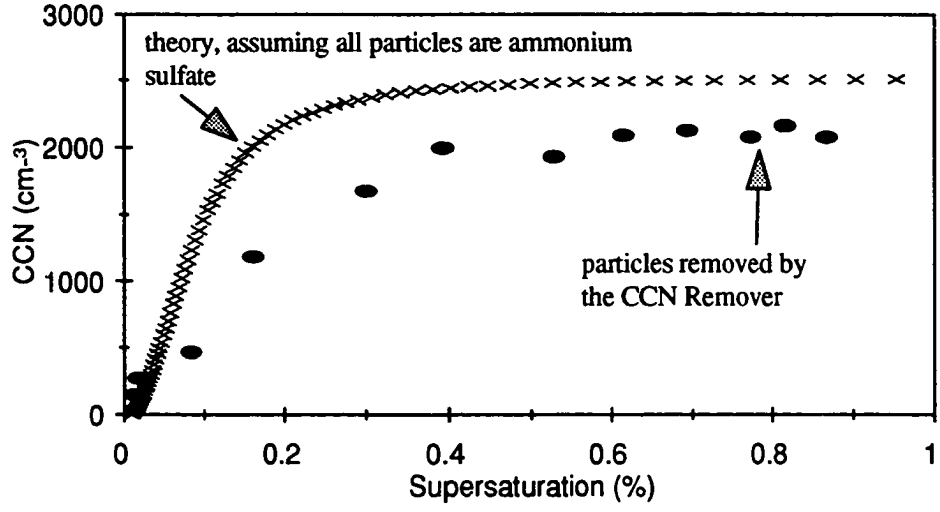

Figure 5-13 A CCN supersaturation spectrum measured by the CCN Remover Spectrometer. The supersaturation scanned from 0% to 0.9% in about 20 min as shown in Figure 5-15. CCN counter read 202 cm^{-3} at S = 0.5%.

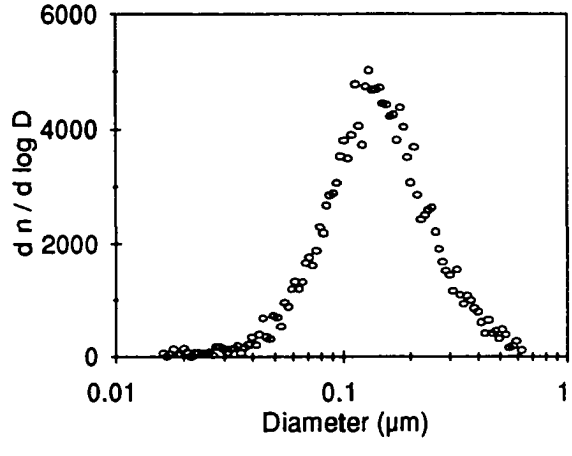

Figure 5-14 Aerosol size distribution at 11:30, August 21, 1995, Cuiaba, Brazil.

5.3 Discussion

It was shown that the prototype CCN Remover operated correctly, although this was a preliminary experiment. The CCN counter's measurements were systematically lower than the CCN Remover's measurements. This is consistent with the laboratory tests.

The SMPS could measure a size distribution every 1.5 min. Meanwhile, the supersaturation in the CCN Remover was scanned. If the supersaturation changes too fast, it would cause considerable errors in the measurements. In the case shown in Figure 5-15, the supersaturation in the CCN Remover could change 0.1% in 1.5 min. The temperature control method should be improved.

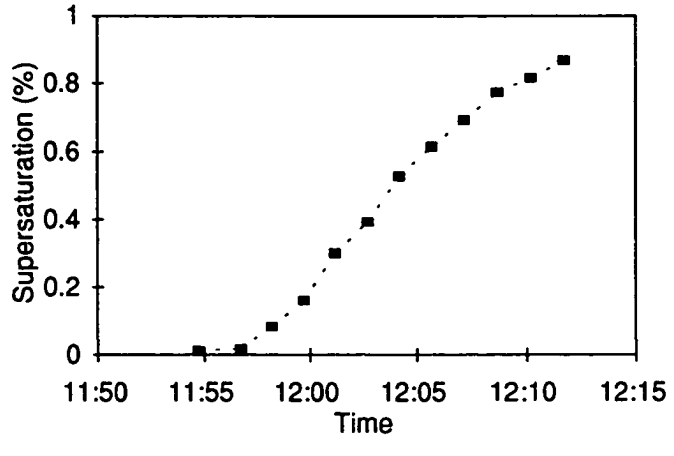

Figure 5-15 The supersaturation was scanned in CCN Remover. August 21, 1995, Cuiaba, Brazil.

CHAPTER 6

CONCLUSIONS

6.1 Summary

(1) A new equation for the supersaturation spectrum of CCN, obtained from data fitting, agrees closely with measurements. The new equation can fit the whole S-shaped CCN supersaturation spectrum if the corresponding size distribution of CCN is bell-shaped. In addition the new equation can be derived from basic physics. It is a distinct improvement on the classical "power law" distribution which is empirical.

(2) A simple theoretical model showed that the size distribution of the so-called accumulation mode of aerosols may tend to the "likelihood distribution" which is bell-shaped. The model considered only the evolution of aerosol size distribution due to coagulation, and assumed that the evolution is related to some perturbations in the atmosphere, such as turbulence and sound waves. When air moves due to the perturbations, smaller aerosols can follow the air better than larger ones. Thus, particles of

different sizes tend to collide with each other due to the differences of moving speeds related the perturbation.

(3) Cloud Condensation Nuclei (CCN) are not easy to measure. The size distribution of CCN has seldom been investigated. With the new CCN Remover Spectrometer and the new CCN measurement method, the properties of CCN, such as the supersautration spectrum, size distribution, and some chemical compositions, can be seen more easily and in considerably more detail than previously possible.

6.2 Future work

Due to the simplified assumptions, the likelihood distribution can describe only a small portion of aerosol. More detailed considerations may extend it to a wider aerosol range. Some preliminary research shows that a unified description of aerosol may come from entropy theory (e.g., for cloud droplets, Zhang, 1994, Liu, 1995). This extension is under development.

Aerosols can be modified by clouds. The soluble, activated nuclei will be modified differently from the inactivated proportion. The CCN size distribution will be very useful when studying the relation of CCN to clouds and climate and to the distribution of ionized particles in the atmosphere.

Due to limited time and budget, the prototype of the CCN Remover Spectrometer is relatively simple. Field measurements and lab tests showed that the CCN Remover can be improved in a number of ways (Appendix D). We hope to pursue vigorously the evolution of the instrument.

Loss of small particles to droplets by diffusion or thermophoresis seems to be an error source in the Remover Spectrometer. We shall further investigate this phenomenon.

A possible application of the new CCN Remover Spectrometer system is to use it as a front end filter to a sensitive sulfur detector. The sulfur in the cloud nuclei themselves can in principle be determined by the amount of sulfur before and after the CCN are removed. It is a central paradigm of climate that the largest CCN are sulfate. However, in some cases the most of CCN may not be sulfate (Hegg, Ferek and Hobbs, 1995), it could be organic (Novakov and Penner, 1993), or sodium chloride. The new Remover Spectrometer may help untangle these hypotheses.

The new equations for CCN supersaturation spectrum and for the likelihood size distribution will be used in the further development of our cloud activation model.

REFERENCES

Aitchison, J., and J. A. C. Brown, 1957: *The Lognormal Distribution with special reference to its uses in economics*. Cambridge University Press. P7.

Albrecht, B. A., 1989: Aerosols, cloud microphysics, and fractional cloudiness. *Science*, **245**, 1127-1230.

Alofs, D. J., and J. C. Carstens, 1975: Numerical Simulation of a Widely Used Cloud Nucleus Counter. *J. Appl. Meteor.*, **15**, 350-354.

Bigg, E. K., 1986: Technique for studying the Chemistry of Cloud Condensation Nuclei. *Atmos. Res.*, **20**, 75-80.

Bigg, E. K., 1980: Comparison of Aerosol at Four Baseline Atmospheric Monitoring Stations. *J. Appl. Meteor.*, **19**, 521-533.

Bigg, E. K., 1977: Some Properties of the Aerosol at Mauna Loa Observatory. *J. Appl. Meteor.*, **16**, 262-267.

Bowling, S. A., 1986: Climatology of High-Latitude Air Pollution as Illustrated by Fairbanks and Anchorage, Alaska. *J. Clim. and Appl. Meteor.*, **25**, 22-34.

Braham, R., 1974: Cloud physics of urban weather modification: A preliminary report. *Bull. Amer. Meteor. Soc.*, **55**, 100-106.

Charlson, R. J., J. E. Lovelock, M. O. Andreae, and S. G. Warren, 1987: Oceanic phytoplankton, atmospheric sulphur, cloud albedo and climate. *Nature*, **326**, 655-661.

Charlson, R. J., R. Vong, and D. A. Hegg, 1983: The sources of sulphate in precipitation (2). Sensitivity to chemical variables. *J. Geophys. Res.*, **88**, 1375-1377.

Charlson, R. J., and H. Rodhe, 1982: Factors influencing the acidity of natural rainwater. *Nature*, **295**, 683-685.

Coakley, J. A., R. L. Bernstein Jr., and P. A. Durkee, 1987: Effect of Ship-track Effluents on Cloud Reflectivity. *Science*, **237**, 1020-1022.

Crow, E. L., and K. Shimizu, edited by, 1988: *Lognormal Distributions, Theory and applications*. Marcel Dekker, Inc., New York. p4.

Dellago, C., and H. Horvath, 1992: On the accuracy of the size distribution information obtained from light extinction and scattering measurements - I. Basic considerations and models. *J. Aerosol Sci.*, **24**, 129-141.

Duce, R. A. 1983: Biogeochemical cycles and the air-sea exchange of aerosols, in *the major biochemical cycles and their interactions*. Ed. Bolin, B., and R. Cook, London, Wiley. P427-456.

Finlayson-Pitts, B. J., 1986: *Atmospheric chemistry*. John Wiley & Sons, Inc.. P755.

Fitzgerald, J. W., 1972: Dependence of the supersaturation spectrum of CCN on aerosol size distribution and composition. *J. Atmos. Sci.*, **30**, 628-634.

Fitzgerald, J. W., 1972: On the Computation of Steady-State Supersaturations in Thermal Diffusion Chambers. *J. Atmos. Sci.*, **29**, 779-781.

Fitzgerald, J. W., 1970: Non-Steady-State Supersaturations in Thermal Diffusion Chambers. *J. Atmos. Sci.*, **27**, 70-72.

Fuchs, N. A., 1964: *The Mechanics of Aerosols*. translated from Russian, The Macmillan Company, New York. p10.

Fukuta, N., and V. Saxena, 1974: Cloud condensation nucleus spectrometer. *Annual Report, Contract No. N000019-73-C-0176, Denver Research Institute*, Univ. of Denver.

Gerber, H. E., W. A. Hoppel, and T. A. Wojciechowski, 1977: Experimental Verification of the Theoretical Relationship Between Size and Critical Supersaturation of Salt Nuclei. *J. Atmos. Sci.*, **34**, 1836-1841.

Ghan, S. J., C. C. Chuang, and J. E. Penner, 1993: A parameterization of cloud droplet nucleation part I: single aerosol type. *Atmos. Res.*, **30**(4), 192-221.

Götz, G., E. Mészáros, and G. Vali, 1991: *Atmospheric Particles and Nuclei*. Akadémiai Kiadó és Nyomda Vállalat, Budapest. P94.

Gras J. L., 1995: CN, CCN and particle size in Southern Ocean air at Cape Grim. *Atmos. Res.*, **35**, 233-251.

Hegg, Dean A., R. J. Ferek, and P. V. Hobbs, 1995: Cloud Condensation Nuclei over the Arctic Ocean in Early Spring. *J. Appl. Meteor.*, **34**, 2076-2082.

Hinds, W. C., 1982: *Aerosol Technology, properties, behavior, and measurement of airborne particles*. John Wiley & Sons, New York. p83, p136, p153-157.

Hobbs, P. V., 1993: *Aerosol-Cloud-Climate Interactions*. Academic Press, Inc., San Diego. 237pp.

Hobbs, P. V., H. Harrison, and E. Robinson, 1974: Atmospheric effects of pollutants. *Science*, **183**, 909-915.

Hoppel, W. A., G. M. Frick, J. W. Fitzgerald, and R. E. Larson, 1994: Marine boundary layer measurements of new particle formation and the effects nonprecipitating clouds have on aerosol size distribution. *J. Geophys. Res.*, **99**, 14,443-14,459.

Hoppel, W. A., J. W. Fitzgerald, G. M. Frick, and R. E. Larson, 1990: Aerosol size Distributions and Optical Properties Found in the Marine Boundary Layer Over the Atlantic Ocean. *J. Geophys. Res.*, **95**, 3659-3686.

Hoppel, W. A., J. W. Fitzgerald, G. M. Frick, R. E. Larson, and E. J. Mack, 1988: Atmospheric Aerosol Size Distributions and Optical Properties Found in the Marine Boundary Layer Over the Atlantic Ocean. Naval Research Laboratory, Washington, D.C., *NRL Report* 9188.

Hoppel, W. A., 1986: Effect of Nonprecipitating Clouds on the Aerosol Size Distribution in the Marine Boundary Layer. *Geophys. Res. Lett.*, **13**, 1, 125-128.

Hoppel, W. A., J. W. Fitzgerald, and R. E. Larson, 1983: Measurements of Atmospheric Aerosols: Experimental Methods and Results of Measurements Off the East Coast of the United States. Naval Research laboratory, Washington, D.C., *NRL Report* 8703.

Hoppel, W. A., and T. A. Wojciechowski, 1976: Accuracy Limitations on CCN Measurements with Thermal Gradient Diffusion Chambers. *J. Appl. Meteor.*, **15**, 107-112.

Hudson, J. G., 1992: Cloud Condensation Nuclei. *J. Appl. Meteor.*, **32**, 596-607.

Hudson, J. G., 1983: Effects of CCN concentrations on stratus clouds. *J. Atmos. Sci.*, **40**, 480-486.

Hudson, J. G., and P. Squires, 1979: An Improved Continuous Flow Diffusion Cloud Chamber. *J. Appl. Meteor.*, **15**, 776-782.

Hudson, J. G., and P. Squires, 1973: Evaluation of a recording continuous cloud nucleus counter. *J. Appl. Meteor.*, **12**, 175-183.

Jensen, J. B., and R. J. Charlson, 1984: On the efficiency of nucleation scavenging. *Tellus*, **36B**, 367-375.

Jiusto, J. E., and G. G. Lala, 1981: CCN-Supersaturation Spectra Slopes (k). *J. Rech. Atmos.* (*Atmos. Res.*), **15**, 3-4, 303-311.

Jiusto, J. E, 1967: Aerosol and cloud microphysics measurements in Hawaii. *Tellus*, **XIX**, 3, 359-368.

Junge, C., and E. McLaren, 1971: Relationship of cloud nuclei spectra to aerosol size distribution and composition. *J. Atmos. Sci.*, **28**, 382-390.

Junge, C., 1958: Atmospheric Chemistry, in *Advances in Geophysics*. Ed. Landsberg, H. E., and J. V. Mieghem, Academic Press Inc., New York. p1-108.

Junge, C., 1963: *Air chemistry and radioactivity*. Academic Press, New York. p153.

Kaufman, Y. J., R. S. Fraser, and R. L. Mahoney, 1991: Fossil Fuel and Biomass Burning Effect on Climate -- Heating or Cooling? *J. Clim.*, **4**, 578-588.

Keady, P. B., F. R. Quant, and G. J. Sem: Differential Mobility Particle Sizer: A new instrument for high-resolution aerosol size distribution measurement below 1 μm. attached, *TSI Model 3934 SMPS user manual*.

Knott, C. G., 1923: *Collected Scientific Papers of John Aitken. LL.D., F.R.S.*. Cambridge at the University Press, London. 591pp.

Laktionov, A., 1965: Measurement of the concentration of cloud condensation nuclei. *Dokl. Akad. Nauk SSSR*, **165**, 3-5.

Landsberg, H. E., 1938: Atmospheric condensation nuclei. *Erg. Kosm, Phys.*, **3**, 155-252.

Lawson, D. R., and J. W. Winchester, 1979: Atmospheric sulphur aerosol concentrations and characteristics from the south American continent. *Science*, **205**, 1267-1269.

Lechner, I. S., G. W. Fisher, H. R. Larsen, M. J. Harvey, and R. A. Knobben, 1989: Aerosol Size Distributions in the Southwest Pacific. *J. Geophys. Res.*, **94**, 14,893-14,903.

Liou, Kou-Nan, and Szu-Cheng Ou, 1989: The Role of Cloud Microphysical Processes in Climate: An Assessment From a One-dimensional Perspective. *J. Geophys. Res.*, **94**, 8599-8607.

Liu, Yangang, Laiguang You, Weinong Yang, and Feng Liu, 1995: On the size distribution of cloud droplets. *Atmos. Res.*, **35**, 201-216.

Lopez, A., J. Servant, and J. Fontan, 1973: Variation des Concentrations et Caractéristiques Physiques des Noyaux d'Aitken Dans un Site Non Pollué. *Atmos. Environ.*, **7**, 945-965.

Maki, L. R., and K. J. Willoughby, 1978: Bacteria as Biogenic Sources of Freezing Nuclei. *J. Appl. Meteor.*, **17**, 1049-1053.

Mészáros, A., 1971: On the Variation of the Size Distribution of Large and Giant Atmospheric Particles as a Function of the Relative Humidity. *Tellus*, **23**, 436-440.

Miller, S. W., and B. A. Bodhaine, 1982: Supersaturation and Expansion Ratios in Condensation Nuclei Counters: An Historical Perspective. *J. Aerosol Sci.*, **13**, 6, 481-490.

Movakov, T., and J. E. Penner, 1993: Large contribution of organic aerosols to cloud-condensation-nuclei concentrations. *Nature*, **365**, 823-826.

Parungo, F. P., C. T. Nagamoto, R. Madel, J. Rosinski, and P. L. Haagenson, 1987: Marine aerosols in Pacific Upwelling Regions. *J. Aerosol Sci.*, **18**, 3, 277-290.

Penner, J. E., R. J. Charlson, J. M. Hales, N. S. Laulainen, R. Leifer, T. Novakow, J. Ogren, L. F. Radke, S. E. Schwartz, and L. Travis, 1994: Quantifying and Minimizing Uncertainty of Climate Forcing by Anthropogenic Aerosols. *Bull. Amer. Meteor. Soc.*, **75**, 3, 375-400.

Philippin, S., and E. A. Betterton, 1995: Cloud Condensation Nuclei in Southern Arizona, Instrumentation and Initial Observations. Submitted to *Atmos. Res.*, Sept. 1995.

Pruppacher, H. R., and J. D. Klett, 1978: *Microphysics of Clouds and Precipitation*. D. Reidel, Hingham, Mass. 714pp.

Radke, L. F., and J. E. Jiusto, 1977: Cloud Condensation Nucleus Counters: A Review. *Ninth International Conference on Atmospheric Aerosols, Condensation and Ice Nuclei.*

Radke, L. F., S. V. Domonkos, and P. V. Hobbs, 1981: A cloud condensation nucleus spectrometer designed for airborne measurements. *J. Rech. Atmos.* (*Atmos. Res.*), **15**, 225-229.

Reist, P. C., 1984: *Introduction to Aerosol Science*. Macmillan Publishing Company. 299pp.

Saxena, V. K., and J. Carstens, 1971: On the operation of thermal diffusion chambers. *J. Rech. Atmos.* (*Atmos. Res.*), **5**, 11-23.

Saxena, V. K., J. N. Burford, and J. L. Kassner Jr., 1970: Operation of a Thermal Diffusion Chamber for Measurements on Cloud Condensation Nuclei. *J. Atmos. Sci.*, **27**, 73-80.

Shaw, G. E., and M. A. K. Khalil, 1989: *Arctic Haze*. The Handbook of Environmental Chemistry, Vol. 4/Part B. Edited by Hutzinger, O., Springer-Verlag Berlin Heidelberg. P70-111.

Shaw, G. E, 1988: Chemical Air Mass Systems in Alaska. *Atmos. Environ.*, **22**, 10, 2239-2248.

Shaw, G. E, 1986: On the physics of Aitken particles in polar air mass systems. *J. Aerosol Sci.*, **17**, 1, 73-78.

Shaw, G. E, 1985a: Cloud Condensation Nuclei Associated with Arctic Haze. *Atmos. Environ.*, **20**, 7, 1453-1456.

Shaw, G. E, 1985b: Aerosol Measurements in Central Alaska, 1982-1984. *Atmos. Environ.*, **19**, 12, 2025-2031.

Shaw, G. E, 1985c: Evaluation of a new aerosol model with a Brownian diffusion technique. *Atmos. Res.*, **20**, 39-51.

Shaw, G. E, 1984: Microparticle size spectrum of arctic haze. *Geophys. Res. Lett.*, **11**, 5, 409-412.

Shaw, G. E, 1983a: Bio-controlled thermostats involving the sulfur cycle. *Climatic Change*, **5**, 297-303.

Shaw, G. E, 1983b: On the Aerosol Particle Size Distribution Spectrum in Alaskan Air Mass Systems: Arctic Haze and Non-Haze Episodes. *J. Atoms. Sci.*, **40**, 5, 1313-1320.

Shaw, G. E, and K. Stamnes, 1980: Arctic haze: perturbation of the polar radiation budget. *Annals of the New York Academy of Sciences*, **338**, 533-539.

Sheridan, P. J., 1994: Aerosol particles in the upper troposphere and lower stratosphere: Elemental composition and morphology of individual particles in northern midlatitudes. *Geophys. Res. Lett.*, **21**, 23, 2587-2590.

Sinnarwalla, A., and D. Alofs, 1973: A cloud nucleus counter with long available growth time. *J. Appl. Meteor.*, **12**, 831-835.

Squires, P., 1971: Diffusion Chambers for the Measurement of the Spectrum of Critical Supersaturations of Cloud Nuclei. *Report on the Second International workshop on Condensation and Ice Nuclei*, Dept. Atmos. Sci., Colorado State University, 7-10.

Smithsonian Meteorological Tables, 1949: Prepared by List, Robert J. Smithsonian Miscellaneous Collections, Vol. 114, City of Washington.

Staebler, R. M., G. den Hartog, B. Georgi, and T. Düsterdiek, 1994: Aerosol size distributions in Arctic Haze during the Polar Sunrise Experiment 1992. *J. Geophys. Res.*, **99**, 25,429-25,437.

Storozhilova, A., 1960: A differential counter for condensation nuclei. *Proc. Surface Forces Conf.*, Moscow, 174-178.

Talbot, L., R. K. Cheng, R. W. Schefer, and D. R. Willis, 1980: Thermophoresis of particles in a heated boundary layer. *J. Fluid Mech.*, **101**, 737-758.

Tomlinson, E. M., and N. Fukuta, 1979: Aspect Ratio of Thermal Diffusion Chambers. *J. Atmos. Sci.*, **36**, 7, 1362-1365.

Tsay, Si-Chee, K. Stamnes, and K. Jayaweera, 1989: Radiative Energy Budget in the Cloudy and Hazy Arctic. *J. Atmos. Sci.*, **46**, 1002-1018.

Twomey, S. A., 1991: Aerosols, clouds and radiation. *Atmos. Environ.*, **25A**, 2435-2442.

Twomey, S. A., M. Piepgrass, and T. L. Wolfe, 1984: An assessment of the impact of pollution on global cloud albedo. *Tellus*, **36B**, 356-366.

Twomey, S. A., 1977: *Atmospheric Aerosols*. Elsevier Scientific Publishing Company, Amsterdam. P94.

Twomey, S. A., 1975: Comparison of Constrained Linear Inversion and an Iterative Nonlinear Algorithm Applied to the Indirect Estimation of Particle. *J. Comp. Phys.*, **18**, 2, 188-200.

Twomey, S. A., 1967: Remarks on the Photographic Counting of Cloud Nuclei. *J. Rech. Atmos. (Atmos. Res.)*, **3**, 85-90.

Twomey, S. A., and T. A. Wojciechowski, 1969: Observation of the geographical variation of cloud nuclei. *J. Atmos. Sci.*, **26**, 684-688.

Twomey, S. A., 1959: The nuclei of natural cloud formation. Part II: the supersaturation on natural clouds and variation of cloud droplet concentration. *Geofis. Pura Appl.*, **43**, 243-249.

Wallace, J. M., and P. V. Hobbs, 1977: *Atmospheric Science - An Introductory survey*. Academic Press, Inc., San Diego. p162, p170.

Wang, Shih Chen, and R. C. Flagan, 1990: Scanning Electrical Mobility Spectrometer. *Aerosol Sci. and Tech.*, **13**, 230-240.

Warner, J., and S. Twomey, 1967: The production of cloud nuclei by cane fires and the effect on cloud drop concentrations. *J. Atmos. Sci.*, **24**, 704-706.

Whitby, K. T., 1978: The physical characteristics of sulphur aerosols. *Atmos. Environ.*, **12**, 135-159.

Whitby, K. T., R. B. Husar, and B. Y. H. Liu, 1972: The aerosol size distribution of Los Angeles smog. *J. Colloid Interface Sci.*, **39**, 237-164.

Wegley, T. M. L., 1989: Possible climate change due to SO_2-derived cloud condensation nuclei. *Nature*, **339**, 365-367.

Wood, A. B., 1955: *A textbook of sound*. The Macmillan Company, New York. P50.

Young, K. C., 1993: *Microphysical Processes in Clouds*. Oxford University Press, New York. 427pp.

Zhang, Xuewen, and Gouguang Zheng, 1994: A simple droplet spectrum derived from entropy theory. *Atmos. Res.*, **32**, 189-193.

Technical Manuals:

Data Acquisition & Control System for the IBM PC and Compatible Computers, Strawberry Tree Incorporated, Computer Instrumentation & Controls, 1988.

Cloud Condensation Nucleus Counter, Model M1, DH Associates, 1993.

Model 3071 DMA (Differential Mobility Analyzer) Instruction Manual, TSI Inc., 1993.

Model 3934 SMPS (Scanning Mobility Particle Sizer) Instruction Manual, TSI Inc., 1993.

Wolfram Research, Inc., Mathematica, Version 2.2, Wolfram Research, Inc., Champaign, Illinois, 1995.

APPENDIX A

Some calculations and graphics for deriving the Likelihood Size Distribution

Mathematica for Students (Wolfram Research, Inc., 1995) is used to solve differential equations and make plots. Some results are listed below. The normal text is the command we type in; the text in italic is the output from Mathematica.

A.1 Solving for v, where v'[t] is the derivative of v[t]

```
v'[t] == w0 U0 Sin[w t] - w0 v[t]
```

v'[t] == U0 w0 Sin[t w] - w0 v[t]

```
DSolve[ {%, v[0] == 0}, v[t], t ]
```

$$\{\{v[t] \to \frac{U0\ w\ w0}{E^{t\ w0}\ (w^2 + w0^2)} +$$

$$\frac{-(U0\ w\ w0\ Cos[t\ w]) + U0\ w0^2\ Sin[t\ w]}{w^2 + w0^2}\}\}$$

A.2 Integral of v(U0 - v), $\int_0^{\pi/\omega} v(U_0 - v)dt$

```
Integrate[      ( (U0*w0*(w/E^(t*w0)-w*Cos[t*w]
          + w0*Sin[t*w]))/(w^2 + w0^2) )
          *( U0 -(U0*w0*(w/E^(t*w0)-w*Cos[t*w]
          + w0*Sin[t*w]))/(w^2 + w0^2) ) ),
          {t, 0, Pi/w} ]
```

```
    2       4     3          2   2        3        4
-(U0  (-2 w  + w  w0 - 4 w  w0  - w w0  - 2 w0 ))
-------------------------------------------------- +
                        2     2 2
                 2 w (w  + w0 )
```

```
        2  4          2  3
   -4 U0  w      2 U0  w  w0          2  2   2
  (---------- + ------------ + 4 U0  w  w0  -
    (Pi w0)/w     (2 Pi w0)/w
   E             E
```

```
       2  2   2
     4 U0  w  w0            2  2   2        2      3
     ------------ - 2 Pi U0  w  w0  - 2 U0  w w0  +
       (Pi w0)/w
      E
```

```
       2   4          2   4           2      2 2
     4 U0  w0  - 2 Pi U0  w0 ) / (4 w (w  + w0 ) )
```

A.3 Limit of v(U0 - v) when ω is large

```
Limit[% * w^2, w -> Infinity]
```

```
     2
Pi U0  w0
```

where % stands for the integrating result from A.2.

A.4 Relaxation time (particle diameter 0.01 ~ 1 μm)

```
coef = 10^(-6)
Plot[(1/coef)*ro*( 1 + 2.52*lmd/(coef*D) )*(coef
D)^2/(18*eta) /. {ro -> 10^3, lmd -> 6.6*10^(-8),
eta -> 1.81*10^(-7)}, {D, 0.02, 1}, DefaultFont ->
{"Courier", 16}, AxesLabel -> {"D (μm)", "Tau (μs)"} ]
```

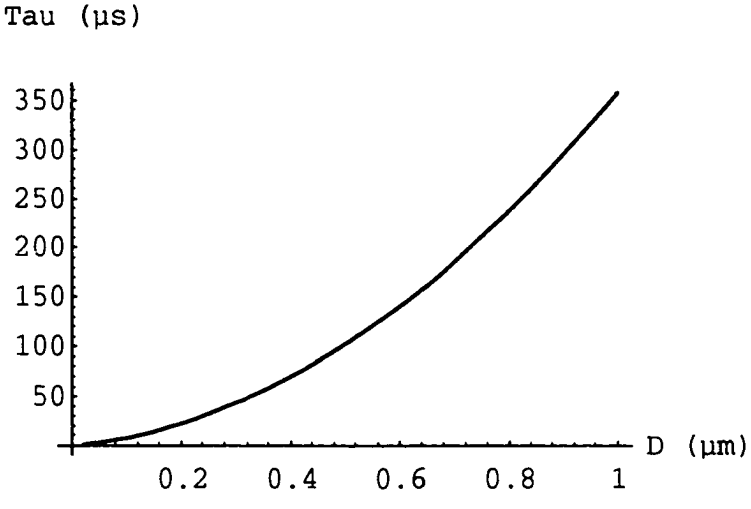

Figure A-1 Relaxation time of particles.
The x-axis is the diameter of particles (0.02 ~ 1 μm), the y-axis is the relaxation time (30 ~ 359 μs).

A.5 *v* as a function of time and ω_0

Assume U_0 = 1 cm s^{-1} in a perturbation. A three dimensional graph of *v* as a function of *D* and *t* shows that small particles, such as 0.1 μm ones, can follow the perturbation well; large particles, such as 1.0 μm ones, are reluctant to move.

```
eta  = 1.81*10^(-7)
ro   = 1000
```

```
U0   = 1
lmd  = 6.6*10^(-8)
coef = 10^(-6)
w    = coef *2Pi * 10^4
w0[x_] := coef*18*eta/(ro*(1+2.52*lmd/10^x)*(coef*10^x)^2)
Plot3D[ ( U0*w*w0[x] * E^(-t*w0[x])
       - U0*w*w0[x]*Cos[t*w] + U0*w0[x]^2*Sin[t*w] )
       / (w^2 + w0[x]^2), {t, 0, Pi/w}, {x, -1, 0},
       DefaultFont -> {"Courier", 12},
       AxesLabel -> {"t (μs) ", "  D (μm)", "v (cm/s)  " },
       Ticks -> { Automatic, { {-1, "0.1"}, {-0.7, "0.2"},
         {-0.52, "0.3"}, {-0.4, ""},  {-0.3, "0.5"},
         {-0.22, ""}, {-0.155, "0.7"}, {-0.1, ""},
         {-0.046, ""}, {0, "1.0"} }, Automatic } ]
```

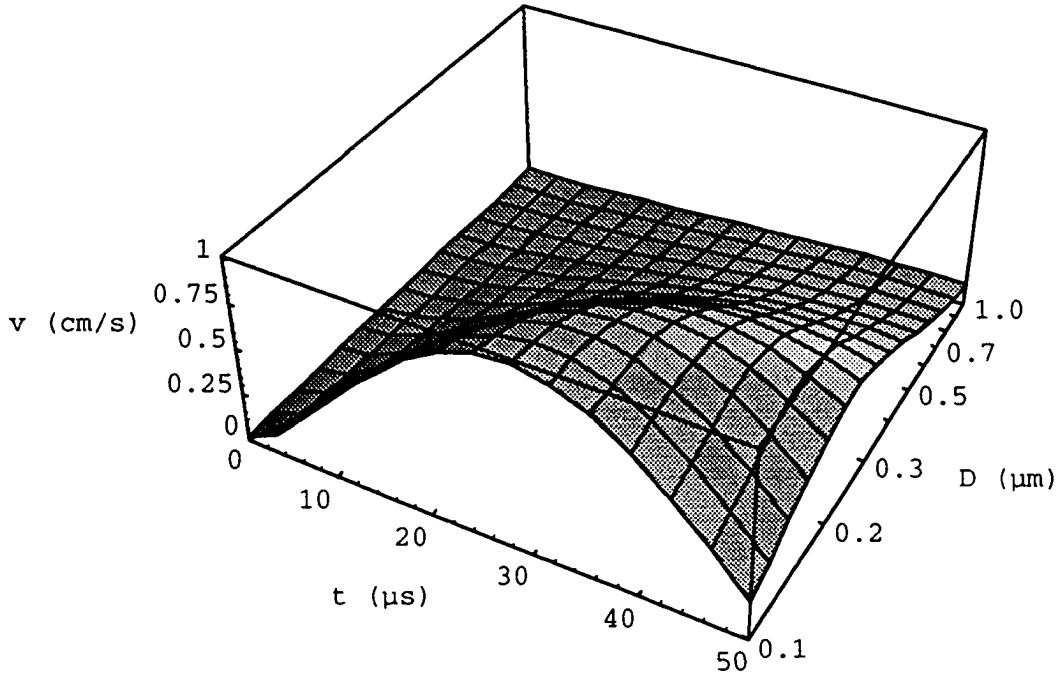

Figure A-2 Speed of particles in a sound wave. The frequency of the sound wave is 10,000 Hz, and $0.1 < D < 1.0$ μm, $0 < t < \pi/\omega$.

APPENDIX B

INSTRUMNTS

B.1 Scanning mobility particle sizer

The measurement of particle size distributions using electrical mobility methods has become the standard method for the characterization of particles smaller than 0.1 μm in diameter since the development of the electrical aerosol analyzer (EAA) and the differential mobility analyzer (DMA) by Knutson, Liu, and their coworkers (1974, 1975). (Wang and Flagan, 1990).

Our scanning mobility particle sizer (SMPS, manufactured by TSI, Inc.) measures particles between about 0.02 and 0.8 μm range. This is about the accumulation mode and CCN particle range.

The measurement result from a SMPS can be converted into DISFTIF file format, which divides the measured range of diameters into about a hundred bins. Each bin has an equal interval in a log scale, and the particle number concentration in each bin is given. The SMPS can make a scan every one minute and a half. To get a more stable result, a longer time is needed.

Since the SMPS is based on the mobility of particles, the size of particles should be regarded as the Stokes diameter. This is the diameter of a sphere of the same density as the particle having the same settling velocity as the particle.

SMPS can be calibrated in the laboratory by using standard polystyrene latex aerosols.

The user manual for SMPS is well written with detailed descriptions and references.

B.2 CCN counter

The CCN counter was described in detail by Philippin and Betterton in their paper (1995). Our CCN counter is exactly the same type as theirs, though I modified ours in a little different way. The quotation below also shows the drawbacks of a typical CCN counter (laser, camera, underestimate, corrections, etc.).

> The M1 thermal gradient diffusion cloud chamber is similar to many others described in the literature (see Kocmond et al., 1980 for example). It consists of two steel plates approximately 9 cm in diameter and 1.25 cm apart and separated by a glass ring enclosing a volume of about 80 cm^3. The upper plate remains at ambient temperature, while the lower plate is thermoelectricity cooled. The temperature difference between the plates is measured using a copper-constantan differential thermocouple, and the temperature of the top plate is measured with a solid-state thermistor (AD590, Omega). A filter paper on the bottom plate and a porous glass

disk beneath the upper plate keep the horizontal surfaces inside the chamber wet.

The chamber is flushed with fresh sample air for 5 seconds at a flow rate of 2.5 L/min with every cycle. Two solenoid valves then isolate the chamber and after about 5 seconds droplets become visible as they fall through a laser beam. It is estimated that the optical system can detect droplets of at least 0.5 μm in diameter (Huffman, 1995, personal communication). The helium-neon laser (6328 Å wavelength, 0.6 mm beam diameter, 3 mW nominal power) is centered in the chamber and oriented at an angle of 90° to a CCD camera (JE 7362, Javelin) which detects the resulting droplets in a volume of approximately 6×10^{-3} cm^3. It is not known how long it takes for thermal and mass equilibrium to be attained in this particular chamber but a horizontal component of the droplet motion cannot be observed so it is assumed that turbulent motion is absent or negligible by the time the first droplets are detected. Results from similar cloud chambers in the past have shown that the time for thermal equilibrium to be achieved is less than 3 seconds (Fitzgerald, 1970, Hudson and Squires, 1973, Squires, 1971). The droplets are counted over a period of 25 seconds before the test sample is replaced and the cycle is repeated. Given a minimum detectable droplet diameter of 0.5 μm, the lower and upper time constraints (5 seconds and 25 seconds, respectively), and an average condensation coefficient of 0.035 (Pruppacher and Klett, 1978), we estimate that all activated nuclei are detected after thermal equilibrium is established and before significant loss from fallout can occur (Hoppel and Wojciechowski, 1976).

The droplets are viewed by a CCD camera and displayed on a monitor. A rectangular portion of the field of view encompassing the laser beam path is digitized in binary format (one when a pixel exceeds a threshold, otherwise zero) and this rectangular digitized field is also displayed on the monitor immediately below and outline of the viewed rectangle. Below the binary digitized image is a third image which shows the status of the factory-set threshold level. The threshold is set to a level that is sensitive enough to record the presence of all droplets yet not so sensitive that it records random noise. The adequacy of the threshold level can be visually checked by comparing the number of droplets seen in the digitized

rectangle to the number seen in the outline of the viewed rectangle. They should be identical.

The viewed rectangle is partitioned among 1024 pixels for digitization. Highlights resulting from reflections are recognized by their persistence and rejected by a drop-counting software that is factory-programmed on a ROM chip. The counting software is also able to recognize a droplet that has already been counted and subsequently fallen under gravity to a lower position in the digitized image. The problem of a single droplet illumination more than one pixel is overcome by counting entities, i.e., clumps of adjacent illuminated pixels. Since the counting software may count several clumped pixels as a single pixel, the instrument counts do not exactly conform to binomial statistics. The underestimation of the "true" number of counts by the "clumped" statistics is systematic and does not exceed 10% if CCN concentrations remain below 1000 per cm^3 (DH Associates, 1992). The correction is calculated as follows: $N_{true} = 1.0237 + 8.476\times10\text{-}5\ N + 5.3\times10\text{-}8\ N^2$, where N_{true} = true number per cm^3 and N = unadjusted number per cm^3. In this study the correction normally amounted to $\leq$ 5% and so was not applied.

The counting software keeps track of raw and volume-integrated counts. Three particle counts are obtained. A time-integrated raw beam count is obtained at the end of each 30 second cycle. Because of the small sampling volume (6×10^{-3} cm^3) this count is usually very low, e.g., 1 count. In order to increase the number, the raw beam count is accumulated until the integrated volume is equivalent to 0.1 cm^3, i.e., for approximately 8 minutes. Finally, the 0.1 cm^3 count is accumulated until a 1 cm^3 count is obtained after approximately 80 minutes. The 0.1 cm^3 count is updated continuously and is often on the order of 10 per cm^3. For a large sample, root-mean-square fluctuations (standard deviation) are expected to be $N^{1/2}$, where N = average number of CCN (Hoppel and Wojciechowski, 1976). This implies that the standard deviation of the 0.1 cm^3 count should be approximately $\pm$3, i.e. 30%. This level of uncertainty is acceptable for quick checks of instrument operation, e.g., response to smoke. The number of active pixel elements is also recorded. This is used for diagnostic purposes in order to detect optical problems.

B.3 Modification of the CCN counter

The CCN counter is modified to let a computer control the supersaturation and data acquisition.

(1) A hole is drilled into the top plate of the thermal diffusion chamber, and a thermocouple is inserted to measure the temperature. It is assumed to be at the same temperature on the bottom surface of the porous glass disk (it is difficult to mount a temperature detector there). Notice that the temperature on the bottom plate is also measured inside the plate. These can cause some errors.

The temperatures are measured by a computer for calculating the supersaturation.

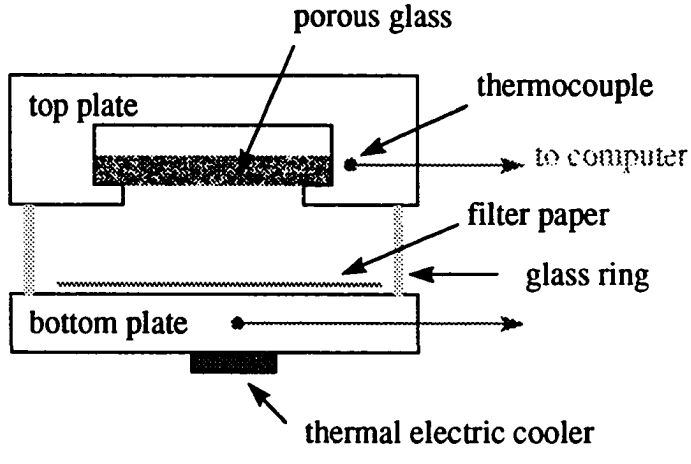

Figure B-1 A cross section of the thermal diffusion chamber in the CCN counter.

(2) A transistor and a switch are added to let a computer control the voltage for the thermoelectric cooler which is mounted beneath the bottom plate of the thermal diffusion chamber.

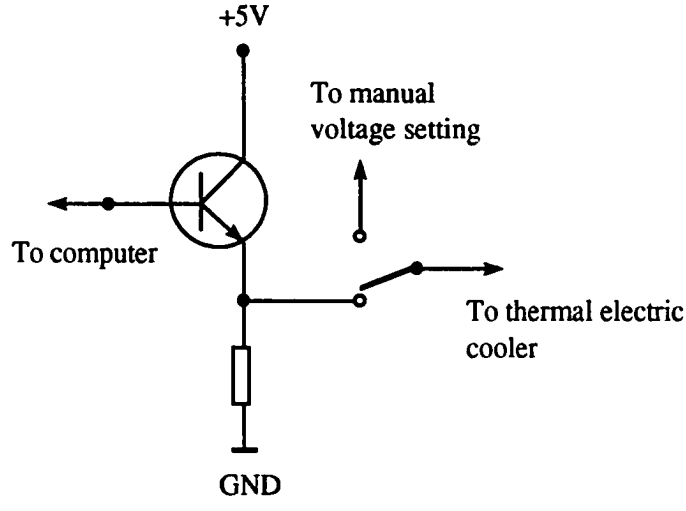

Figure B-2 The circuit added to the CCN counter to let a computer control the thermal electric cooler.

B.4 Supersaturation in a thermal diffusion chamber

The supersaturation (S) in a thermal diffusion chamber is calculated from the Clausius-Clapeyron equation. It depends on T, and dT; where T is the temperatures on the top plate, dT is the temperature difference between the top and bottom plates. The calculation shows that control the temperature difference only may not be enough. The calculation was done in Mathematica.

A. Error analysis

According to Chapter 2, the CCN number (concentration) can be described by

$$N = A[1 - \exp(-BS^{4/3})]$$

Let us consider the uncertainty of N due to the uncertainty of S. Assume A and B are constant, then

$$\frac{dN}{dS} = \frac{4}{3} ABS^{4/3} \frac{1}{S} \exp(-BS^{4/3})$$

and

$$\frac{\Delta N}{N} = \frac{\frac{4}{3} BS^{4/3} \exp(-BS^{4/3})}{1 - \exp(-BS^{4/3})} \frac{\Delta S}{S}$$

Assume $B = 3.5$, $S = 0.3$, $\Delta S/S = 0.1$, then $\Delta N/N \approx 0.09$, which means that if S change 10%, then N will also change about 10%. The following examples will show that if T changes 10°C, then S can change 10%. Therefore, assuming the environment is at a constant temperature can cause a little extra error. It is better to control S directly than to control dT only. It is also shown that the assumption that the diffusivity of water vapor in air and the thermal conductivity of moist air are independent of temperature can result in an error in the supersaturation of 9% (Fitzgerald, 1972).

B. *S* vs. d*T* at *T* = 25°C

```
T = 273 + 25
dT = 3
dT1 = 0
dT2 = 7
Plot[S[T, dT], {dT, dT1, dT2},
  DefaultFont -> {"Courier", 16}, AxesLabel -> {"dT", "S"}]
```

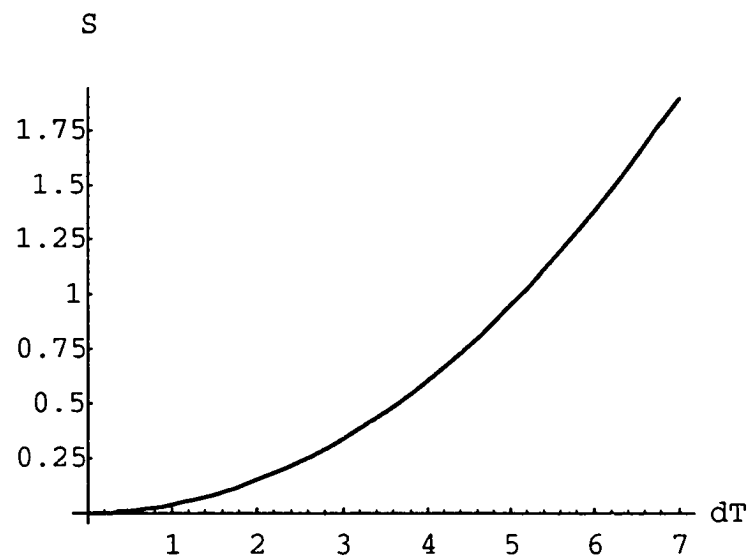

Figure B-3 Supersaturation vs. the temperature difference between the top and bottom plates, d*T*, at *T* = 25°C.

C. *S* vs. *T* (between 15°C and 40°C) with d*T* fixed at 3°C

```
T0 = 298
dT = 3
T1 = 273 + 15
T2 = 273 + 40
Plot[S[T, dT], {T, T1, T2}, DefaultFont -> {"Courier", 16},
     AxesLabel -> {"T (K)", "S at dT = 3"},
     AxesOrigin -> {T1, S[T0,dT]}]
```

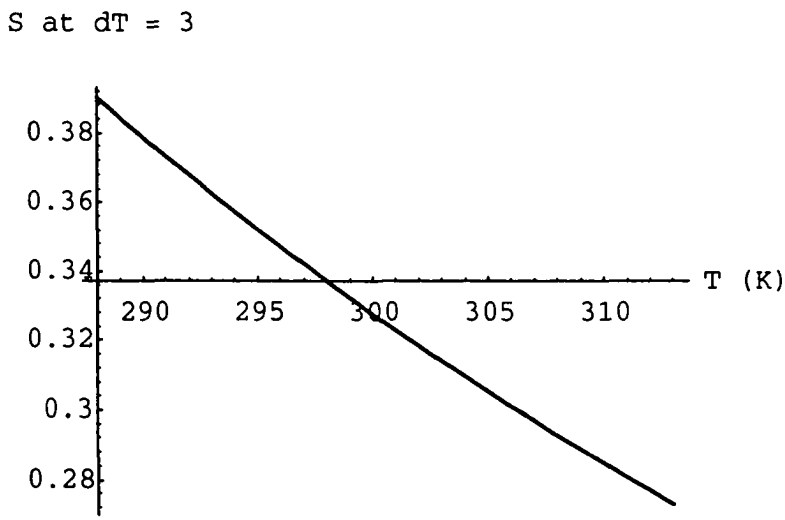

Figure B-4 Supersaturation vs. the temperature on the top plate, *T*, at d*T* = 3°C.

D. Relative error of *S* (*T* = 15°C ~ 40°C, d*T* = 3°C)

```
T0 = 298
dT = 3
T1 = 288
T2 = 313
Plot[(S[T, dT] - S[T0, dT]) / S[T0, dT], {T, T1, T2},
  DefaultFont -> {"Courier", 16},
  AxesLabel -> {"T (K)", "relative error of S at dT = 3"},
  AxesOrigin -> {288, 0}]},
  Ticks -> {Automatic, {{0.15, "15%"}, {0.1, "10%"},
           {0.05, "5%"}, {-0.05, "-5%"}, {-0.1, "-10%"},
           {-0.15, "-15%"}} }]
```

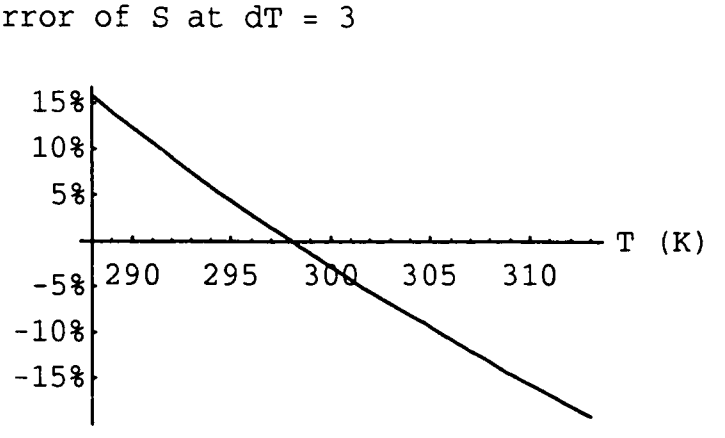

Figure B-5 Relative error of supersaturation. Keep d*T* = 3°C, the supersaturation at *T* = 15°C will be 15% higher that at *T* = 25°C.

E. *S* vs. *T* and *dT*

```
T1 = 273 + 15
T2 = 273 + 40
dT1 = 0
dT2 = 7
e0 = 611
L = 2.5 10^6
Rv = 461
e[T_] := e0 Exp[(L/Rv) (1/273 - 1/T)]
S[T_, dT_] := 100( ( (e[T]/T + e[T-dT]/(T-dT) )/2 )
                / ( e[T-dT/2]/(T-dT/2) ) - 1 )
Plot3D[S[T, dT], {T, T1, T2}, {dT, dT1, dT2}, DefaultFont ->
{"Courier",12}, AxesLabel ->{"T (K) ", "dT (°C)", "S (%) "}]
```

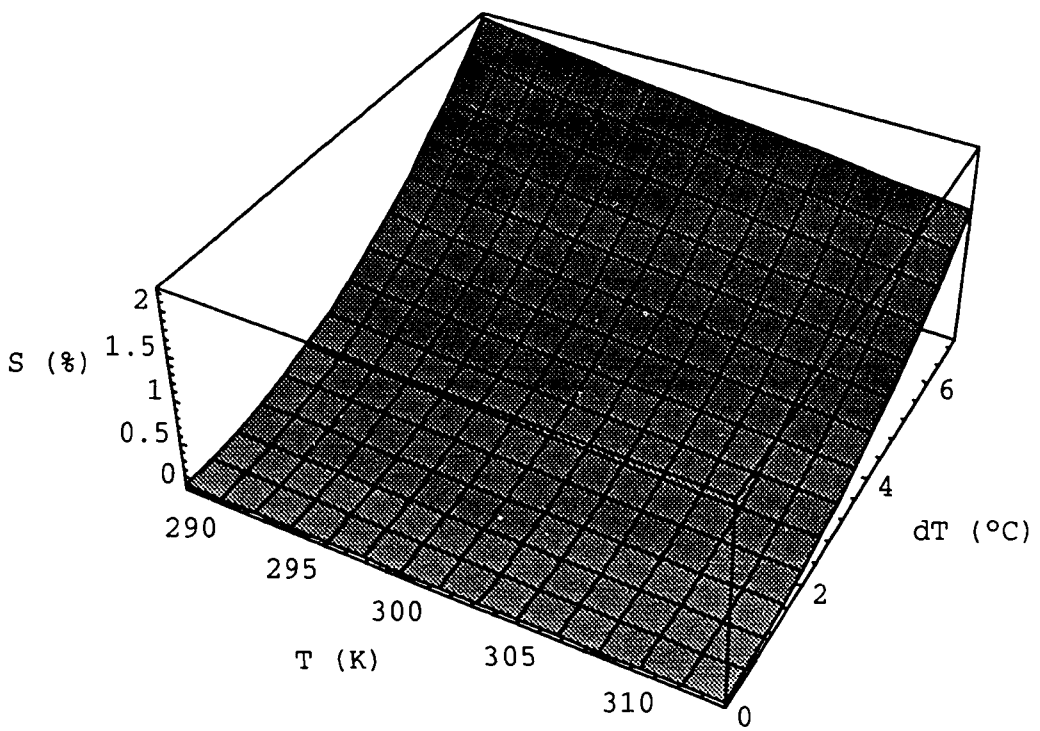

Figure B-6 Supersaturation (*S*) vs. temperature (*T*) on the top plate and the temperature difference between the top and the bottom plates in a thermal diffusion chamber is (d*T*).

APPENDIX C

COMPUTER PROGRAMS

C.1 A thermal-diffusion-chamber model

```
' Trajectory of droplets
'   - a simplified simulation of how fast droplets grow and fall

'   units: IS

'   references: (Y) Microphysical Processes in Clouds,
'                   K. C. Young,
'                   New York, Oxford University Press,
'                   1993
'                   QC 921.5 Y68

'               (P) Microphysics of Clouds and Precipitation,
'                   Hans R. Pruppacher, James D. Klett,
'                   D. Reidel Publishing Company, Boston,
'                   1978
'                   QC 921.5 P78

startTime = TIMER                   'record CPU time

'use time as file name for output
file1$ = LEFT$(DATE$, 2) + MID$(DATE$, 4, 2) + LEFT$(TIME$, 2)
         + MID$(TIME$, 4, 2)
file1$ = file1$ + ".txt"
CLS
PRINT "output: "; file1$

OPEN file1$ FOR OUTPUT AS #1
OPEN "debug.prn" FOR OUTPUT AS #3 'for debugging

nTime% = 61             'simulation time ~ 1 minute
dtPRN = 1               'record the height of a droplet every 1 s

'trajectory of a droplet, radius, time and height
nPRN% = nTime% / dtPRN
nLayers% = 7

DIM zInis(nLayers%)
DIM tPRN(nPRN%, nLayers%)
```

```
DIM rPRN(nPRN%, nLayers%)
DIM zPRN(nPRN%, nLayers%)

es0 = 6.11          'saturation water vapor pressure at 0 C (mb)
es0 = es0 * 100     '(Pa)
g = 9.81            'gravity
Mv = 18             'molecular weight of water
Rgas = 8314.36      'gas constant
Rv = 461.5          'gas constant for water vapor
ro = 1000           'density of droplet
roCCN = 1770        'density of CCN, assume to be (NH4)2SO2
iHoff = 3           'Van't Hoff factor
MCCN = 132          'molecular weight of ammonium sulfate
C = .0154           'for critical size, r in µm

coef1 = 2 * ro / 9 * g          'a coefficient in Stokes' law
roRv2 = 2 / (ro * Rv)

H = .02             'height of the chamber
Tb = 298.15         'temperature at the bottom plate, 25°C
'temperature difference between the top and the bottom plates
dTtop = 3           '°C
Ttop = Tb + dTtop
dt = .001           'time step (1 ms)

zInis(1) = .0025    '(m)
zInis(2) = .005
zInis(3) = .0075
zInis(4) = .01
zInis(5) = .0125
zInis(6) = .015
zInis(7) = .0175

rIni = .036           'initial radius (µm) of CCN
rIni = rIni * .000001 '(m)

' assume the temperature and the water vapor change linearly in
the chamber
' the supersaturation reaches the maximum on mid-plan
z = H / 2                       'to get the SS_max and
r_critical
zH = z / H                      'relative height
dTz = dTtop * zH                'dT at z
Tz = Tb + dTz                   'T at z
TzC = Tz - 273.15               'T at z in Celsius

' specific latent heats of evaporation, (P) p89 (4-85a)
'  Lv  = 1000  * 4.18  * 597.3  * (273.15  / Tz ) ^ gama
gama = .167 + .000367 * Tz
Lv = 2496714 * (273.15 / Tz) ^ gama
LvMvR = Lv * Mv / Rgas
```

```
' supersaturation by Clausius-Clapeyron equation, (Y) P5
'   and gas law
tmp = EXP(LvMvR * dTtop / (Tb * Ttop)) / Ttop
tmp = (1 - zH) / Tb + tmp * zH
tmp = tmp * Tz * EXP(-1 * LvMvR * dTz / (Tb * Tz))
SStmp = tmp - 1
SSMax = SStmp * 100                'in %

'from Köhler curve
rC = C / (SSMax ^ (2 / 3))         'critical size
rC = rC * .000001                  '(m)

FOR iLayers% = 1 TO nLayers%
  t = 0                            'initialization
  z = zInis(iLayers%)              'initial height of CCN

  Tz = Tb + dTtop * z / H      'T at z
  TzC = Tz - 273.15            'T at z in Celsius

' surface tension, (P) p104 (5-12)
  sigma = .0761 - .000155 * TzC

' Köhler curve, (Y) p53
  aHat = roRv2 * sigma / Tz
  bHat = iHoff * rIni ^ 3 * roCCN / ro * Mv / MCCN
                             'assume at t=0 CCN turns into haze
  r = SQR(bHat / aHat)       'the haze size (SS=0) of the CCN
  rHaze = r                  'the initial droplet size

  iPRN% = 1
  rCount% = dtPRN / dt       'make a record every dtPRN / dt cycle
  PRNCount% = rCount%

  nLoop& = nTime% / dt
  FOR i& = 1 TO nLoop&       'FOR loop

'during dt, the droplet falls dz, grows dr
    t = dt * (i& - 1)        'new time

    IF PRNCount% = rCount% THEN
'size (r) and height (z) of a droplet at time (t)
      tPRN(iPRN%, iLayers%) = t
      rPRN(iPRN%, iLayers%) = r
      zPRN(iPRN%, iLayers%) = z
      PRNCount% = 0          'reset counter
      iPRN% = iPRN% + 1
    END IF
    PRNCount% = PRNCount% + 1

' dynamic viscosity, (P) p323 (10-107a)
'eta  = .1  * (1.718  + .0049  * TzC ) * .0001
    eta = .00001718# + .000000049# * TzC
```

```
' terminal velocity by Stokes approximation, (Y) P170
'coef1  = 2 * ro  / 9 * g
    Vt = coef1 / eta * (r * r)

    dz = Vt * dt                'droplet fall
    z = z - dz                  'new height

    zH = (z + .5 * dz) / H
'use the T at the middle of dz for growth
    dTz = dTtop * zH            'dT at z
    Tz = Tb + dTz               'T at z
    TzC = Tz - 273.15           'T at z in Celsius

' specific latent heats of evaproation, (P) p89 (4-85a)
'  Lv  = 1000  * 4.18  * 597.3  * (273.15  / Tz ) ^ gama
    gama = .167 + .000367 * Tz
    Lv = 2496714 * (273.15 / Tz) ^ gama
    LvMvR = Lv * Mv / Rgas

' supersaturation by Clausius-Claperyron equation, (Y) P5
'   and gas law
    tmp = EXP(LvMvR * dTtop / (Tb * Ttop)) / Ttop
    tmp = (1 - zH) / Tb + tmp * zH
    tmp = tmp * Tz * EXP(-1 * LvMvR * dTz / (Tb * Tz))
'supersaturation of the new environment, not it (%)
    SS = tmp - 1

' surface tension, (P) p104 (5-12)
    sigma = .0761 - .000155 * TzC

' Kohler curve, (Y) p53
    aHat = roRv2 * sigma / Tz

'supersaturation of the droplet on Köhler curve
    SSdrop = aHat / r - bHat / r ^ 3

' thermal conductivity, (P) p418 (13-16)
'  Ka  = 4.18  * (5.69  + .017  * TzC ) * 0.001
    Ka = .0237842 + .00007106# * TzC

' saturation vapor pressure
    esz = es0 * EXP(LvMvR * TzC / (273.15 * Tz))

' diffusivity of water vapor in air, (P) p413 (13-3)
' assume p = p0 = 1013.25 mb
    Dv = .0000211 * (Tz / 273.15) ^ 1.94

' growth equation, (Y) p120 (5.15)
    tmp1 = Lv * Lv / (Ka * Rv * Tz * Tz)
    tmp2 = Rv * Tz / (Dv * esz)
    coef2 = ro * (tmp1 + tmp2)
    drdt = (SS - SSdrop) / (r * coef2)
```

```
    dr = drdt * dt              'diffusion growth of the droplet
    r = r + dr

'if the SS in evironment is smaller than SSdrop,
'  the droplet evaporates
'r should be >= rHaze in the chamber, if not,
'  dt is probably too large
    IF r < rHaze THEN
      PRINT #3, "(let r=rHaze)", t, r, dr, rHaze
      r = rHaze
'due to the Kohler curve,
'SSdrop may increase while r increase before the critical size
'should use the new balance size, to simplify, keep rHaze
    END IF

    IF z <= 0 THEN
      GOTO printOut                 'before reaching the bottom
    END IF

  NEXT i&

printOut:

  PRINT #1,
  PRINT #1, "dT:", dTtop
  PRINT #1, "SS max:", SSMax
  PRINT #1,
  PRINT #1, "rIni:", rIni
  PRINT #1, "rHaze:", rHaze
  PRINT #1, "rC:", rC
  PRINT #1,
  PRINT #1, "dt:", dt
  PRINT #1, "simulation time:", nTime% - 1
  PRINT #1, "CPU time: "; TIMER - startTime
  PRINT #1,
  PRINT #1, "layer:", zInis(iLayers%)
  PRINT #1,

  FOR i% = 1 TO nTime% / dtPRN
'after CCN touch the bottom, all records are 0
    PRINT #1, i%, tPRN(i%, iLayers%), zPRN(i%, iLayers%),
                  rPRN(i%, iLayers%)
  NEXT i%

NEXT iLayers%

CLOSE
STOP
```

C.2 Data acquisition

```
REM control program for DH associates' CCN counter Model M1

REM CCNSCAN:    based on QBASUBR V4.0 1-3-89
REM             modified for CCN counter, 1994
REM reference:  (1) manual of AD and DA boards
REM                 (Strawberry Tree Inc.)
REM             (2) manual of CCN counter
REM                 (DH Associates)
REM             (3) manual of QuickBasic
REM                 (Microsoft)
REM             (4) Smithonian Meteorological Table
REM                 P350, P381
REM hardware:   CCN counter,
REM             AD board,
REM             DA board,
REM             terminal boxes and accessories

' ***************** USING QUICKBASIC ENVIRONMENT **********************
' *                                                                    *
' * Start Quick Basic by typing:                                       *
' *       QB QBASUBR /LQBLIB.QLB                                       *
' * You must have QBLIB.QLB and QBLIB.LIB in the QuickBasic directory *
' *================ USING THE COMMAND LINE COMPILER ==================*
' *  Link with QBCALL.OBJ after compiling:                             *
' *       BC QBASUBR           (compile)                               *
' *       LINK QBASUBR QBCALL  (link)                                  *
' *  This program compiles using Microsoft Quick Basic 4.0             *
' *  Do not change the name AM1 used for calls                         *
' *  Use CALL AM2 for "1" command as in the examples in the manual     *
' *  Use CALL AM3 for driver calls which require 2 integer arrays and  *
' *  the command string as arguments.                                  *
' *  Note:  AM3 was created to appease QuickBasic's strong typing.     *
' *         AM3 allows QuickBasic to pass 2 integer arrays without     *
' *         error instead of one integer array and one real array as   *
' *         used normally in CALL AM1.                                 *
' *                                                                    *
' ********************************************************************
```

See the computer connected to the CCN Remover for detail.

APPENDIX D

FUTURE WORK ON CCN REMOVER SPECTROMETER

The CCN Remover Spectrometer is composed of an aerosol sizing system and a CCN Remover. The aerosol sizing system we use is a commercial one; no modification is needed at this time. The CCN Remover is a thermal diffusion chamber. To improve the performance of the CCN Remover Spectrometer, we need to consider:

A. A better temperature control in the CCN Remover

It is found that if the temperature on the top plate of the thermal diffusion chamber is not controlled, then when the bottom plate is cooled, the temperature on the top plate will also drop. Thus, the supersaturation keeps changing, introducing a considerable error.

Since the supersaturation is calculated from the temperatures measured on the top and the bottom plates of the chamber, more accurate measurements of temperatures is desired. The temperature distributions across the top and the bottom plates will be monitored.

B. A better air flow control

In the present design of the CCN Remover, due to the sheath air, the sample air is diluted. The fluctuation in the air flow rates will cause errors. A better flow control is needed.

C. Speed up measurements

To speed up measurements and to get more accurate data, more than one CCN Remover can be used simultaneously. Therefore, while one Remover is performing measurement, the supersaturations in other Removers can be set to new values and reach stable states, and the chambers are also flushed.

D. Building materials

Distilled water is the working fluid in the thermal diffusion chamber. Inexpensive materials such as aluminum, filter paper and cotton cloth may contaminate distilled water in the chamber and cause errors in supersaturation and measurements. Stainless steel, porous glass or sintered metal plates will be used when we build new chambers.